Investigating Sex Differences in Knee Osteoarthritis: Meniscus Models Under Simulated Microgravity

by

Zhiyao Ma

A thesis submitted in partial fulfillment of the requirements for the degree of

Doctor of Philosophy

Department of Surgery
University of Alberta

Abstract

Knee osteoarthritis (KOA) is a degenerative joint disease that impacts all structures within the knee joint, often leading to chronic pain and disability. The meniscus, a crucial fibrocartilaginous structure within the knee, plays a key role in joint biomechanics. It is well established that damage or degeneration of the meniscus significantly contributes to the progression of KOA. Additionally, recent studies have shown that the meniscus is one of the first structures to be affected in the early stages of KOA. This early involvement underscores the meniscus's importance in KOA research. Despite well-documented differences in KOA prevalence and severity between males and females, the molecular mechanisms behind these sex-specific differences are not well understood. This gap in knowledge hinders the development of targeted therapies that can more effectively address the unique aspects of KOA in each sex. To address this, studies in this thesis use simulated microgravity (SMG) to induce KOA-like changes in meniscus models. SMG effectively mimics mechanical unloading, a condition known to exacerbate osteoarthritic changes by disrupting normal biomechanical stimuli. By employing SMG, this thesis aims to investigate the sex-specific molecular mechanisms that contribute to the development and progression of KOA in various meniscus models, with in-depth tissue level and bioinformatics analysis elucidating the key molecules, pathways, and regulatory networks involved.

Chapter 1 provides a comprehensive review of the mechanical environment of the knee meniscus, examining how various forms of mechanical stimuli influence meniscus cell phenotype and extracellular matrix production. It also introduces SMG as an emerging

method to study the effects of mechanical unloading on engineered meniscus models, setting the stage for experimental investigations in subsequent chapters. Building on this, Chapter 2 focuses on the short-term responses of primary meniscus fibrochondrocytes seeded on 3D type I collagen scaffolds to SMG, presenting a detailed transcriptome study that tracks molecular pathways and signaling networks over time. Significant gene expression changes are identified, with JUN highlighted as a potential marker for sex differences. Extending these findings, Chapter 3 examines the long-term effects of SMG on engineered meniscus models to understand the broader impact of prolonged mechanical unloading and investigates tissue-level differences. Additionally, it explores the effects of cyclic hydrostatic pressure (CHP) to study mechanical loading. Chapter 4 builds on the SMG study from Chapter 3, using the same engineered meniscus models, to provide a deeper focus on the transcriptome profile. This chapter identifies the cell surface marker CD36 as an indicator of higher osteoarthritis development propensity in a subgroup of females. Finally, Chapter 5 investigates the role of CD36 in sex differences related to KOA using human total knee arthroplasty meniscus samples and a CD36 knockout mice model. The findings indicate that CD36 plays a significant role in mediating meniscus calcification and hypertrophic differentiation, with notable sex-specific differences. Chapter 6 summarizes the thesis and suggests future research directions.

The findings of this thesis provide valuable insights into the sex-specific molecular responses of meniscus models to mechanical unloading induced by SMG, using both human and mouse models. Understanding these differences is crucial for developing targeted therapeutic strategies for KOA, given the varying prevalence and severity of the

disease between sexes. This research enhances our knowledge of the molecular mechanisms behind KOA and sex differences. It underscores the effectiveness of SMG as a platform for inducing KOA-like changes and screening potential biomarkers, such as CD36, to identify individuals with a higher propensity for osteoarthritis development. These insights can aid in developing suitable therapeutic targets for managing KOA.

Preface

This thesis, titled " Investigating Sex Differences in Knee Osteoarthritis: Meniscus Models Under Simulated Microgravity " is an original work by Zhiyao Ma. The use of human specimens received research ethics approval from the University of Alberta's Health Research Ethics Board, Biomedical Panel, study ID: Pro00018778. The animal research was conducted in accordance with the protocol approved by the University of Alberta Animal Care and Use Committee, study ID: AUP00001363.

The research presented herein has been peer-reviewed and published as detailed below. Each of the first three chapters and part of chapter 4 (chapter 4.1 and 4.2) corresponds to articles that were published in scientific journals. The detailed references and authors' contributions are listed as follows. Articles marked with ***** were equal first-authorships

Chapter 1: Z. Ma Z, Vyhlidal MJ, Li DX, Adesida AB. Mechano-bioengineering of the knee meniscus. *Am J Physiol Cell Physiol.* 2022; 323(6):C1652-C63. Z.M.: Conceptualization, methodology, data collection, formal analysis, writing original draft, review, and editing. M.J.V.: Data collection, formal analysis, writing review, and editing. D.X.L.: Data collection, formal analysis, writing review, and editing. A.B.A.: Conceptualization, resources, supervision, writing review, and editing.

Chapter 2*: Ma Z, Li DX, Lan X, Bubelenyi A, Vyhlidal M, Kunze M, Sommerfeldt M, Adesida AB. Short-term response of primary human meniscus cells to simulated microgravity. *Cell Commun Signal.* 2024;22(1):342. Z.M.: Conceptualization, methodology, data collection, formal analysis, writing original draft, review, and editing. D.X.L.: Conceptualization, methodology, data collection, investigation, writing review, and editing. X.L.: Investigation, writing review, and editing. A.B.: Investigation, writing review, and editing. M.V.: Investigation, writing review, and editing. M.K.: Data collection and investigation. M.S.: Surgical harvest and collection of tissue specimens. A.B.A.: Conceptualization, resources, supervision, writing review, editing, and project administration.

Chapter 3*: Ma Z, Li DX, Kunze M, Mulet-Sierra A, Westover L, Adesida AB. Engineered Human Meniscus in Modeling Sex Differences of Knee Osteoarthritis in Vitro. *Front Bioeng Biotechnol.* 2022; 10:823679. Z.M.: Conceptualization, methodology, data collection, formal analysis, writing original draft, review, and editing. D.X.L.: Conceptualization, methodology, data collection, formal analysis, writing original draft, review, and editing. A.M.-S.: Data collection and investigation. M.K.: Data collection and investigation. L.W.: Data collection, formal analysis, and mechanical testing. A.B.A.: Conceptualization, resources, supervision, writing review, and editing.

Chapter 4*: Ma Z, Li DX, Chee RKW, Kunze M, Mulet-Sierra A, Sommerfeldt M, Westover L, Graf D, Adesida AB. Mechanical Unloading of Engineered Human Meniscus Models Under Simulated Microgravity: A Transcriptomic Study. *Sci Data*. 2022; 9(1):736. Z.M.: Conceptualization, methodology, data collection, formal analysis, writing original draft, review, and editing. R.C.: Conceptualization, methodology, data collection, formal analysis, writing review, and editing. D.X.L.: Conceptualization, methodology, data collection, formal analysis, writing original draft, review, and editing. A.M.-S.: Data collection and investigation. M.K.: Data collection and investigation. L.W.: Data collection, formal analysis, and mechanical testing. M.S.: Procuring clinical specimens, writing review, and editing. D.G.: Co-applicant for financial support, writing review, and editing. A.B.A.: Conceptualization, resources, supervision, writing review, and editing.

As of August 2024, chapter 5 and chapter 6 have not been peer-reviewed nor published.

Additionally, during the completion of this work, Zhiyao Ma contributed to several full-length manuscripts accepted and published in peer-reviewed journals that are not contained in this thesis. These publications include:

1. **Accepted *** Ma Z, Chawla S, Lan X, Zhou E, Mulet-Sierra A, Kunze M, Adesida AB. Functional heterogeneity of meniscal fibrochondrocytes and microtissue models is dependent on modality of fibrochondrocyte isolation. *Cell Prolif*. 2024.
2. Lan X, Ma Z, Dimitrov A, Kunze M, Mulet-Sierra A, Ansari K, Osswald M, Seikaly H, Boluk Y, Adesida AB. Double crosslinked hyaluronic acid and

collagen as a potential bioink for cartilage tissue engineering. *Int J Biol Macromol*. 2024;273 (Pt 1):132819.

3. * Li DX, Ma Z, Szojka AR, Lan X, Kunze M, Mulet-Sierra A, Westover L, Adesida AB. Non-hypertrophic chondrogenesis of mesenchymal stem cells through mechano-hypoxia programing. *J Tissue Eng*. 2023; 14:20417314231172574.
4. Aissiou AK, Jha S, Dhunnoo K, Ma Z, Li DX, Ravin R, Kunze M, Wong K, Adesida AB. Transcriptomic response of bioengineered human cartilage to parabolic flight microgravity is sex-dependent. *NPJ Microgravity*. 2023;9(1):5.
5. Lan X, Ma Z, Kunze M, Mulet-Sierra A, Osswald M, Ansari K, Seikaly H, Boluk Y, Adesida AB. The Effect of Crosslinking Density on Nasal Chondrocytes' Redifferentiation. *Ann Biomed Eng*. 2023.
6. Szojka ARA, Li DX, Sopcak MEJ, Ma Z, Kunze M, Mulet-Sierra A, Adeeb SM, Westover L, Jomha NM, Adesida AB. Mechano-Hypoxia Conditioning of Engineered Human Meniscus. *Front Bioeng Biotechnol.* 2021; 9:739438.
7. Lan X, Ma Z, Szojka ARA, Kunze M, Mulet-Sierra A, Vyhlidal MJ, Boluk Y, Adesida AB. TEMPO-Oxidized Cellulose Nanofiber-Alginate Hydrogel as a Bioink for Human Meniscus Tissue Engineering. *Front Bioeng Biotechnol*. 2021;9:766399.

Acknowledgement

First and foremost, I would like to express my deepest gratitude to my supervisor, Dr. Adetola Adesida, for his continuous support, guidance, and encouragement throughout my PhD journey. His insightful feedback and unwavering belief in my abilities have been instrumental in shaping this research.

I extend my heartfelt thanks to the members of my supervisory committee, Dr. Daniel Graf and Dr. Lindsey Westover, for their valuable insights, constructive criticism, and support. Their expertise and suggestions have significantly contributed to the improvement of this thesis. I would also like to acknowledge Dr. Maria Febbraio for providing the mice used in this project. Her assistance, generosity, and guidance have been crucial for the success of this research.

I am also deeply thankful to the technical staff in Dr. Adesida's lab, Aillette Mulet-Sierra and Melanie Kunze, for their invaluable assistance and support. Additionally, I would like to extend my gratitude to my colleagues and friends in the lab, Michelle Lan, Alex Szjoka, David Li, and Margaret Vyhlidal, for their friendship and encouragement. Their encouragement and assistance have made the challenging moments more manageable and the achievements more enjoyable.

My heartfelt appreciation goes to my parents, Yafeng Ma and Juye Chen, whose unwavering support and belief in me have been the foundation of my journey. Their endless sacrifices, encouragement, and unconditional love have provided me with the strength and motivation to pursue my dreams. My parents have always been my greatest cheerleaders, celebrating my successes and comforting me during challenges. Their guidance, wisdom, and patience have shaped who I am today, and I am forever indebted to them for their invaluable contributions to my life and education. Without their support, none of this would have been possible. I dedicate this thesis to them as a small token of my immense gratitude and love.

Thank you all.

Table of Contents

List of Tables

List of Figures

Chapter 1

Mechano-bioengineering of the knee meniscus

This Chapter has been previously published as:

Ma Z, Vyhlidal MJ, Li DX, Adesida AB. Mechano-bioengineering of the knee meniscus. *Am J Physiol Cell Physiol*. 2022; 323(6):C1652-C63.

1.1 Introduction

Once considered a functionless structure akin to an embryonic remnant, the meniscus is now recognized as the critical structure for proper knee mechanics (1). The meniscus contributes to many essential biomechanical functions of the knee, such as load transmission, stability, and joint lubrication (2, 3). The ability of the meniscus to assist in routine joint function is primarily a result of the heterogeneous macro and microstructure shaped by mechanical loading (4). The biochemical composition and functionality of the tissue are maintained by resident meniscus cells that tailor extracellular matrix (ECM) synthesis in response to mechanical cues. The process by which meniscus cells respond to mechanical cues, known as mechanotransduction, is essential as abnormalities in the signaling pathways can contribute to the development of knee osteoarthritis (KOA). KOA is a chronic disease characterized by cartilage deterioration that causes substantial pain and joint immobility (5). Annually, KOA burdens the workforce considerably and accounts for a significant fraction of disability leave (6, 7). Current treatment options, such as hyaluronic acid and corticosteroid injections, for KOA, are temporary and aim at reducing pain in the short term. Total joint arthroplasty is a longer-term solution (~20 years) that is more feasible, but the procedure is commonly considered and performed in individuals aged over 65 yr, as this is when individuals usually present with end stage of the disease and other treatment options have been exhausted (8, 9).

Tissue engineering is being explored as an alternative option for KOA treatment to generate replacement tissues that can offer longer-term solutions for individuals of all

ages. Various cells, materials, and biomechanical stimuli have been explored to enhance tissue formation and develop a tissue that reflects the meniscus's unique architecture and function. The use of mechanical stimulation in meniscus tissue engineering has shown some mixed results. Still, for the most part, it has led to tissues that more closely resemble the native meniscus. Understanding exactly how cells function and respond to mechanical stimulation in bioengineered meniscus constructs is essential as it may allow us to develop methods to amplify certain cellular events and enhance tissue development. This review summarizes recent findings over the last 10 years of the cellular responses to various mechanical stimuli used in meniscus tissue bioengineered. We hope this will bring light to specific cellular mechanisms that can be further investigated to gain better insight into the physiology of bioengineered meniscus tissues and lead to the development of clinically relevant tissues.

1.2 Meniscus form and function

1.2.1 Meniscus anatomy

Knee menisci are crescent-shaped fibrocartilaginous structures located on the medial and lateral aspects of the knee joint between the tibia plateau and corresponding femoral condyle (10). Each meniscus is attached to the underlying bone at the anterior and posterior horns by the enthesis, a complex gradient tissue composed of fibrocartilage near the meniscus attachment site that transitions to bone (11, 12). The enthesis is essential for mechanical fixation and load distribution throughout the meniscus (13). During early human development, the meniscus is fully vascularized at the time of formation until ~3 mo, when blood vessels begin to disappear from the inner region. By around 11 yr of age, the inner region of the meniscus is entirely avascular (14). This gradual elimination of blood supply from the inner region is suggested as the result of mechanical stimulation by increased keen joint motion and body weight (15).

In adults, the meniscus adopts a more heterogeneous, zonal-dependent structural organization that can be characterized into two regions based on morphology, biochemical composition, and access to blood supply (4, 16). The peripheral one-third of the meniscus (red zone) is vascularized with a thick and convex morphology. The inner

two-thirds of the meniscus (white zone) tapers to a thin free edge and is avascular in adults (17). The middle zone is then referred to as the red-white zone (18-20). Overall, the meniscus is a highly hydrated tissue composed of 72% water and 28% organic matter that is primarily different types of collagens and proteoglycans (21). However, its anisotropic structure leads to zonal variations in biochemical content. In the outer regions, type I collagen dominates over 80% of the total dry weight, and other types of collagens contribute less than 1%. In contrast, in the inner region, type II and type I collagens together account for 70% of the dry weight in an ~3:2 ratio (22-24). Proteoglycan content depositions are also higher in the inner regions and the horns of the meniscus (21, 25). This variation in biochemical composition results in circumferential rope-like collagen bundles in the outer regions, whereas the inner regions appear more like hyaline cartilage.

Aside from its regional-dependent matrix properties, a spectrum of different cell populations is also found in the human meniscus (Figure 1.1) (14). Although controversial terminologies have been used in the literature to define the cell types in the meniscus, it is commonly accepted that the cells can be categorized by their morphology and location in the meniscus (26). Cells on the superficial layer are found to be oval or fusiform in shape, whereas they are more rounded in deeper regions of the tissue (Figure 1.1) (27). Cell morphology also transitions from a fibroblast-like phenotype in the outer zone to a chondrocyte-like phenotype in the middle and inner zone (27, 28). Further investigations on meniscus cell types and their distributions via flow cytometry and single cell RNA sequencing have identified at least seven types of cells (29, 30). Among them, the heterogeneous population of cells responsible for the meniscus extracellular matrix synthesis are recognized as meniscus fibrochondrocytes (MFC) (3). Together these zonal differences observed at the cellular, protein, and structural level are evidence of unique functional properties, which may reflect a cellular adaptation to external stimuli.

1.2.2 The physio-mechano environment of the meniscus

In the adult meniscus, the fully developed geometry, anchoring, and zonal-dependent ultrastructure allow the tissue to adapt to different mechanical stresses during joint

loading. The meniscus is compressed by an axial tibiofemoral force through the joint motion from daily activities (Figure 1.1). Due to its wedge shape and the concave superior surface, the bulk compression force is converted to surface shear, vertical compression, and horizontal hoop forces (Figure 1.1) (31). The vertical compression force is concentrated in the inner region of the meniscus and is opposed by the tibial reaction force, whereas the horizontal hoop force is mainly distributed to the outer region and is balanced by the horn attachments. The horizontal hoop force is further converted into circumferential and radial tensile forces by the alignment of collagen fibers (Figure. 1.1) (11, 14). Given the meniscus's active role in experiencing mechanical stimulation, studies have quantitatively examined the mechanical properties of the human meniscus. The ranges of compression resisting aggregate modulus, tension-resisting circumferential, and radial tensile moduli were determined to be 100– 150 kPa, 100–300 MPa, and 120 kPa, respectively (32, 33).

For MFC to adequately respond to these external forces and contribute to the zonal-dependent development of the tissue, they likely have molecular mechanisms that respond to these effects. The process by which cells sense and respond to mechanical stimuli is referred to as mechanotransduction. In the case of MFC, mechanical forces are converted into biological responses that alter the gene and subsequent protein expression of ECM proteins and remodeling enzymes, among others. In the next section, we will highlight the current knowledge on MFC mechanotransduction.

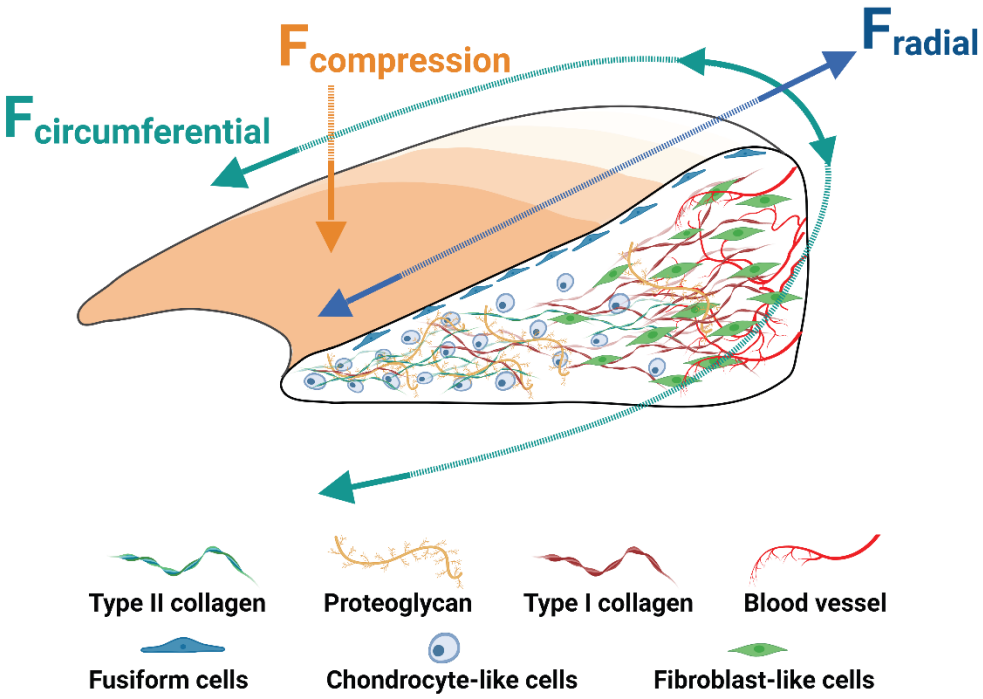

Figure 1.1 Simplified schematic of meniscus ultrastructure and force distribution during loading.

Cells in the meniscus are generally categorized based on three main phenotypes. The cells lining the surface of the meniscus are fusiform cells. In the inner region, cells show round chondrocyte-like morphology, and in the outer region, cells demonstrate elongated fibroblast-like morphology. Type II collagen and proteoglycans are mainly deposited by cells in the inner region. In the outer region, the primary component of ECM is type I collagen. During loading, the meniscus' inner region experiences mostly compression force, and the outer region is mainly subjected to tensile forces in both circumferential and radial directions. Created with BioRender. com. ECM, extracellular matrix.

1.2.3 Mechanotransduction in the meniscus

Currently, the knowledge of MFC mechanotransduction remains scarce. Various studies have looked at the role of different proteins, ion channels, and receptors, but there is a lack of consensus and a clear understanding of the precise mechanism of mechanotransduction in MFC (34-38). Analogous mechanisms found in knee articular chondrocytes (AC) have been proposed for MFC, such as those involving integrins and ion channels like transient receptor potential cation channel subfamily V member 4 (TRPV4), but evidential support is limited (35, 38). Integrins are cell-adhesion receptors that act as an interface between the extracellular and intracellular environment and play

an essential role in regulating cytoskeletal remodeling in response to mechanical cues in different cell types (39). TRPV4, on the other hand, is a nonselective cation channel that functions in calcium signaling and is known to enhance anabolic gene expressions, such as collagen type II and aggrecan expression in knee AC in response to physiological loading (40). It is thought that TRPV4 may similarly function in MFC by regulating calcium signaling of MFC in response to mechano-osmotic stimuli (35). PIEZO1 is another ion channel that has gained a lot of attention in knee AC, particularly for its proposed catabolic role in matrix metabolism (40). Activation of PIEZO1, which can be stimulated by injurious loading or inflammatory factors like interleukin-1, is thought to enhance the gene expression of matrix metalloproteinases and mediate cartilage deterioration (40). Currently, PIEZO1 has not been specifically investigated in MFC, but given its role in knee AC, it is quite likely that it may confer a similar function.

We have proposed the potential role of caveolae in MFC mechanotransduction based on recent findings in tissue engineered human meniscus (41). Caveolae are small plasma membrane invaginations of 60–80 nm in size known to function as Mechan transducers in cells frequently exposed to mechanical stress, such as cardiomyocytes, adipocytes, and vascular endothelial cells (42). The mechanotransducive mechanisms carried out by caveolae are largely similar across different cell types. In a low-tension state, caveolae can regulate the activity of different signaling pathways due to their association with several proteins, ion channels, and receptors (42, 43). On the other hand, exposure to high tension leads to caveolar flattening and disassociation of proteins like the EH domain containing 2 (EHD2) and cavin-1 that can translocate to the nucleus and influence gene expression (41, 42). Mechanical stimulation of the meniscus likely causes localized tension and compressive forces in the cellular microenvironment that may trigger caveolae on the cell membranes and lead to a biological response. However, further research is required to better understand this mechanism and meniscus mechanobiology overall.

1.3 Mechanical stimulation of engineered meniscus

Many different modalities of mechanical stimulation have been applied to tissue-engineered meniscus constructs to mimic what the native meniscus and resident cells experience in physiological conditions. These loading types have also been combined with other relevant variables such as cell type, biochemical cues, biomaterials for the matrix microenvironment, and oxygen conditions to determine the optimal culture strategy for engineering biomechanically functional tissue constructs. This section aims to highlight key findings from studies utilizing different types of mechanical stimulation and in combination with other culture variables. Table 1.1 summarizes the studies that were investigated for this review.

Table 1. 1 Summary of studies using mechanical stimulation on engineered meniscus models in the last 10 years.

Loading type	Reference	Cell type	Scaffold material	Loading regime			Other variables	Conclusion
				Duration	Amplitude	Frequency		
Mechanical Boundary Constraints	(44)	Mouse ESC	Bovine Type I collagen	11 days	N/A	N/A		↑Cell mediated gel contraction (vertical to constraint direction) ↑ *OSX* expression ↑Deposition of aligned collagen Presence of cartilage nodules
	(45)	Bovine MFC	Rat Tail Type I collagen	8 weeks	N/A	N/A	Collagen gel concentration	Maintenance of size and shape Formation of anisotropic fiber ↑ Collagen accumulation ↑ Mechanical property and development of anisotropic tensile properties
	(46)	Bovine MFC	Rat Tail Type I collagen	4 weeks	N/A	N/A		Maintenance of size and shape Development of aligned fibers ↑ Mechanical property over culture time
	(47)	Bovine MFC	Rat Tail Type I collagen	4 weeks	N/A	N/A		Maintenance of size and shape Formation of aligned collagen fiber ↑ Mechanical property over culture time
	(48)	Bovine MFC	Rat Tail Type I collagen	30 days	N/A	N/A	Glucose and TGF-β1 supplement	Does-dependent effect of TGF-β1 on collagen fiber organization Synergistic effect of mechanical anchoring and TGF-β1 on collagen fiber formation ↑ Mechanical property
Static Tension	(49)	Bovine MFC	PCL nanofibers/silicon membrane	15 minutes	3 %, 6 %, and 9% strain	0.05% strain/s		Considerable difference of Ca^{2+} regulation between native and engineered meniscus ↑ Number of cells respond to tension with increasing strain level
Dynamic Tension	(44)	Mouse ESC	Bovine Type I collagen	4 hours	3 % and 6 % strain	0.5 Hz		↑ *YAP1, WWTR1, TRPV4, MRTFO* expression by 6% strain loading No effect by 3% strain loading
	(50)	Human ASC	PDMS membrane	Up to 6 hours	5 %, 10 %, 15 %, 20 %, and 25 % strain	0.5 Hz, 1 Hz, and 1.5 Hz	FBS, ITS+, ASP, DEX, TGF-β3 supplement	Optimal effect for fibrogenic differentiation by 10% strain at 1Hz for 3 hours in chondrogenic medium

Table 1.1 — Continued

Dynamic Compression	(51)	Human BMSC	PU	2 weeks, 8h/day	0-10% strain	0.5 Hz	Perfusion	Perfusion and on-ff cyclic compression showed pro-chondrogenic effect ↑ Mechanical property ↑ Type I procollagen production
	(52)	Human BMSC	Bovine Type I collagen	2 weeks, 8h/day	0-10% strain	0.5 Hz	Perfusion	↑ Cell proliferation ↑ Type I and III procollagen production ↑ Mechanical property
	(53)	Porcine MFC	PCL base with agarose or GelMA	4 weeks, 1h/day	0-10% strain	1 Hz	TGF-β1 supplement	Maintenance of cell viability ↑ Mechanical property ↑ GAG production by agarose impregnation ↑ Collagen production by GelMA impregnation
	(54)	Human MFC	Bovine Type I collagen	3 weeks, 4h/day	30-40% strain	1 Hz	Oxygen Tension, pre-culture duration	Additive effect of dynamic compression and low oxygen tension Dose-dependent response of gene expression by dynamic compression ↑ Mechanical property ↓ *COL10A1* expression
	(55)	Human MFC	Bovine Type I collagen	5 minutes	30-40% strain	1 Hz	Oxygen Tension	Induction of an inflammatory matrix remodeling response ↑ *SOX9* and *COL1A1* expression
	(56)	Human MFC	Bovine Type I collagen	2 weeks, 1h/day	0-10% strain	1 Hz	Oxygen Tension, TGF-β3 supplement	↑ Mechanical property Necessary role of TGF- β3 for meniscus-like ECM formation No significant effect on mRNA markers for fibrocartilage formation
	(57)	Huma AC and BMSC	Type I/III collagen	3 hours, 10 min on/off	0-25% strain	1 Hz	Osteoarthritis	↑ Mechanical property ↑ *COL10A1, MEF2C, ALPL*, and *IBSP* expression level in OA derived group ↓ *COL2A1* expression in OA derived group

Table 1.1 — Continued

Dynamic Hydrostatic Pressure	(58)	Rabbit CPC, CC, FPSC	Alginate	4 weeks, 4h/day	0-5 MPa	0.5 Hz	Cell type	↑ Migration and proliferation of FPSCs and CPCs to different extents ↑ Production of ECM components ↑ Expression of chondrogenic genes More prominent effect in CPCs
	(59)	Human ASC	N/A (pellet)	2 weeks, 4h/day	7.5 MPa	1 Hz		↑ *SOX9, COL2A1,* and *ACAN* expression ↑ GAG production ↑ Vimentin production and organization
	(60)	Human MFC	N/A (pellet)	1 weeks, 4h/day	0.55-5.03 MPa	1 Hz	Cell source	Maintenance of size ↑ Chondrogenesis Earlier onset of chondrogenesis by cells from outer zone
	(55)	Human MFC	Bovine Type I collagen	5 days, 1h/day	0.5 MPa	1 Hz	Oxygen Tension	↑ *c-FOS* and *SOX9* expression level
	(61)	Human MFC	Bovine Type I collagen	3 weeks, 1h/day	0.9 MPa	1 Hz	Donor sex	↑ *ACAN* and *COL2A1* expression level ↓ *COL10A1* expression level ↑ GAG/DNA ratio Regulation of OA-related pathways Noticeable sex-dependent differences
Physiological Loading	(53)	Porcine MFC	PCL base with agarose and GelMA	4 weeks	0-10% strain	1 Hz	TGF-β1 supplement	↑ Ratio of type II collagen in agarose-impregnated inner region ↑ Ratio of type I collagen in GelMA-impregnated outer region
	(46)	Bovine MFC	Rat Tail Type I collagen	4 weeks, 2h/day	5% and 10% strain	1 Hz		↑ GAG production ↑ Collagen accumulation ↑ Mechanical property Development of heterogenous ECM organization like native tissue
	(62)	Bovine MFC	Alginate	Up to 4 weeks, 2h/day	15% strain	1 Hz	Post-culture duration	↑ Mechanical property ↑ Matrix formation Loss of ECM in the medium with prolonged post-culture duration
	(63)	Rabbit BMSC	PCL	2 weeks, 1h/day	10% strain	1 Hz	CTGF and TGF-β1 supplement	Formation of a physiological anisotropic profile with zonal, layer-specific expression of type I and II collagen Long-term chondro-protection of knee joint *in vivo*

Table 1.1 — Continued

Simulated Microgravity	(59)	Human ASC	N/A (pellet)	2 weeks	N/A	11 rpm		↓ Deposition of GAG and type II collagen ↓ *COL2A1* and *COL10A1* expression
	(64)	Human BMSC	N/A (pellet)	3 weeks	N/A	4.2-7.2 rpm		Alteration of Wnt-signaling pathway towards the direction of decreasing chondrogenesis
	(65)	Human MFC and ASC	Bovine Type I collagen	3 weeks	N/A	20-30 rpm	Cell interaction	↑ Cartilaginous matrix formation in coculture of MFC and ASC ↑ *COL10A1* and *MMP-13* expression ↓ *GERM1* expression
	(61)	Human MFC	Bovine Type I collagen	3 weeks	N/A	30-40 rpm	Donor sex	↓ *ACAN* and *COL2A1* expression Modulation of OA-related pathways Demonstration of sex-related differences

Studies were identified by performing a systematic search of the literature. Cochrane Library, EMBASE, MEDLINE, and Scopus were the databases from which records were retrieved and analyzed. A detailed flowchart outlining the strategy and search parameters is presented in the Supplementary Figure. 1.1. AC, articular chondrocytes; ASC, adipose-derived stem cells; ASP, ascorbic acid; BMSC, bone marrow derived stromal cells; CC, chondrocytes; CPC, cartilage progenitor cells; CTGF, connective tissue growth factor; DEX, dexamethasone; ESC, embryonic stem cells; FBS, fetal bovine serum; FPSC, fat pad-derived stem cells; ITS+, insulin; MFC, meniscus fibrochondrocytes; PCL, Poly(ε-caprolactone); PDMS, polydimethylsiloxane; PU, polyurethane; TGF-β1, transforming growth factor-beta1; TGF-β3, transforming growth factor-beta 3.

1.3.1 Mechanical boundary constraints

Mechanical boundary constraints have been established as a relatively simple form of mechanical stimulation to guide the formation of ECM structures by acting against the contraction forces in engineered constructs (66-68). Mechanical boundary constraints are achieved by anchoring the implants at the horns or two ends (45-48). The main objective of applying mechanical boundary constraints is to guide the formation of native tissue-like anisotropic collagen fibers. Several studies have used engineered meniscus with bovine MFC and type I collagen scaffolds (45-48). Parameters such as mechanical stimulation duration, initial collagen gel concentration, and culture medium supplement (glucose and transforming growth factor-beta 1 (TGF-β1)) were manipulated, and the resulting collagen fiber alignment was examined. In addition, the effect of anchoring on tissue biochemical composition and mechanical properties was also investigated.

Gross inspection of constructs showed that mechanical anchoring was very effective at maintaining the size and shape of engineered meniscus constructs (45-48). The morphology of anchored constructs was comparable to the original shape throughout the culture period (45-47), whereas the unclamped groups reduced the area to 40% by 8 wk (45). The initial concentration of collagen gel (10 or 20 mg/mL) did not affect contraction, but lower concentrations (10 mg/mL) led to a 20% loss at 8 wk (45). In terms of collagen alignment, unorganized constructs at baseline experienced varying degrees of alignment as early as 2 wk from anchoring. By 4 wk, collagen alignment was observed throughout the entire tissue construct (45, 46) in the anchored group, and a native tissue-like, region-dependent circumferential and radial alignment pattern were achieved by 8 wk (45). The organization of the unclamped group was improved slightly, but no region-dependent alignment was observed (45, 46). One study also applied mechanical anchorage to engineer the meniscal enthesis and regulate the bone-collagen interface organization (47). Mechanical fixation at the bony ends induced tissue integration of collagen fibers into the decellularized bony tissue (47). Another study with differentiated mouse embryonic stem cells (ESC) embedded in bovine type I collagen also showed that deposited collagen fibers aligned along the direction of anchorage (44).

The effect of mechanical anchoring on biochemical synthesis appeared opposite to that of collagen fiber alignment. Compared with the unclamped group, anchoring led to a significant decrease in total glycosaminoglycan (GAG) content in the meniscus constructs at the end of 8 wk of culture (45). To better understand the negative correlation between GAG deposition and collagen fiber alignment, the same research group utilized a gradient of biochemical factors and mechanical anchoring to study the interaction between biochemical and biomechanical stimulation (48). Their results show that the influence of the TGF-β1 growth factor is more prominent under a less proteoglycan-synthesis-promoting environment (500 mg/L compared with 4,500mg/L glucose), and the optimal fiber formation is achieved at an intermediate concentration of TGF-β1 (0.5 ng/mL) with mechanical anchoring (48).

It has been well established that the anisotropic ultrastructure is the foundation of the highly adapted mechanical property of meniscus (27). Constructs under mechanical anchorage demonstrated a gradual increase of equilibrium and tensile modulus (45, 46, 48). By the time of 8 wk, the anchored constructs developed an equilibrium modulus that is close to native meniscus tissue. However, even though the tensile modulus in the clamped group was about two times greater than the unclamped group, the values remained several orders of magnitude smaller when compared with the tensile modulus of native tissue (11, 32). This suggests that static boundary constraints as a form of mechanical stimulation are not enough to achieve native tissue-level mechanical capacity in engineered tissue constructs.

1.3.2 Static and dynamic tension

The unique shape and ultrastructure of the meniscus allow the tissue to convert axial compression primarily experienced by the inner region into circumferential and radial tension in the outer region (11, 14, 69). These tensile forces help guide the alignment of collagen fibers and regulate the phenotype of local cells (70). Therefore, both static and dynamic tension are relevant forces experienced by the meniscus. Many studies that apply tensile mechanical stimulation to engineered constructs focus on optimizing the loading regime to produce anabolic outcomes in ECM production and understanding the mechanotransductive mechanism at the cellular and molecular level (44, 49, 50). To

systematically define the optimal tensile loading regime for promoting the native meniscus tissue-like phenotype formation, a combination of ranges of loading duration (up to 6 h), strain amplitude (5%–25%), and loading frequency (0.5–1.5 Hz) was applied to human adipose-derived stromal cells (ASC) on polydimethylsiloxane (PDMS) membrane (50). Gene expression measurements showed that select chondrogenic markers responded uniquely to each combination of loading parameters; the combination of 3 h of tensile loading at 10% strain and 1 Hz frequency proved most effective in promoting the expression of the chondrogenic markers. Noticeably, cells survived most strain levels for 6 h except for 25% strain, at which cell necrosis and death were observed with staining analysis (50).

As a ubiquitous secondary messenger in downstream signaling pathways, calcium (Ca^{2+}) channel activation has been shown to respond to various types of loading (34, 35, 71, 72). In the context of meniscus tissue engineering, understanding the specific Ca^{2+} response to mechanical stimulation is essential for optimizing loading regimes for anabolic outcomes. Since the Ca^{2+} response is highly dependent on the cell-matrix interaction, a study was designed to compare the tension-induced Ca^{2+} signaling in MFC embedded in different matrix microenvironments (49). The Ca^{2+} responding profile in native tissue was considerably different compared with cells embedded in polycaprolactone (PCL) nanofibers or silicone membranes (49). Interestingly, the level of the applied tensile strains did not affect the responding profile of single cells but affected the fraction of cells that showed Ca^{2+} channel activation. For the PCL and silicone group, the fraction of Ca^{2+} activated cells plateaued between 6% and 9% strain, whereas native tissues showed no saturation (49). Other well-studied mechanotransduction markers *YAP1*, *WWRT1*, *TRPV4*, and *MRTFA* were also activated by the 6% dynamic tensile strain on a tissue engineering model using bovine type I collagen as the matrix microenvironment (44).

1.3.3 Dynamic compression

Dynamic compression has been one of the most utilized loading modalities in cartilage and meniscus engineering due to its high physiological relevance (51-57, 73). Several loading regimes have been applied to a wide variety of tissue-engineered constructs with different combinations of cells and biomaterials as the matrix microenvironment (74).

The main goal of applying dynamic compression to engineered meniscus models is to understand the mechanobiology of the meniscus and promote more native tissue like phenotypes in engineered constructs. Efforts have also been devoted to studying the interaction of mechanical loading with other relevant stimulations such as oxygen tension (54-56), perfusion (51, 52), and biochemical cues (53). In addition, dynamic compression has also been used to understand the alteration of cartilage cell mechanobiology affected by osteoarthritis (OA; (57)).

Like many of the other loading modalities, the outcome of dynamic compression stimulation on engineered meniscus constructs is heavily influenced by the loading regime. It is critical to identify optimal loading parameters, as inappropriate loading regimes can result in undesirable outcomes (75). In engineered human meniscus models with MFC embedded in bovine type I collagen scaffolds, loading duration ranging from 15 min to 3 wk have been studied in combination with strain levels ranging from10% to 40%, and the outcomes were assessed in terms of ECM composition, modulation of selected chondrogenic markers, alteration of the global transcriptome profile, and the influence on mechanical properties (54-56). For the same loading duration, the stress response to 30%–40% strain was approximately five times greater than from 10% to 20% strain. The modulation of the mechano-sensitive gene *c-FOS*, chondrogenic marker *SOX9*, and the oxygen stress-sensitive gene *PTGS2* also showed a dose-dependent response to strain levels with 30%–40% inducing significantly higher expression of all three markers (54). Based on these results, dynamic compression at 30%–40% strain levels seemed to be the more effective regime for the specific tissue engineering model (54). When comparing the effect of loading duration (single incident of 5 min vs. regular incidents over 5 days) at a 30%– 40% strain level, the RNA sequencing data of the global transcriptome profile showed that genes regulating the expression of molecules involved in early mechanotransduction pathways were among the highest regulated genes in both the short- and long-term loading studies. Interestingly, inflammatory-related genes and signaling pathways were also regulated in both loading durations (54, 55). When proceeding to longer-term loading (regular incidents over 3 wk), the dynamic modulus showed a sigmoidal growth curve with no plateau observed. In contrast, hypertrophic markers *COL10A1* and *MMP13* were found to be highly suppressed (54). Collectively,

these findings suggest that the magnitude of gene responses to dynamic compression is closely related to the aggression of loading, and an extended loading period under optimal loading regimes can lead to superior mechanical property development in the engineered meniscus. In another human-engineered meniscus model using human bone mesenchymal stromal cells (BMSCs) and polyurethane (PU) based scaffolds, the regime of the individual loading incidents was studied (51). ECM composition and mechanical property assessments showed that for the same loading duration, on-off dynamic compression resulted in a higher equilibrium modulus and better ECM formation as compared with a single continuous loading regime (51).

In physiological conditions, the activity and synthesis of ECM by meniscus cells are regulated by a multitude of different factors, and mechanical stimulation often works synergistically with other factors such as oxygen tension and biochemical cues. Given the avascular nature of the inner meniscus in adults and the fact that the entire meniscus is embedded in the hypoxic (low oxygen tension) synovial fluid (76), oxygen tension is believed to be an essential regulatory factor of the meniscus phenotype (77-79). The effect of hypoxia (3% O2) alone and in combination with dynamic compression has been examined in engineered human meniscus models (54-56). In both short- and long-term (single incident of 5 min vs. regular incidents over 5 days) studies with a 30%–40% strain dynamic compression, a large panel of genes were regulated only by hypoxia, and an anabolic and anti-catabolic expression profile for hyaline cartilage was induced (54, 55). However, when hypoxia was applied together with a lower strain level (10%), no effect was observed in regulating the matrix-forming phenotype of cartilage (56). These results indicate a synergistic interaction between oxygen tension and dynamic compression in the engineered meniscus model.

As for the interaction between biochemical cues and dynamic compression, reported results are controversial. One study found that the supplementation of transforming growth factor-beta 3 (TGF-β3) was necessary for matrix formation regardless of loading (56), whereas another study suggested that the supplement of TGF-β1 had a negative effect on meniscus matrix formation in the presence of dynamic compression (53). Several reasons could potentially explain the opposing results. First, the cells and

biomaterial used in these two studies were different, and the effect of growth factors depends largely on the cell type and cell-matrix interaction (Table 1.1). Second, although TGF-β1 and -β3 share the same 70%–80% sequence identity and they both signal through the same receptor, different isoforms of the growth factor family have been suggested to have distinct biological effects (80). Third, the regimes of loading applied are different, and this may play a role in the interaction between biomechanical and biochemical cues. Another factor applied in combination with dynamic compression is perfusion of culture media (51, 52). Results from a study using human BMSC cultured on PU and bovine type I collagen scaffolds showed that perfusion promoted the development of meniscus phenotype and worked synergistically with dynamic compression (51, 52). Dynamic compression has also been applied to engineered meniscus models to study the mechanobiology involved in the physiological alteration of chondrocytes in OA. One study applied a single incident of 25% strain dynamic compression on tissue constructs derived from normal AC and BMSC of patients with OA and measured the differences in gene profile alteration. They concluded that tissues derived from osteoarthritic cells had lower tolerance to physiological loading, which was thought to be due to the NFκB-related pathways functioning differently in the diseased cells (57).

1.3.4 Dynamic hydrostatic pressure

Dynamic hydrostatic pressure is a modality of mechanical stimulation that partially mimics physiological loading patterns and can be recreated easily *in vitro* with specialized bioreactor systems (81). The reported effects of dynamic hydrostatic pressure on chondrogenesis were mostly positive in terms of ECM deposition (82-85). More specifically, a study investigated the effects of dynamic hydrostatic pressure on a rabbit-engineered-meniscus model using articular chondrocytes, cartilage progenitor cells (CPC), and fat pad derived stem cells (FPSC) to determine the optimal cell source in combination with this modality of mechanical stimulation (58). Analysis of cell migration, ECM deposition, and gene expression profiling revealed that dynamic hydrostatic pressure had a prechondrogenic effect on all three cell types, with CPC being the most effective cell source (58).

Another study using MFC in a human-engineered meniscus model demonstrated that even for the same cell type, MFC isolated from the inner and outer regions of the meniscus responded differently to dynamic hydrostatic pressure (60). MFC from the outer region responded in a timely manner, whereas MFC from the inner region showed a delayed response. Further, donor sex also played a role in the response of the inner region MFC (60). A sex-dependent response to dynamic hydrostatic pressure was observed at both the transcriptome and tissue matrix level in engineered meniscus models using male and female tissue-derived cells (61).

1.3.5 Physiological loading

To achieve clinical use, tissue-engineered meniscus models need to maintain function in an anatomically representative loading environment which varies from primary compression in the inner zone to primary tension in the outer zone (69). Despite enormous efforts devoted to optimizing an individual type of mechanical stimulation, single modalities of loading thus far have not created a zonal variant tissue construct to match the structural and functional properties of the native meniscus. In addition, the biochemical composition, fiber alignment, and especially the mechanical properties of engineered constructs using single modality loading are inferior to those of native tissue. In this sense, a more integrative and physiologically representative loading regime was proposed to achieve an anisotropic biochemical and biomechanical profile of the engineered meniscus (46, 53, 62, 63). The distribution of physiological meniscus loading patterns is mainly achieved by matching the geometry of the tissue construct and loading platens. This can be achieved using several bio fabrication techniques. One group used three dimensional (3D) printing with PCL to generate a wedge shaped ring construct with desired dimensions, and the loading platen was also specially designed to match the shape of the printed construct to apply a physiological distribution pattern of loading (53, 63). Another group used injection moulding to create anatomically shaped meniscus models with selected materials, and the loading platen was fabricated from magnetic resonance imaging (MRI) data of the matching condyle shape (46, 62). Computational simulations were also conducted to validate the physiological pattern of the proposed loading system (46, 63). To further improve the anisotropic development of engineered

constructs, one study used different materials on top of a PCL base (53). Chondrogenic phenotype-driving material agarose was impregnated in the inner region of printed constructs, and the fibrogenic phenotype-driving material gelatin methacryloyl (GelMA) was impregnated in the outer region (86, 87).

The regional anisotropy evaluation of 3D printed, and injection molded constructs showed promising outcomes. On the transcription level, the inner and outer regions of the engineered meniscus showed significantly different profiles. The expression of fibrogenic genes (*COL1A2*, *FN1*, and *TNC*) was significantly higher in the outer region, whereas the inner region showed higher expression of chondrogenic markers (*COL2A1*, *ACAN*, and *SOX9*; (53)). The gene-level observation also correlated positively with protein level deposition, where a higher amount of type I collagen was detected in the outer region, and more type II collagen and GAG were deposited in the inner region (53, 63). In addition to the regional-dependent deposition of ECM components, the organization of collagen fibers also showed patterns that resembled native meniscus. The fiber diameter increased up to fourfold at the end of 4 wk of physiological loading and formed circumferentially and radially aligned morphologies that resemble the native tissue (46). Besides achieving heterogeneity at the cellular and ECM level, recapitulating the anisotropic biomechanical properties is even more critical for the long-term application. The physiological loading was able to improve the overall tensile and equilibrium modulus of tissue constructs by 10-fold larger as compared with baseline values. Further, the anisotropic characteristics of the tensile modulus were reported to develop as early as 2 wk when comparing the circumferential and radial directions (46). Although the mechanical properties were still inferior to native tissue from *in vitro* physiological loading (46, 63), 24 wk of *in vivo* implantation in rabbits increased tensile and aggregate moduli to values that are comparable to native menisci (63). In addition, the gross and microscopic assessment of the whole joint after the implantation period showed that the engineered meniscus had a chondroprotective effect.

1.4 Simulated microgravity

The effects of mechanical loading and the crucial role of loading regimes have been well demonstrated by the aforementioned studies (Table 1.1). As a highly mechanosensitive

tissue, the response of the meniscus to mechanical stimuli is also reflected with mechanical unloading. One way to achieve mechanical unloading is by microgravity, where the forces of gravity are minimized. With space flights gaining more relevance as more long-term missions are underway (88), it is crucial to understand the impact of low gravity on the physiology of the neuroendocrine system (89), immune system (90), and musculoskeletal system (91, 92).

There are three primary methods to achieve microgravity to investigate the effects of mechanical unloading on cartilage- related tissues, spaceflight, parabolic flight, and simulated microgravity (SMG) using bioreactors (93). First, experiments can be conducted on the International Space Station (ISS), wherein real microgravity is experienced and is the optimal platform for long-term microgravity exposure. Second, short-term real microgravity can be achieved through parabolic flight maneuvers on aircraft such as the Airbus A300 Zero-G. However, due to the cost and limited accessibility, parabolic flight experiments are likely not feasible for large-scale applications. Third, simulated microgravity (SMG) can be achieved by using specialized bioreactors in ground-based facilities. Current methods to generate SMG include the random positioning machine (RPM), fast-rotating clinostats, and the rotating wall vessel (RWV) bioreactor (94, 95). Although SMG cannot account for external influences presented during spaceflight, it compensates for the effect of gravity and prevents sedimentation (93), therefore providing an accessible and practical platform to study cartilage-related tissue under unloading conditions in low gravity.

The reported effects of SMG on cartilage-related tissues are controversial (91, 92, 96, 97). Beneficial results were observed when applying SMG to articular chondrocytes cultured in monolayer where newly divided cells went into suspension, aggregated to cell clusters, and preserved their phenotype (96). A higher collagen II/collagen I expression ratio was also observed in chondrocytes cultured in the ISS as compared with those cultured under normal gravity (91). However, when applied to native and engineered cartilage tissues, SMG showed more adverse effects. Mice intervertebral disks cultured under an SMG environment showed a reduction in total GAG amount and upregulation of OA-related genes (92). Articular cartilage also showed a reduction of thickness and

increased ultrasound roughness, which are characteristics of cartilage degradation and damage (97).

For engineered human meniscus models exposed to SMG, some prochondrogenic effects have been observed (64, 65). This was, however, at the cost of significant upregulation of OA-related genes like *COL10A1* and *MMP13* as well as OA modulated pathways such as Wnt signaling (59, 65). Moreover, the osteoarthritis-driving effect of SMG showed a cell interaction (65) and biological sex-dependent differences (61). When taken together, SMG appeared to induce OA-like pathological development in cartilage-related tissues and could perhaps serve as an *in vitro* platform to study the molecular mechanisms of OA.

1.5 Conclusion

Mechanical stimulation plays a crucial role in the development and maintenance of meniscus tissue. With the advancement of meniscus tissue engineering, many different types of mechanical stimulation have been applied to engineer meniscus constructs from the combination of a variety of cell types and biomaterials. Mechanical loading, in general, promoted the development of fibrocartilage-like phenotype at both molecular and tissue levels. The regime of each loading type needs to be carefully designed to achieve optimal effect, and the interaction with other factors, such as biochemical stimulation, oxygen tension, and pre-and post- culture duration, need to be considered. In addition, what cell type or combination of cell types is most suited for the bioengineering of the meniscus and how the optimal cells will recapitulate the architecture of functional ECM of the meniscus are perhaps one of the most outstanding questions. SMG is an emerging area in meniscus tissue engineering, where the mechanical unloading microenvironment could be used as a platform to induce OA-like changes in engineered tissue models. Knowledge about the effect of various types of mechanical stimulation on engineered meniscus could potentially lead to the definition of the optimal loading regimes. With this, a combinatory approach where optimal loading regimes are used in conjunction with other treatments such as biochemical cues, bioinductive scaffold materials, and oxygen tension is promising for engineering clinically applicable meniscus tissues.

1.6 Supplemental data

Supplementary Figure 1.1. PRISMA flowchart of documents retrieved by literature search. Of the total 473 documents retrieved, 451 were excluded as they were unrelated to the scope of this review.

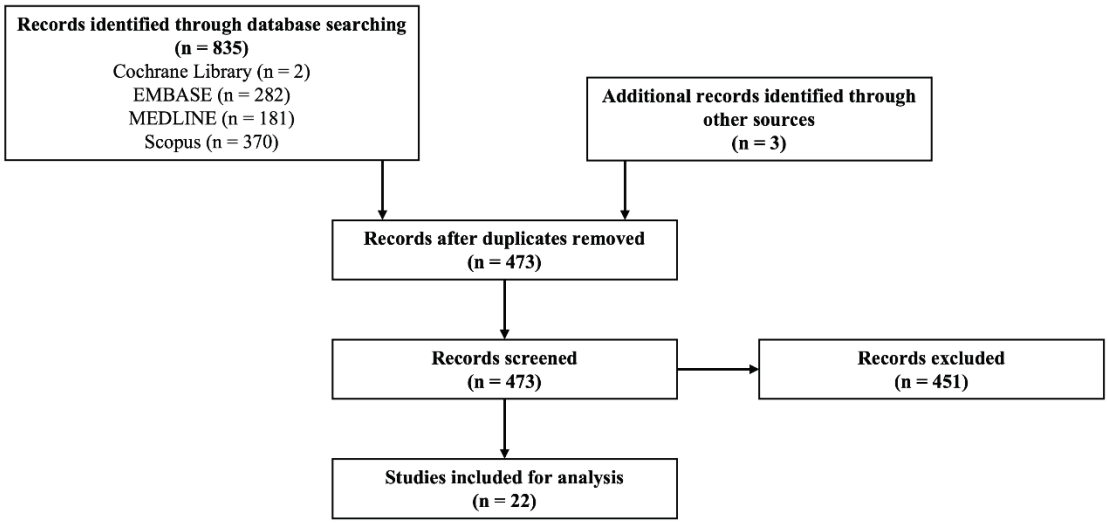

An advanced literature search was conducted on April 03, 2022 and re-run July 08, 2022 and included works published in the last 10 years (2012-current) that were in English. Search terms were divided into 3 sets and were mapped to subject headings if available. '*' was used for truncations to broaden the search.

Full search terms were: (bioengineer* OR tissue-engineer* OR tissue engineer* OR engineer* OR bio engineer* OR bio-engineer* OR biological engineer*) AND (menisc* OR tibial menisc* OR knee menisc* OR knee articular cartilage) AND (cell mechanotransduc* OR cellular mechanotransduc* OR mechanosensory transduct* OR mechanic* OR mechanobiolo* OR mechanotransduc* OR signal transduc* OR mechanical signal transduc*).

1.7 Acknowledgement

Graphical abstract was created with BioRender.com.

This article is part of the special collection "Musculoskeletal Biology and Bioengineering." Frank Zaucke, PhD, Thomas Hawke, PhD, and Liliana Schaefer, MD, served as Guest Editors of this collection.

1.8 Grant

This work was supported by the Alberta Cancer Foundation Grant ACF-MIBRP 27128, Canada Foundation for Innovation Grant CFI 33786, Canadian Institutes of Health Research Grant CIHR MOP 125921, Natural Sciences and Engineering Research Council of Canada Alexander Graham Bell Scholarship-Master's Program, Natural Sciences and

Engineering Research Council of Canada Grant NSERC RGPIN-2018-06290, University Hospital Foundation Grants RES0028185 and RES0045921, University Hospital Foundation Cliff Lede Family Charitable Foundation Grant RES00045921, University of Alberta Pilot Seed Grant Program (UOFAB PSGP), Faculty of Graduate Studies and Research, University of Alberta (FGSR) Walter H Johns Graduate Fellowship, and University of Alberta Women and Children's Health Research Institute Innovation Grant UOFABWCHRIIG 3126.

1.9 Disclosure

No conflicts of interest, financial or otherwise, are declared by the authors.

Chapter 2

Short-term Response of Primary Human Meniscus Cells to Simulated Microgravity

This Chapter has been previously published as:

Ma Z, Li DX, Lan X, Bubelenyi A, Vyhlidal M, Kunze M, Sommerfeldt M, Adesida AB. Short-term response of primary human meniscus cells to simulated microgravity. *Cell Commun Signal*. 2024;22(1):342.

2.1 Introduction

Osteoarthritis (OA) is a degenerative disease that commonly affects mechanical load-bearing joints, with the highest prevalence in the knee. The most notable feature of knee osteoarthritis (KOA) is the atrophy of articular cartilage. However, damage and inflammation of tissues that support the knee, such as the meniscus, also contribute to the overall deterioration of the joint (98). The crucial role of the meniscus in the early onset of KOA was demonstrated by spatial biomechanical mapping of the human knee joint, which revealed that KOA altered the biomechanical properties of menisci before the articular cartilage (5). Despite the critical impact of the meniscus on the development of KOA, there is a notable gap in research focused on the cellular and molecular mechanisms of meniscus alteration in KOA. While most studies have concentrated on how traumatic meniscus injuries and tears initiate and progress OA in the knee (99-101), few have explored the underlying cellular and molecular dynamics. The prevalence and severity of KOA are disproportionally higher in females (102, 103). This discrepancy may be attributed to anatomical differences in the knee (103), as well as genetic factors and sex hormones (98, 104). However, no single factor can fully explain the observed sex difference in KOA. Furthermore, these factors exert their effects by modifying relevant molecules at the cellular level. Hence, it is imperative to understand the molecular and cellular differences to gain insight into the sex differences in KOA.

Research into OA and the differences between sexes is hindered by the shortcomings of existing *in vivo* and *in vitro* models (105, 106). These models struggle to accurately represent the complex and multifaceted nature of OA, especially its initiation and early progression mechanisms. While animal models shed light on OA's development and possible interventions, discrepancies in biomechanics, molecular pathways, and progression rates limit their applicability to human OA. *In vitro* studies, though useful for examining specific molecular phenomena, risk oversimplification and often involve cells that lose their original tissue-specific properties, moving away from an accurate portrayal of OA's biological and pathological dynamics in humans. This issue becomes even more pronounced when exploring sex differences, as variations in responses to OA development and treatments between male and female models mirror the differences seen in human OA prevalence and severity. Consequently, there is an urgent need for the development of more suitable models that can specifically address these sex differences, focusing on cellular signaling discrepancies. Mechanical stressors, including prior knee injuries, muscle weakness, joint misalignment, and obesity, are widely considered significant contributors to the development of KOA (102, 103, 107). This notion is supported by studies demonstrating that mechanical loading is essential for normal joint function, and prolonged mechanical unloading of joints can lead to degenerative changes resembling KOA (108, 109). The utilization of real and simulated microgravity (SMG) has become a prominent tool for studying the effects of mechanical unloading on cartilage tissue at both the cellular and tissue levels (97, 110, 111). In several studies, SMG was found to activate the Wnt-signaling pathway (110), leading to increased cartilage catabolism, reduced glycosaminoglycan (GAG) content, increased *MMP3* and *MMP13* expression, and an upregulation of cell apoptosis (61, 65, 92, 112). Although there are fewer investigations examining the effects of short-term microgravity culture compared to long-term culture, several studies using parabolic flight maneuvers demonstrated an acute adaptation of cellular activity to altered mechanical environments (113, 114), but further research is necessary to elucidate the underlying mechanisms that govern the response of primary cells that are devoid of *in vitro* expansion culture on traditional tissue culture plastic.

Considering the above, this study aims to create an *in vitro* model via tissue engineering by seeding primary human meniscus fibrochondrocytes from healthy females and males into porous collagen scaffolds to generate 3D meniscus models. To preserve the original phenotype of the isolated meniscus fibrochondrocytes, both the cell recovery period and the scaffold pre-culture time were minimized (26). These models were used to investigate OA-like phenotypes through global transcriptome analysis after 7 days in SMG conditions, and to determine if sex-specific expression patterns related to KOA under prolonged unloading are replicated under brief SMG conditions.

2.2 Methods

2.2.1 Ethical approval

The experimental protocols and tissue procurement procedures adhered to the ethical guidelines prescribed by the Biomedical Panel of the University of Alberta's Health Research Ethics Board (Study ID: Pro00018778).

2.2.2 Plate coating

T75 culture flasks (Sarstedt, Germany) was coated with native human-derived extracellular matrix (ECM) (HumaMatrix Coat, 1 mg/mL, Humabiologics Inc, AZ, USA). Specifically, this matrix was obtained from the human placenta donated by parents who have undergone a minimum of 36 weeks of gestation and whose babies were delivered by Caesarean section. The source materials for the ECM met all relevant industry standards, and the donors were screened and found negative for HIV-1, HIV-2, hepatitis B, hepatitis C, syphilis, and other infectious diseases. The ECM coating solution was prepared by diluting it to a concentration of 0.1 mg/mL in 10-20 mM hydrochloric acid solution with a pH range of 1.9-2.1. Subsequently, 125 $\mu L/cm^2$ of the ECM coating solution was evenly spread on the culture plate surface. The plate was then incubated at 37°C for 2 hours, excess solution was removed, and the coated surface was left to air-dry overnight without the lid in a cell culture hood. The residual acid was rinsed off the coated surface with sterile phosphate-buffered saline before use.

2.2.3 Human meniscus fibrochondrocytes (MFC) isolation and plating

MFC were isolated from fresh inner avascular meniscus specimens obtained from 3 male subjects (22, 27, and 32 years old) and 3 female subjects (24, 32, and 38 years old) who had undergone partial meniscectomy by a sports medicine orthopaedic surgeon for acute injury but with no history of osteoarthritis. The MFC were isolated by 22-hour digestion at 37°C using type II collagenase (0.15% w/v; 300 U/mg solid; Worthington, NJ, USA) in high glucose DMEM (4.5 mg/mL D-Glucose) supplemented with 5% v/v inactivated FBS (Sigma-Aldrich Co., MO, USA). Isolated primary cells were seeded at a density of 1×10^4 cells/cm^2 on the ECM-coated plate and cultured in a standard DMEM-complete medium containing high glucose DMEM supplemented with 10% v/v FBS (Sigma-Aldrich), 100 U/mL penicillin, 100 µg/mL streptomycin, 2 mM L-glutamine, and 10 mM HEPES (Sigma-Aldrich) under normal oxygen tension (~21% O2) at 37°C for 48 hours.

2.2.4 Scaffold seeding

After 48 hours of culture, adherent primary cells were detached using trypsin-EDTA (0.05% w/v) and seeded onto cylindrical type I collagen scaffolds (diameter = 4mm, height = 3.5mm, pore size = 115 ± 20µm, Integra Lifesciences, USA) (115) at a density of 5×10^6 /cm^3 (116) Cells from each donor were used to seed scaffolds and generate cell-seeded meniscus constructs independently. The cell-seeded scaffolds were then pre-cultured for 48 hours in serum-free standard chondrogenic medium (high glucose DMEM, HEPES (10 mM), penicillin-streptomycin-glutamine (PSG), dexamethasone (100 nM), ascorbic acid 2-phosphate (365 µg/mL), human serum albumin (125 µg/mL), 40 µg/mL L-proline (all from Sigma-Aldrich), and ITS+ premix (Corning, Discovery Labware, Inc., MA, USA)) supplemented with 10 ng/mL TGF-β3 (Proteintech Group, United States, #HZ-1090).

2.2.5 Mechanical stimulation

After 48 hours of pre-culture, the cell-seeded meniscus constructs were randomly allocated to static control and SMG group. The static control group was cultured in a non-adherent tissue culture well plate while the SMG group was cultured using a commercially available bioreactor (RCCS-4; Synthecon Inc., TX, USA). The rotation

speed of the bioreactor was adjusted to maintain the constructs in a free-falling position, with a speed of 30 rpm applied from day 1 to 2, and 34 rpm from day 3 to 7. During the 7-day experimental period, both the static and SMG groups were cultured in a serum-free chondrogenic medium, supplemented with TGF-β3 (same as pre-culture period), with the volume of culture medium per cell-seeded meniscus construct consistently maintained across both conditions. Samples were collected at day 0 (common control), and from both groups at day 1, day 3, and day 7 (n=2 for each time point).

2.2.6 RNA extraction and RT-qPCR

The constructs collected at each time point were immediately preserved in Trizol reagent (Life Technologies, United States) and stored at -80°C until RNA extraction. The PuroSPIN Total RNA Purification KIT (Luna Nanotech, Canada) was used for RNA extraction and purification according to the manufacturer's instructions. The extracted RNA underwent bulk RNA sequencing and reverse transcription-quantitative polymerase chain reaction (RT-qPCR). For RT-qPCR, a panel of selected chondrogenic (*ACAN, COL1A2, COL2A1,* and *SOX9*), OA-related (*COL10A1, IHH, MMP13,* and *SPP1*), as well as the mechano-transduction marker *TRPV4* was examined. The gene expression levels were normalized against the average of three reference genes (*ACTB, B2M,* and *YWHAZ*). The cycle threshold (CT) values of these housekeeping genes across all included donors under both static and SMG conditions is included in Supplementary Table 2.6.

2.2.7 Bioinformatics

The Biomedical Research Centre at the University of British Columbia used the Illumina NextSeq 500 platform for bulk RNA sequencing, generating 20 million paired end reads with a read length of 42 bp x 42 bp. RNA sequencing data was analyzed using Partek Flow software (Partek Inc, St. Louis, MO, USA). Raw input reads were trimmed and aligned to the reference human genome hg38 using the STAR 2.7.3a aligner. Genes with maximum read counts below 50 were filtered out, and normalization was performed using the Add 1.0, TMM, and Log 2.0 parameters. Statistical analysis was conducted using ANOVA with biological sex and time points as factors. Differentially expressed

genes (DEGs) were identified for each comparison by applying p-values, adjusted p-values (q-values), and fold change (FC) criteria. Partek was used for principal component analysis (PCA), Gene Ontology (GO) and KEGG pathway enrichment analyses, as well as visualization of DEGs using volcano plot and Venn diagrams. Hub protein networks were created for specific groups of DEGs using the Search Tool for the Retrieval of Interacting Genes/Proteins (STRING) online platform. A weighted protein network was constructed for a designated set of DEGs in which all potential protein-protein interactions had a confidence score greater than 0.4. Hub proteins were identified using the Kleinberg hub score metric, and the resulting hub protein network included directly connected proteins. Network visualizations were produced using Cytoscape.

2.2.8 Statistical analysis

Prism 9 (GraphPad) and Partek Flow software were utilized to conduct statistical analyses. For RT-qPCR results, statistical analysis employed to compare the expression level across all time points was repeated measures one-way ANOVA with Dunnett's multiple comparisons test. For RNA sequencing results, student t-test was employed to compare the expression level of two selected time points or between male and female groups. Multiple test correction FDR step-up (q-value) was performed on the p-values of each comparison.

2.3 Results

2.3.1 Dataset overview

In this study, RNA sequencing and RT-qPCR were used to analyze gene expression changes over a short-term culture in SMG with 6 donors (3 males and 3 females) and 4 time points per donor (Figure 2.1a). The RNA sequencing preprocessing pipeline retained 13,537 genes for downstream analysis. The quality assessments of extracted RNA were conducted before sequencing and after each step of preprocessing (Supplementary Table 2.1). The authenticity of the RNA sequencing data was verified by comparing it to RT-qPCR data, showing a high correlation (R^2 value of 0.9588) between the two transcriptomic techniques (Supplementary Figure 2.1).

2.3.2 Analysis of transcriptomic trajectory of meniscus constructs

In order to evaluate the alteration of transcriptome profile over time, PCA was employed to examine the temporal changes in the transcriptome profiles across all donors during SMG culture. PC1 and PC2 captured a temporal trajectory, with PC1 (24.01%) accounting for slightly more variation than PC2 (21.84%) (Figure 2.1b). SMG culture duration had little impact on gene expression until day 3, and by day 7, donors tended to converge towards a similar transcriptional pattern. Key contributors to the change in transcriptome trajectory were identified (Supplementary Table 2.2), including genes associated with inflammatory processes (*IL21R*, *ILF2*, and *TNFRSF11B*) and bone development (*BMP6* and *BMPR2*). DEG analysis was performed to identify genes that showed significant statistical differences ($|FC| \geq 2$ and q-value < 0.05) at each time point (Figure 2.1c). Comparison of the volcano plots over time revealed that the impact of SMG became more evident as the number of DEGs, and the extent of regulation considerably increased. The expression of several genes involved in early inflammatory processes (*CXCL* families), the NF-κB signaling pathway (*IL36RN*), and the matrix remodeling process (*ADAMTS6*) were consistently and significantly regulated during the SMG culture period (Figure 2.1c).

To further assess the impact of SMG culture duration on transcriptome profile alteration, the strength of correlation between the expression level changes of each gene and SMG culture time was determined. Among 13,537 genes, 5,064 genes showed a significant correlation with SMG culture duration (q-value ≤ 0.05), with 570 genes exhibiting a strong correlation ($|\text{partial correlation coefficient}| \geq 0.8$). Of these strongly correlated genes, 386 were positively correlated with SMG culture time while 184 were negatively correlated (Figure 2.1d) (Supplementary Table 2.3). The KEGG pathways (Supplementary Table 2.3) that were enriched by the group of genes that showed strong positive correlations include the glycosaminoglycan degradation pathway (*HEXA* and *HGSNAT*), the rheumatoid arthritis pathway (*CTSK* and *ATP6V* family), inflammation-related pathways (*GSK3B, NCK2, HRH1,* and *ITPR1*), Wnt signaling pathways (*APCDD1L, FZD1, GPC4, GSK3B,* and *MMP7*), hedgehog signaling pathway (*EVC* and *GSK3B*), and PPAR signaling pathways (*ACSL1, FABP4,* and *PLIN2*).

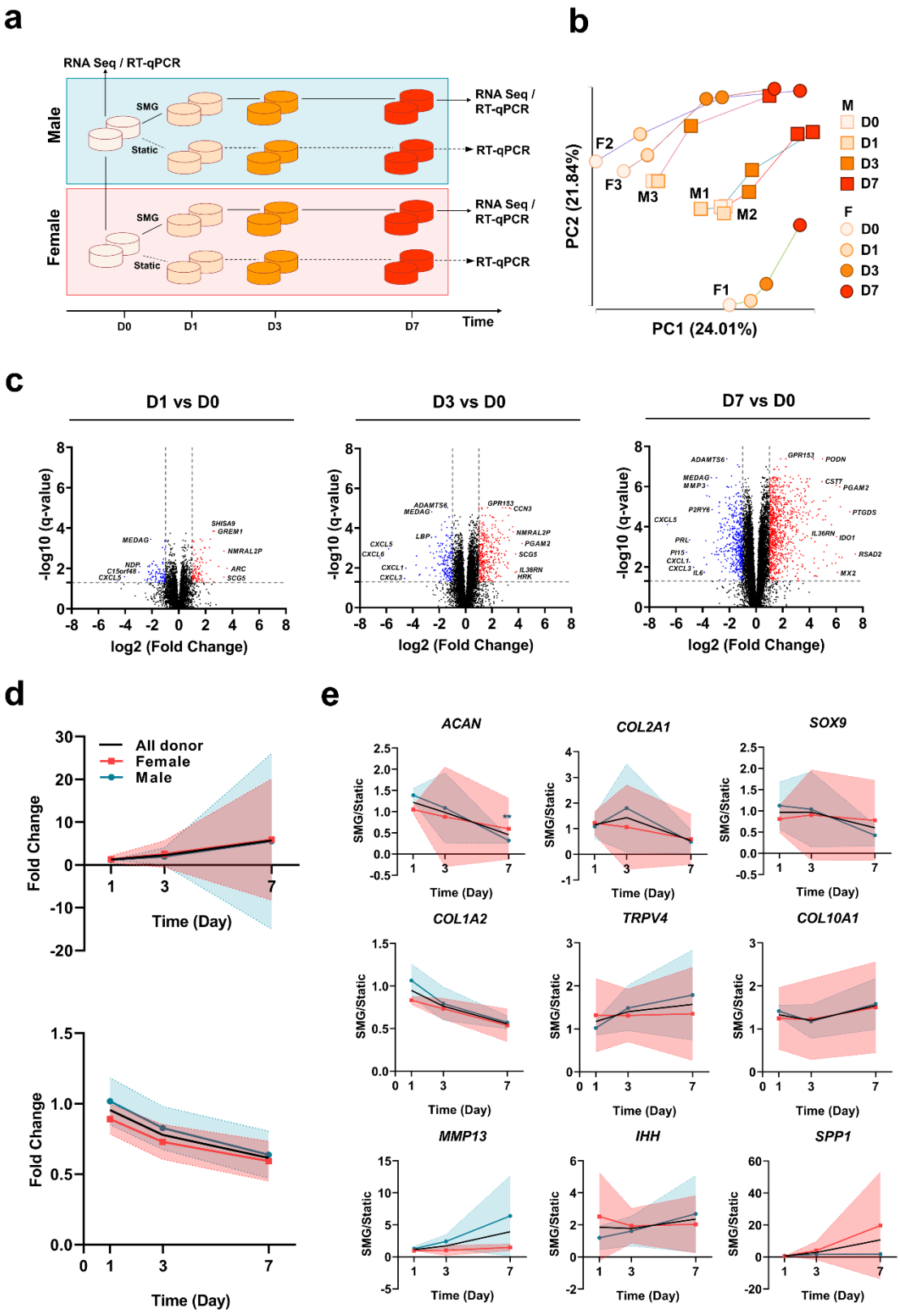
a
RNA Seq / RT-qPCR
Male
SMG
Static
RNA Seq / RT-qPCR
RT-qPCR
Female
SMG
Static
RNA Seq / RT-qPCR
RT-qPCR
D0
D1
D3
D7
Time
b
PC2 (21.84%)
PC1 (24.01%)
F2
F3
M3
M1
M2
F1
M
D0
D1
D3
D7
F
D0
D1
D3
D7
c
D1 vs D0
D3 vs D0
D7 vs D0
-log10 (q-value)
log2 (Fold Change)
SHISA9
GREM1
MEDAG
NMRAL2P
NDP
C15orf48
CXCL5
ARC
SCG5
ADAMTS6
MEDAG
GPR153
CCN3
NMRAL2P
PGAM2
SCG5
IL36RN
HRK
LBP
CXCL5
CXCL6
CXCL1
CXCL3
ADAMTS6
MEDAG
MMP3
GPR153
PODN
CST7
PGAM2
PTGDS
IL36RN
IDO1
RSAD2
MX2
P2RY6
CXCL5
PRL
PI15
CXCL1
CXCL3
IL6
d
All donor
Female
Male
Fold Change
Time (Day)
e
ACAN
COL2A1
SOX9
COL1A2
TRPV4
COL10A1
MMP13
IHH
SPP1
SMG/Static
Time (Day)

Figure 2.1 RNA sequencing and RT-qPCR-based transcriptome across all donors. a. Schematic for analyzing temporal trajectories of cell-seeded meniscus constructs, initiated from a static control. Samples were collected on day 0 under static control, as well as on day 1, 3, and 7 under SMG condition for RNA-seq analysis. For RT-qPCR analysis, samples were collected on day 0 under static control and on day 1, 3, and 7 for both SMG and static conditions. b. Principal component analysis (PCA) of temporal transcriptome trajectory for all donors (n = 6). The first two principal components (PC1 and PC2) were plotted, with male and female donors represented by different shapes (square for male and circle for female), and different time points represented by different colors. c. Volcano plot of the whole transcriptome on day 1, 3, and 7 compared to day zero for all donors. Upregulated DEGs (fold change ≥ 2, q-value ≤ 0.05) were labelled with red color and downregulated DEGs (fold change ≤ -2, q-value ≤ 0.05) were labelled with blue color. d. Characterization of the temporal expression trajectory of genes significantly correlated with SMG culture time (absolute partial correlation coefficient ≥ 0.8, q-value ≤ 0.05). To assess the temporal correlation, the expression level of each gene in the SMG group was compared at each time point with the expression level of the same gene on day 1 in the static group (fold change). The fold change in expression level was then compared to the trend of culture time to determine the temporal correlation of each gene. Top: positively correlated genes. Bottom: negatively correlated genes. Shaded area: Standard Deviation (SD) e. Characterization of the temporal expression trajectory of selected chondrogenic/OA-related signature genes. Data for females, males, and all donors combined were presented as mean values along with their corresponding standard deviations. Shaded area: Standard Deviation (SD). ** $p \leq 0.005$ compared to day 1.

2.3.3 Examination of early KOA onset mechanisms in the SMG model

Changes in chondrogenesis and OA-like phenotype were first confirmed using a panel of selected markers by RT-qPCR (Figure 2.1e). Chondrogenic markers (*ACAN, COL1A2, COL2A1,* and *SOX9*) initially comparable between groups decreased over time in the SMG culture, while OA-related markers (*IHH, MMP13, SPP1*, and *COL10A1*) increased. *TRPV4* was activated and upregulated in the SMG group, indicating mechanical stimulation responsiveness. Due to large donor variability, only the expression level of

ACAN was statistically significant at day 7; however, the general trend across all donors aligned with this pattern. DEGs from RNA sequencing were then compared between time points (Figure 2.2a), showing a substantial increase in the number of DEGs from day 1 to day 7. Some DEGs were consistently regulated throughout the culture period, suggesting that SMG consistently regulated a specific group of genes with an expanding effect over time.

Functional enrichment analysis was performed to explore the KEGG pathways and GO terms significantly enriched by all DEGs at each time point (Figure 2.2b, Supplementary Figure 2.2). The findings revealed a consistent overrepresentation of several GO terms, including "extracellular space and regions", "response to stimulus", and "signaling receptor binding". At later time points, additional functional terms such as matrix remodeling and immune system pathways were identified. For KEGG pathway analysis, significant enrichment was observed in pathways such as "calcium signaling pathway," "complement and coagulation cascades," "PPAR signaling pathway," and "rheumatoid arthritis," which could potentially play a crucial role in the early onset of KOA (Figure 2.2b).

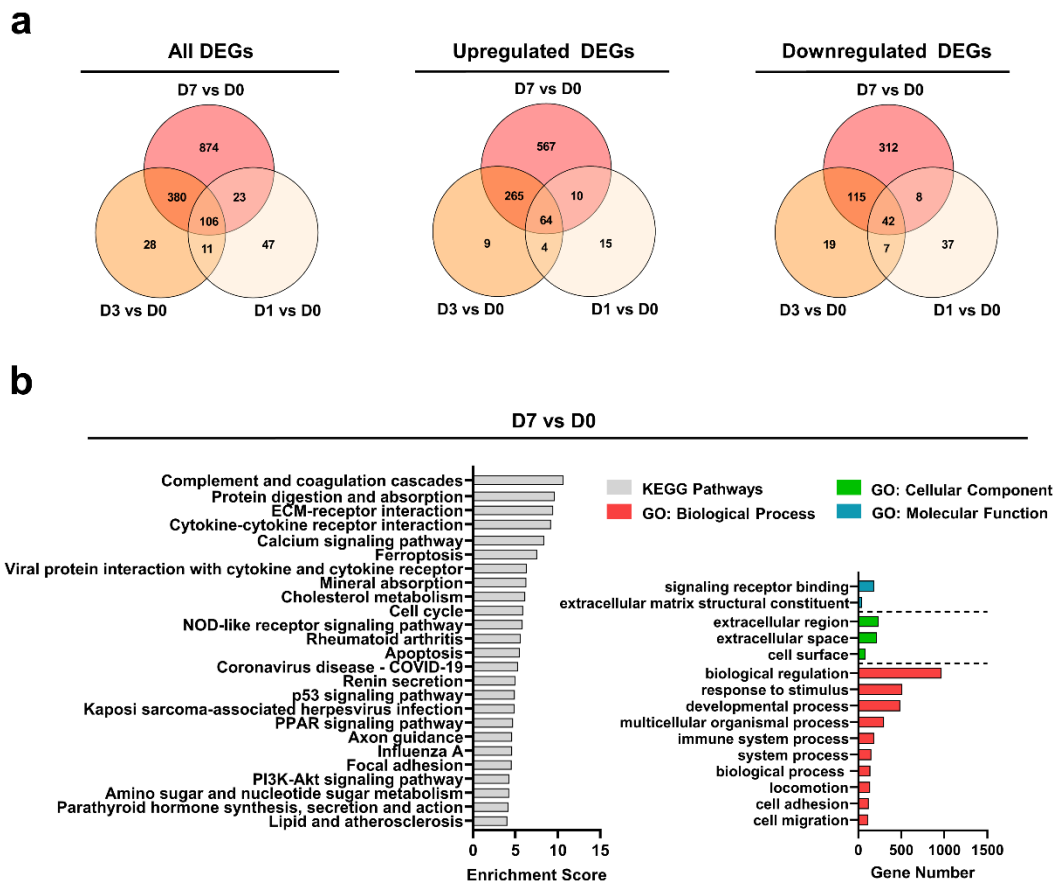

Figure 2.2 Functional enrichment of altered transcriptome induced by SMG across all donors.

a. Venn diagram of the comparison between all DEGs, upregulated DEGs, and downregulated DEGs in all donors (n = 6) across three time points. Each circle represents a distinct time point with the number of uniquely regulated genes indicated in the non-overlapping areas, while overlapping areas show the number of genes that are commonly regulated across multiple time points. b. Top non-redundant Gene Ontology (GO) terms and KEGG pathways enriched by all DEGs on day 7.

To elucidate the underlying molecular mechanism responsible for the OA-inducing effect of SMG, the hub protein networks were constructed for all DEGs at each time point (Supplementary Figure 2.3-2.5). The networks comprised 27, 86, and 111 genes on days 1, 3, and 7, respectively (Supplementary Table 2.4), with CCL2, IL6, and CDK1 serving

as the hub proteins. CCL2 and IL6 are known to participate in immunoregulatory and inflammatory processes, while CDK1 plays a critical role in cell cycle regulation. Notably, several proteases including the MMP family and ADAMTS5 were highly connected to the hub protein IL6 in the network (Supplementary Table 2.4). More than half of the top 25 KEGG pathways enriched by the panel of genes corresponding to the filtered protein network overlapped on day 1 and 3, including several pro-inflammatory signaling pathways and OA-related pathways, such as "IL-17 signaling pathway," "TNF signaling pathway," and "rheumatoid arthritis" (Supplementary Table 2.4).

2.3.4 Examination of sex-dependent responses to SMG

After establishing SMG's capability to generate an OA-like phenotype in cell-seeded meniscus construct models, the donors were stratified by sex. The models derived from male and female primary MFC were analyzed separately to investigate sex-specific responses to SMG and identify molecular mechanisms that may contribute to the disproportionate incidence and severity of OA in females.

DEGs were identified for male and female donors at each time point. SMG regulated 1,182 genes in female donors on day 7, while the number of DEGs increased gradually from 218 genes on day 1 to 1,216 genes on day 7 for male donors. Only a small proportion of DEGs were shared on day 3, while approximately half of the DEGs were the same on day 7 when comparing male and female donors at the same time points (Figure 2.3a). This trend was also observed when the up and downregulated DEGs were separated (Supplementary Figure 2.6). The results of the PCA analysis revealed a noticeable impact of SMG on the transcriptome profile over culture time for both male and female donors (Figure 2.3b). Key genes associated with OA development were among the most significantly regulated DEGs in female donors on day 7, such as *LOX* (-5.13-fold), *MMP3* (-17.37-fold), *MMP11* (74.71-fold), and *COL10A1* (29.53-fold) (Figure 2.3c).

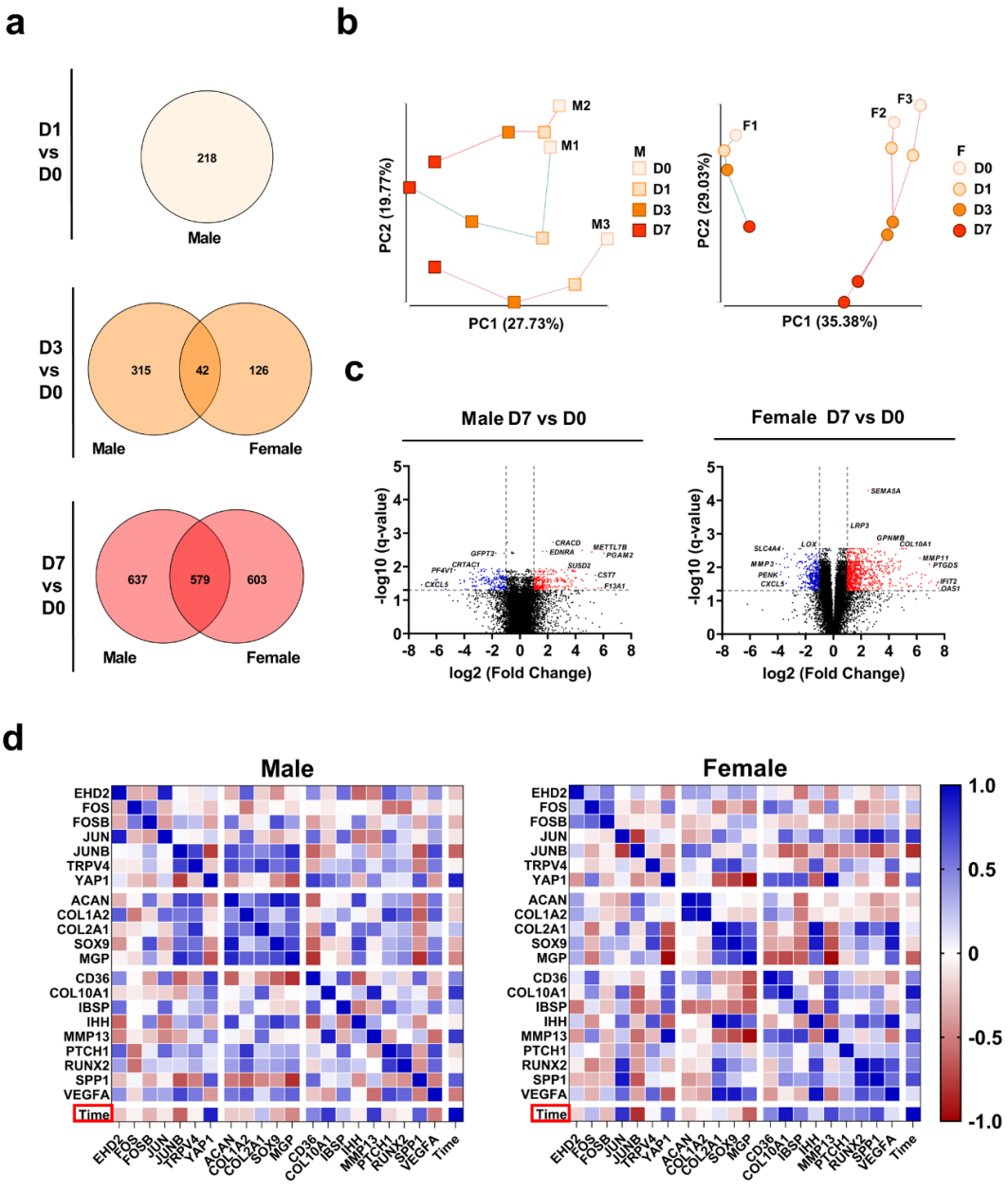

Figure 2.3 RNA sequencing based transcriptome profiling and trajectory analysis for male and female donors.

a. Venn diagram of the comparison between all DEGs regulated in male (n = 3) and female (n =3) donors across three time points. b. Principal component analysis (PCA) of temporal transcriptome trajectory for male and female donors. The first two principal components (PC1 and PC2) were plotted. c. Volcano plot of the whole transcriptome on

day 1, 3, and 7 compared to day 0 for male and female donors. Upregulated DEGs (fold change ≥ 2, q-value ≤ 0.05) were labelled with red color and downregulated DEGs (old change ≤ -2, q-value ≤ 0.05) were labelled with blue color. d. Pearson correlation heatmap of select markers and culture time for male and female donors. Heatmap was generated by calculating the pairwise Pearson correlation coefficient, with the color of each cell representing the corresponding coefficient value.

Correlation analysis was conducted to investigate the relationship between well-established cartilage and OA-related markers within male and female donor groups. Correlation heatmaps were created using selected signature markers divided into mechano-transduction (*EHD2, FOS, FOSB, JUN, JUNB, TRPV4,* and *YAP1*), chondrogenesis (*ACAN, COL1A2, COL2A, SOX9,* and *MGP*), and OA development (*CD36, COL10A1, IBSP, IHH, MMP13, PTCH1, RUNX2, SPP1,* and *VEGFA*) subcategories (Figure 2.3d). The expression levels of chondrogenic markers showed a negative correlation with SMG culture time in both male and female donors, while the correlation with OA markers was positive, especially for females. The correlation patterns of OA markers and chondrogenic markers differed for males and females, particularly with regards to *ACAN* and *COL1A2*, which exhibited opposing trends. These suggested the potential unique interaction mechanism between these markers within each sex group. Finally, among the chosen mechano-transduction markers, *JUN* and *JUNB* exhibited the most notable sex-specific differences in their correlation patterns with other markers.

Functional enrichment analysis showed that both male and female donors demonstrated comparable GO enrichment on day 3 and day 7, with general biological processes such as cell adhesion and migration, extracellular matrix components, and molecular function of signaling receptor binding being the primary terms. The KEGG pathway "mineral absorption" was enriched in both males and females on day 3 and day 7, along with several pathways related to the cell cycle and apoptosis. Inflammation and immune response were significant functional enrichments for male donors on both day 3 and day 7, but not for female donors (Figure 2.4a, Supplementary Figure 2.7).


a
Male D7 vs D0
Complement and coagulation cascades
Mineral absorption
ECM-receptor interaction
Axon guidance
Alcoholic liver disease
Protein digestion and absorption
Cytokine-cytokine receptor interaction
Calcium signaling pathway
Parathyroid hormone synthesis, secretion and action
Focal adhesion
Cholesterol metabolism
Amoebiasis
PI3K-Akt signaling pathway
Viral protein interaction with cytokine and cytokine receptor
Prostate cancer
Rheumatoid arthritis
Staphylococcus aureus infection
Hypertrophic cardiomyopathy
Arrhythmogenic right ventricular cardiomyopathy
PPAR signaling pathway
Ferroptosis
Phenylalanine metabolism
Basal cell carcinoma
Melanoma
TNF signaling pathway
0 5 10 15
Enrichment Score
KEGG Pathways
GO: Cellular Component
GO: Biological Process
GO: Molecular Function
signaling receptor activity
molecular transducer activity
sulfur compound binding
extracellular matrix structural constituent
extracellular matrix binding
extracellular region
extracellular space
cell junction
cell surface
collagen trimer
biological regulation
developmental process
response to stimulus
multicellular organismal process
system process
homeostatic process
locomotion
cell adhesion
cell migration
0 300 600 900
Gene Number
Female D7 vs D0
Cell cycle
DNA replication
Apoptosis
Small cell lung cancer
Ferroptosis
Lysosome
Protein digestion and absorption
Mineral absorption
Fanconi anemia pathway
p53 signaling pathway
Amino sugar and nucleotide sugar metabolism
Progesterone-mediated oocyte maturation
ECM-receptor interaction
Cholesterol metabolism
Mismatch repair
Phenylalanine metabolism
Homologous recombination
Renin secretion
Axon guidance
Nucleotide metabolism
MicroRNAs in cancer
Cellular senescence
Parathyroid hormone synthesis, secretion and action
NF-kappa B signaling pathway
Ubiquinone and other terpenoid-quinone biosynthesis
0 5 10 15
Enrichment Score
KEGG Pathways
GO: Cellular Component
GO: Biological Process
GO: Molecular Function
signaling receptor binding
extracellular matrix structural constituent
extracellular region
extracellular space
kinetochore
cellular process
biological regulation
developmental process
response to stimulus
homeostatic process
locomotion
cell adhesion
cell migration
cell division
collagen metabolic process
collagen catabolic process
0 500 1000 1500
Gene Number
b
Male D7 vs D0 Upregulated
NID1
LAMA1
LAMA2
COL8A2
ITGA8
ANTXR2
COL18A1
ITGA7
MMP14
ITGA4
CSPG4
SPP1
MMP15
AGRN
COL14A1
POSTN
COL4A2
PDGFRB
ITGA2
BGN
THBS2
COL6A3
TIMP3
COL21A1
COL5A3
COL4A1
COL11A1
CTHRC1
ADAMTS12
COLGALT1
BMP4
NOTCH3
COL10A1
Female D7 vs D0 upregulated
KDR
MMP13
AGTR1
CPT1A
HRK
NOTCH3
MMP11
PDGFRB
PPARGC1A
MAP3K12
CTSK
SOCS1
MEF2C
FGF13
IRS2
HSPA1A
ETV5
MMP2
CXCL12
STAT2
MDK
MMP7
SQSTM1
APP
DUSP6
PIK3R1
PMAIP1
MMP17
SPHK1
GJA1
SPP1
NQO1
HIST2H2BE
TIMP3
DDX58
FGFR1
PPP1R15A
MAFB
HDAC9
JUN
HMOX1
IFIH1
HIST1H2AC
NOTCH1
MMP14
MAFG
RELB
IRF1
GADD45A
TRAF1
LEF1
B2M
MAF
IRAK1
DDIT3
HIST1H2BD
EGR2
EGR1
BIRC3
GCLC
WNT11
MECOM
DUSP5
MAP4K4
DUSP10
CDK5R1
TRAF5
PLEKHO1
NFATC4
TNIK
HMGA1
ROR2
CHRNA1
ETV1

Figure 2.4 Functional enrichment of altered transcriptome induced by SMG for male and female donors.

a. Top non-redundant Gene Ontology (GO) terms and KEGG pathways enriched by all DEGs in male and female donors on day 7. b. Hub protein networks for upregulated DEGs on day 7 in male and female donors. Hub protein was defined as the protein with the highest connectivity. A network was generated by including the hub protein and its direct connections with all other proteins. The size and density of color of each protein in the network reflected its level of connectivity, with larger and denser colors indicating higher connectivity. The hub protein in the network was highlighted with a blue circle. The hub protein for male donors was identified as COL4A2, and for female donors was JUN.

To investigate further the molecular mechanism underlying sex-dependent differences, hub gene networks were constructed for male and female donors separately, considering all DEGs combined, up-regulated DEGs, and down-regulated DEGs (Figure 2.4b, Supplementary Figure 2.8). Upon comparing males and females, it was found that the corresponding hub protein from up-regulated DEGs on both day 3 and day 7 in females were primarily associated with Wnt signaling (CTSK, IRAK1, JUN, PIK3R1, LEF1, MMP7, NFATC4, ROR2, and WNT11), VEGF signaling (KDR, PIK3R1, and SPHK1), and NF-κB signaling pathways (BIRC3, CXCL12, DDX58, GADD45A, IRAK1, RELB, TRAF1, and TRAF5). In contrast, the hub components of upregulation in males were ECM components and matrix remodeling enzymes (Supplementary Table 2.5).

2.4 Discussion

The absence of adequate model systems for studying the molecular pathogenesis of KOA impedes our comprehension of the entire disease spectrum. Studies that use end-stage disease samples may not capture essential molecular changes that occur earlier in the disease progression, leading to an incomplete understanding of the underlying mechanisms. By employing tissue engineering techniques and coating cell contact surfaces with human-derived extracellular components, this model maintains meniscus fibrochondrocytes (MFC) in a state closely resembling their native environment. The meniscus models engineered with primary cells were analyzed by RNA sequencing to

establish a transcriptome profile over time and examine the initial changes in molecular profile that contribute to the early onset of KOA.

The molecular mechanisms underlying the connection between meniscus injury and the onset and progression of KOA are intricate and not completely understood. However, it is hypothesized that meniscus injury initiates a series of cellular and molecular reactions that culminate in an inflammatory response within the knee joint, which contributes to the development of KOA (117). In our study, we used cell-seeded meniscus constructs and demonstrated that molecular patterns and pathways related to inflammation and immune response were significantly enriched at nearly all time points in the SMG treatment. The inflammatory response involves various immune cells, growth factors, cytokines, and chemokines, and prior research has suggested that inflammatory-related molecules primarily drive the enzymatic cascade of OA, which leads to cartilage matrix degradation (118, 119). After knee injury, IL6 and TNF-α levels rise within 24 hours (120) and can persist for up to 18 months post-injury (121). They regulate various signaling pathways and promote the recruitment and activation of immune cells such as macrophages among the most significantly enriched pathways on both day 1 and 3. Although the precise process behind inflammatory-induced cartilage catabolic activity remains unclear, several studies suggest that inflammatory cytokines play a crucial role in regulating various catabolic enzymes, including proteases from the MMP and ADAMTS families (122, 123). Our study also demonstrated this correlation, as evidenced by the hub protein network on day 3 for all donors. Several MMPs and ADAMTS5 were closely linked to the hub protein IL6 and other proteins in the network.(124). CCL2 is another signaling molecule induced after joint injury, primarily recruiting monocytes, and modulating downstream immune response cascades (125). In our study, the short-term SMG model effectively captured the initial inflammatory events associated with joint injury and early onset KOA observed in various *in vitro* and *in vivo* models, with CCL2 and IL6 being the hub protein on day 1 and day 3, respectively. This finding aligns with the observation that regulating these two molecules are critical in modulating the inflammatory response during the acute phase of joint injury, and the onset of KOA. In addition, the functional enrichment analysis showed that TNF and MAPK signaling pathways, IL-17 signaling pathway, as well as complement and coagulation cascades were

In addition to the activation of the inflammation cascade and the degradation of ECM components, another important event that marks the early stage of KOA is the proliferation of chondrocytes (126, 127). In normal articular cartilage, chondrocytes usually do not undergo proliferation or terminal differentiation. However, in diseased cartilage, there is an augmentation in chondrocyte proliferation and hypertrophic differentiation (128), along with the start of vascularization and focal calcification. Cyclin-dependent kinases (CDKs) are a family of proteins that play a key role in regulating the cell cycle, with CDK1 being the first CDK gene to be identified and conserved across all organisms (129). The importance of CDK1 in skeletal system development has been demonstrated through loss-of-function experiments on chondrocytes in mouse models (130). In the context of disease state, CDK1 has been identified as a hub gene in several studies (131, 132). The findings of our study support that CDK1 plays a crucial role in the early onset of KOA. CDK1 was identified as the hub protein for all differentially expressed genes on day 7 when all donors were combined. Notably, the impact of CDK1 was more pronounced in female donors than in male donors. Specifically, CDK1 was the hub protein exclusively for female donors on day 7, while IL6 was the hub protein for male donors. In addition, the top enriched KEGG pathways demonstrated significant cell proliferation-related activities such as "cell cycle" and "DNA replication" that were only present in female donors.

Cartilage development and maintenance rely on mechanical stimulation. Chondrocytes sense environmental stimuli via the pericellular matrix (133) and convert them into biological signals through various receptors on their cell membranes, known as mechanotransduction (71). In healthy joints, this process is crucial for preserving cartilage tissue's integrity and function. However, in OA joints, an imbalance between the mechanical loading and the ability of chondrocytes to respond to mechanical signals can lead to cartilage breakdown and joint degeneration (108, 134). Chondrocyte mechanotransduction involves various signaling molecules and pathways. Our study assessed the expression of these molecules and compared the expression patterns between males and females. The results showed that *JUN* exhibited the most significant difference in expression correlations with other assessed factors between male and female donors. The JUN proteins are part of the AP-1 transcription factor family and was identified as a

regulator of gene expression and a trigger for downstream signaling cascades in response to mechanical stimuli in chondrocytes (135). The hub protein network analysis in this study demonstrated a sex-dependence of JUN's expression, where JUN was identified as the hub protein only in female donors. Moreover, the network showed that several proteins from the MMP family and the calcification-related protein SPP1 were highly connected to JUN, suggesting the potential role of JUN in regulating the expression of genes involved in the matrix degradation and calcification processes.

In addition to its role in mechanotransduction, JUN can also crosstalk with other well-established signaling pathways involved in OA. For example, JUN participates in Wnt signaling pathways, which regulate the expression of genes involved in cell proliferation, differentiation, and survival (136, 137). Numerous studies have shown that, in the context of KOA, there is an upsurge in Wnt signaling that can result in chondrocyte hypertrophy, inflammation, and cartilage deterioration. (138, 139) In this study, the hub protein network of upregulated DEGs for males and females was analyzed, along with the enriched pathways corresponding to the genes in the network. For females with JUN as the hub protein, Wnt signaling pathways were among the top enriched KEGG pathways, along with several other OA-relevant pathways such as VEGF signaling, and NF-kappa B signaling pathways. On the other hand, for males, the hub components of upregulations were ECM components and matrix remodeling enzymes.

One limitation of our study involves using day 0 baseline samples as a common control instead of matched static samples from each time point for RNA sequencing data analysis. Using matched time-point controls in static conditions could potentially enhance the precision of our findings by more distinctly isolating the effects of simulated microgravity. Another limitation of this study lies in the need for validation experiments to link the transcriptional data with functional outcomes, which is crucial for confirming the model's predictive power for OA progression and sex differences. Despite this, the study's innovative use of a refined *in vitro* model and SMG conditions successfully narrows down potential targets for early KOA development and sex disparities, marking a significant step forward in the search for effective treatments. This approach solidifies

the model's role as a valuable screening platform for identifying promising molecular targets.

2.5 Conclusion

In conclusion, our study opens the perspective that short-term SMG induced molecular events mimicking early KOA in refined human meniscal models developed from non-osteoarthritic primary MFC that can be leveraged for therapeutic discovery and development. Transcriptomic analysis revealed a significant enrichment of genes and pathways related to inflammation and immune response in the early onset of KOA. Notably, our study suggests that sex dimorphism in cellular proliferation and JUN expression may be the key factors responsible for the progression of early-onset KOA.

2.6 List of abbreviations

Osteoarthritis (OA), knee osteoarthritis (KOA), meniscus fibrochondrocytes (MFC), simulated microgravity (SMG), extracellular matrix (ECM), Differentially expressed genes (DEGs),

2.7 Supplementary information

Supplement Figure 2.1 Correlation assessment between RT-qPCR and RNA sequencing data. The data points represented individual donors.

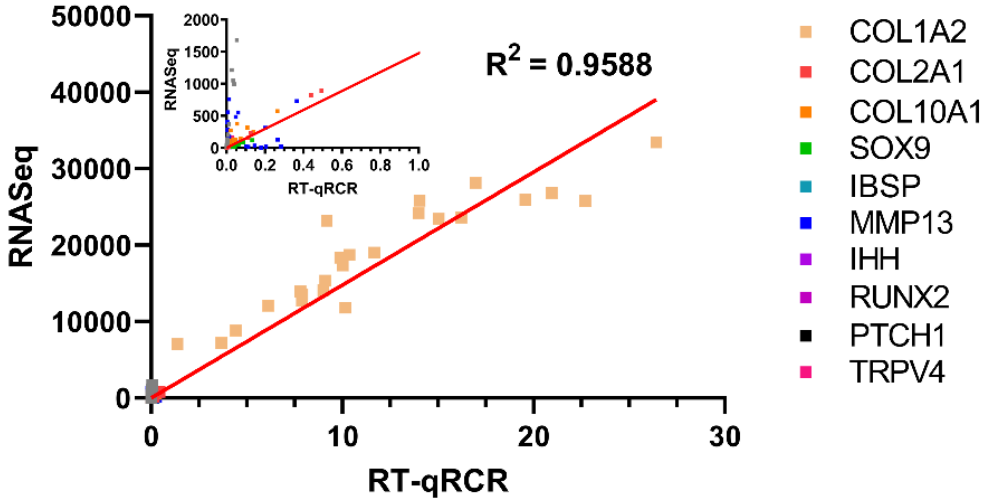

Supplement Figure 2.2 Top non-redundant Gene Ontology (GO) terms and KEGG pathways enriched by all DEGs on day one and three.

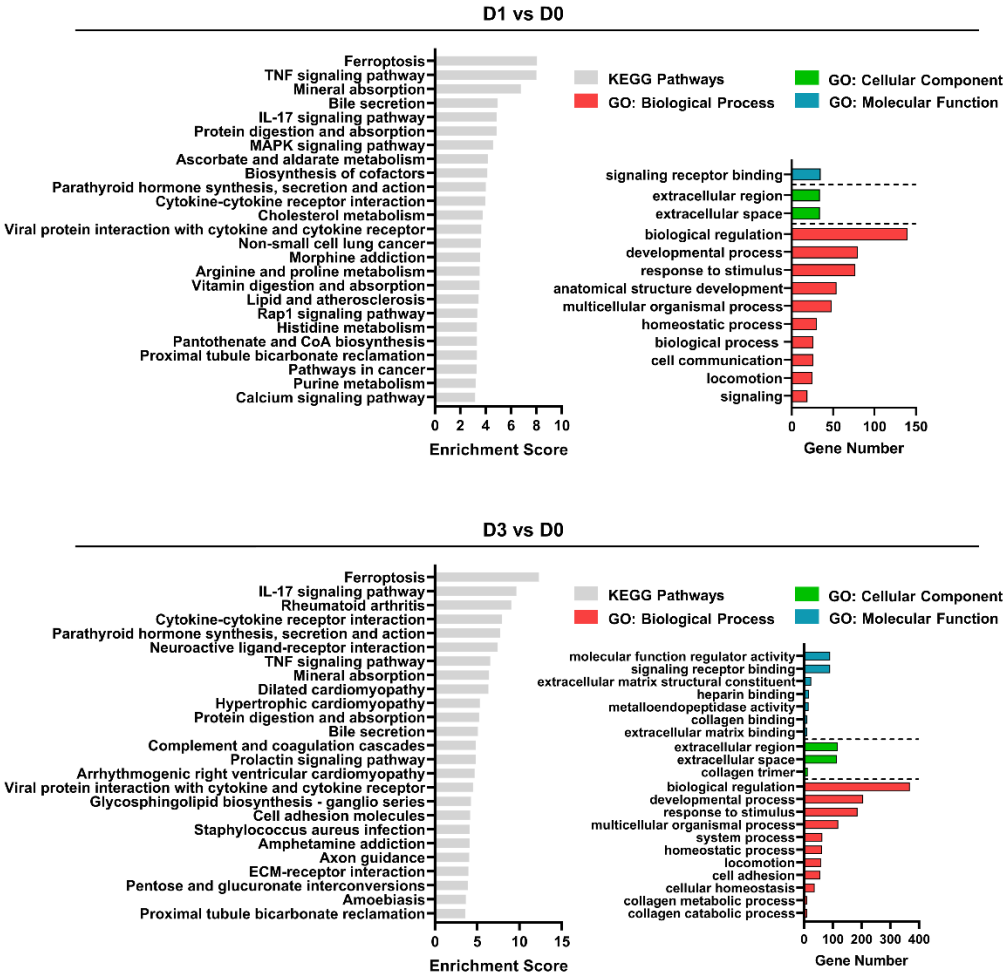

Supplement Figure 2.3 Hub protein network on day one for all donors. Hub protein was defined as the protein with the highest connectivity. A network was generated by including the hub protein and its direct connections with all other proteins. The size and density of color of each protein in the network reflected its level of connectivity, with larger and denser colors indicating higher connectivity. The hub protein in the network was highlighted with a blue circle. The hub protein in the network was CCL2.

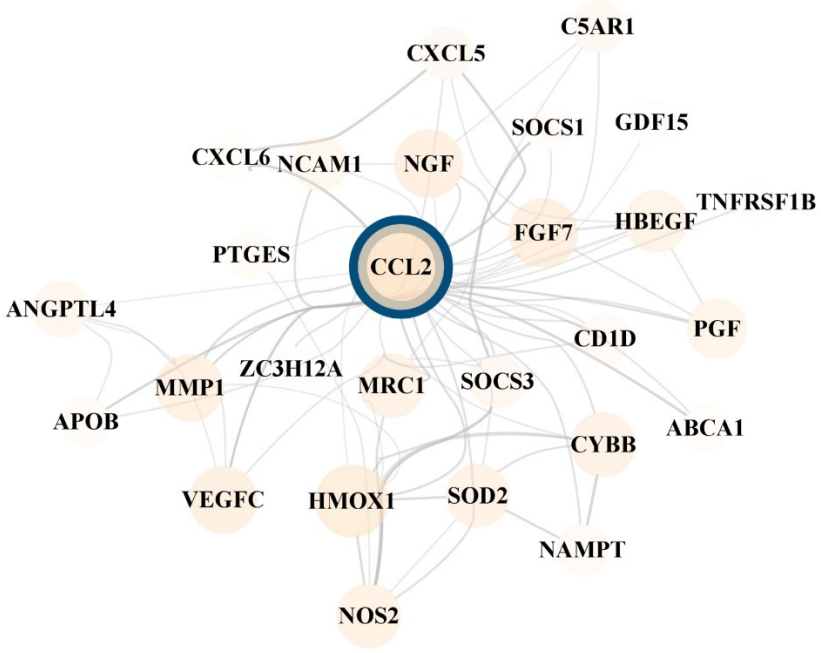

Supplement Figure 2.4 Hub protein network on day three for all donors. The hub protein in the network was IL6.

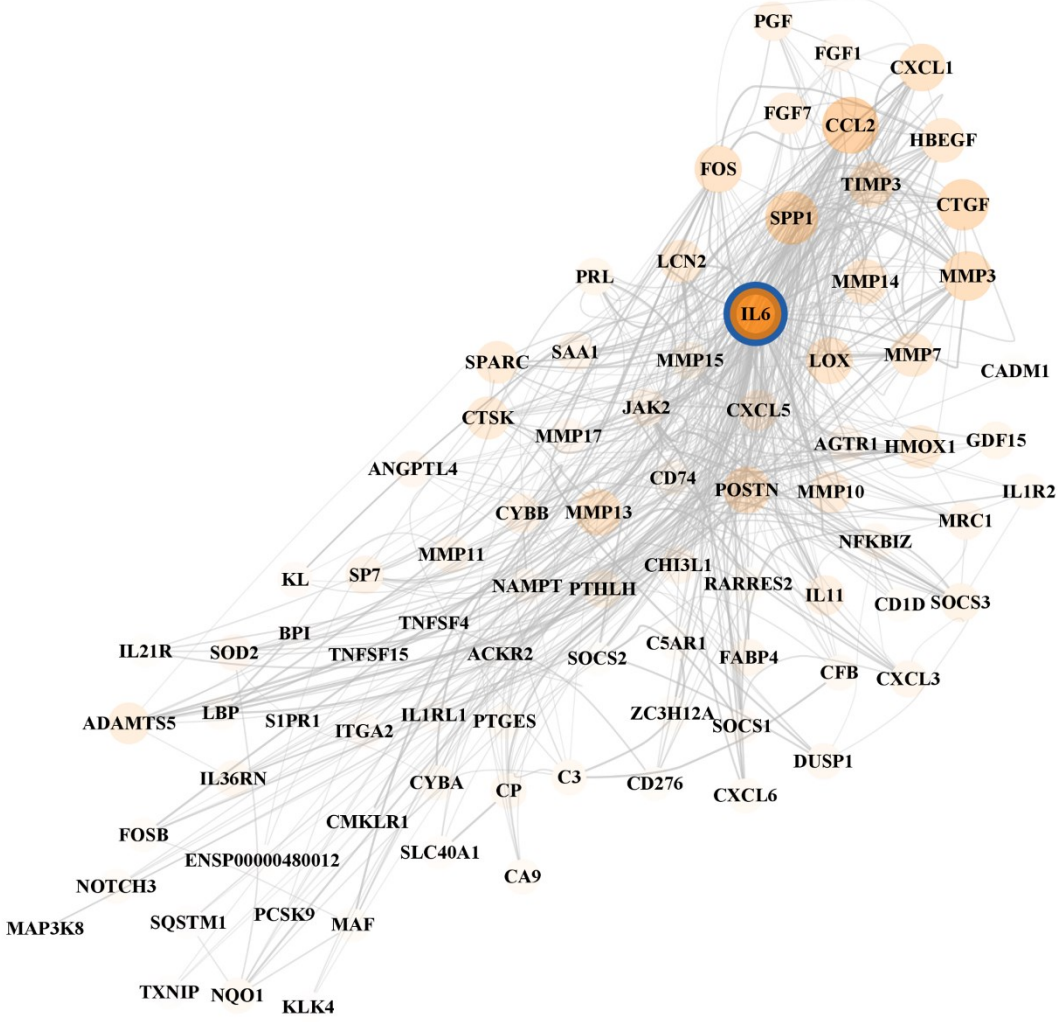

Supplement Figure 2.5 Hub protein network on day seven for all donors. The hub protein in the network was CDK1.

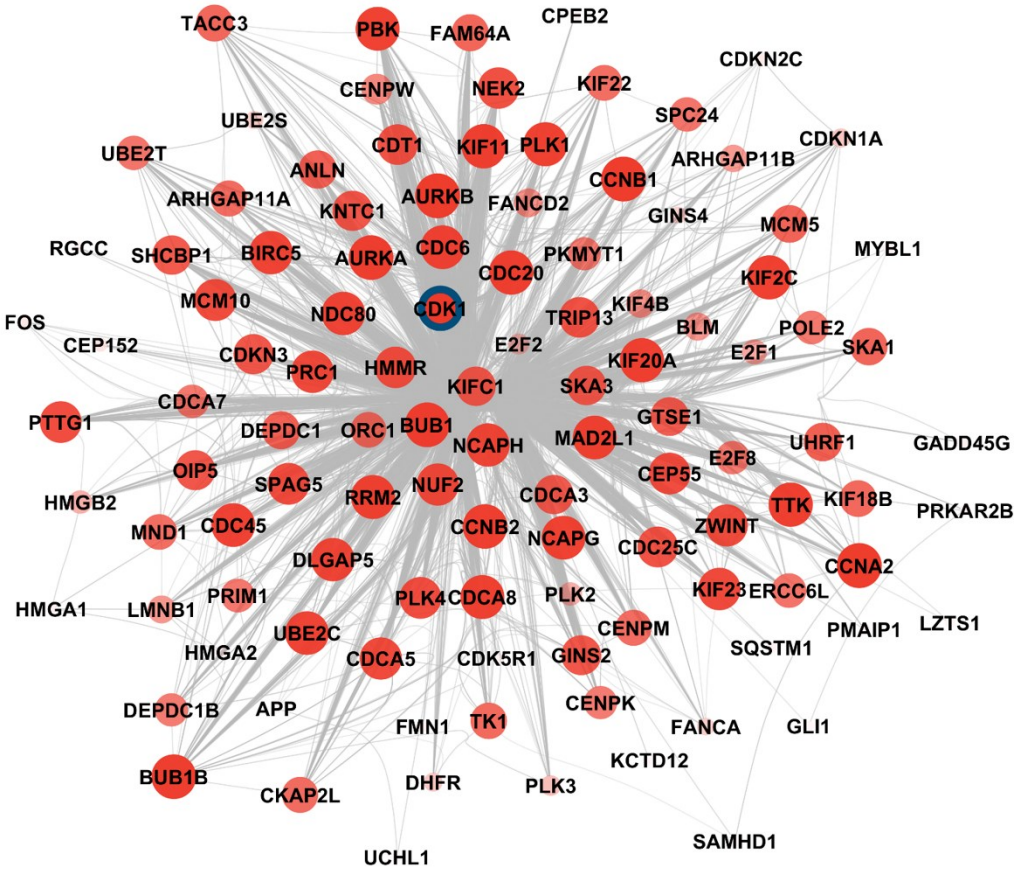

Supplement Figure 2.6 Venn diagram of the comparison between upregulated and downregulated DEGs in male and female donors across three time points.

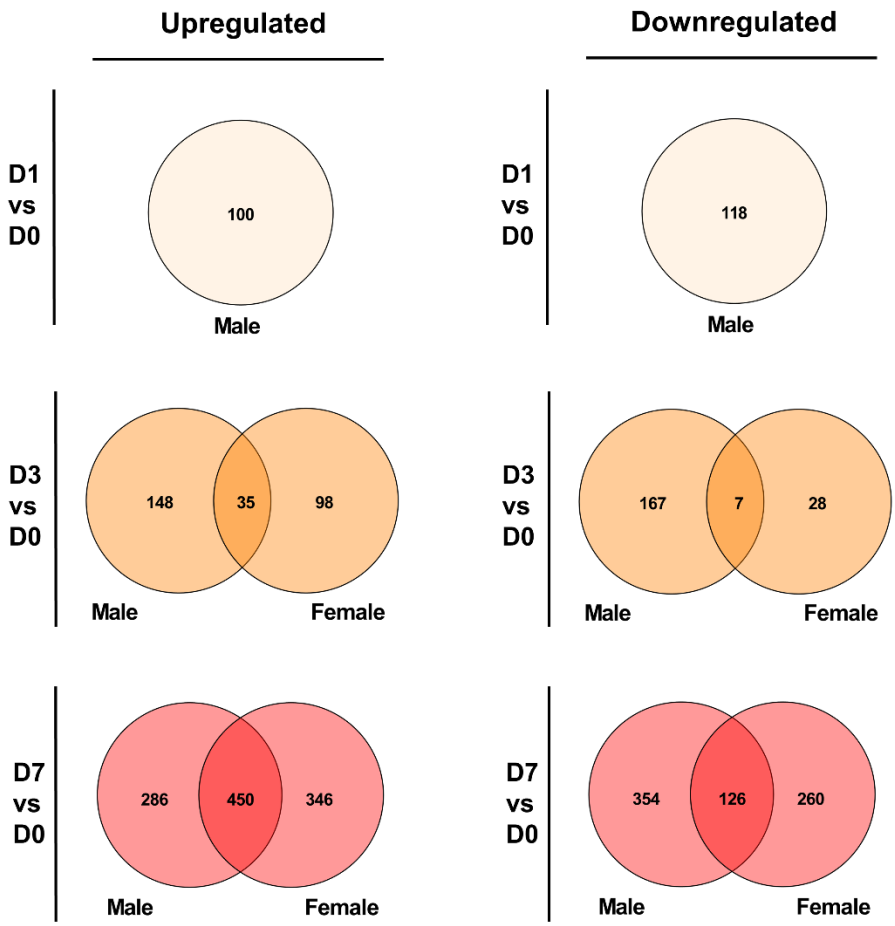

Supplement Figure 2.7 Functional enrichment of altered transcriptome induced by SMG for male and female donors. Top non-redundant Gene Ontology (GO) terms and KEGG pathways enriched by all DEGs on day one and day three for male donors, and on day seven for female donor.

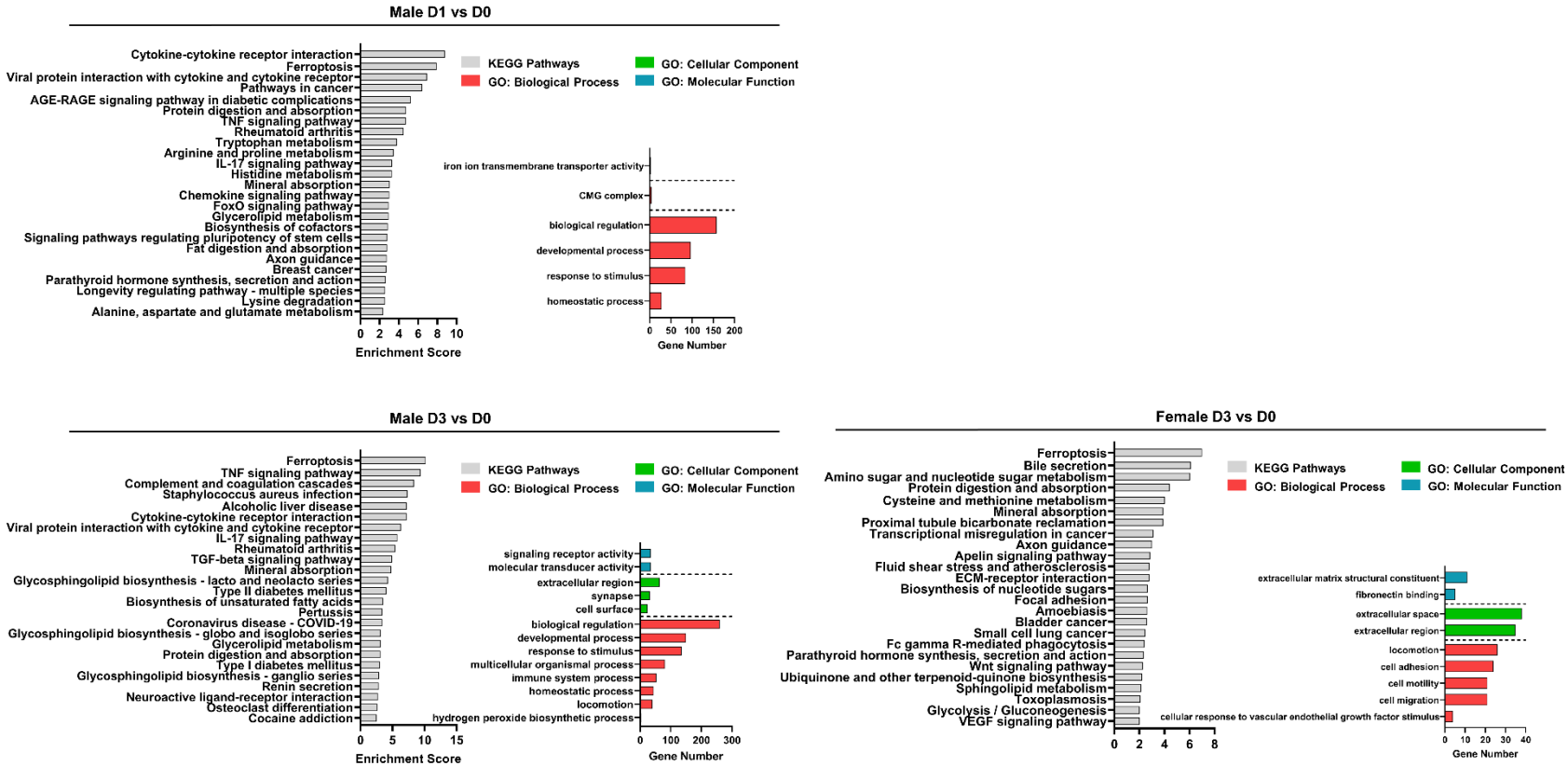

Supplement Figure 2.8 Hub protein network on day three and day seven for male and female donors. In male donors, NFKBIA was identified as the hub protein for all DEGs on day three, THBS2 for upregulated DEGs on day three, and IL6 for all DEGs on day seven. Meanwhile, in female donors, CTGF was identified as the hub protein for all DEGs on day three, KDR for upregulated DEGs on day three, and CDK1 for all DEGs on day seven.

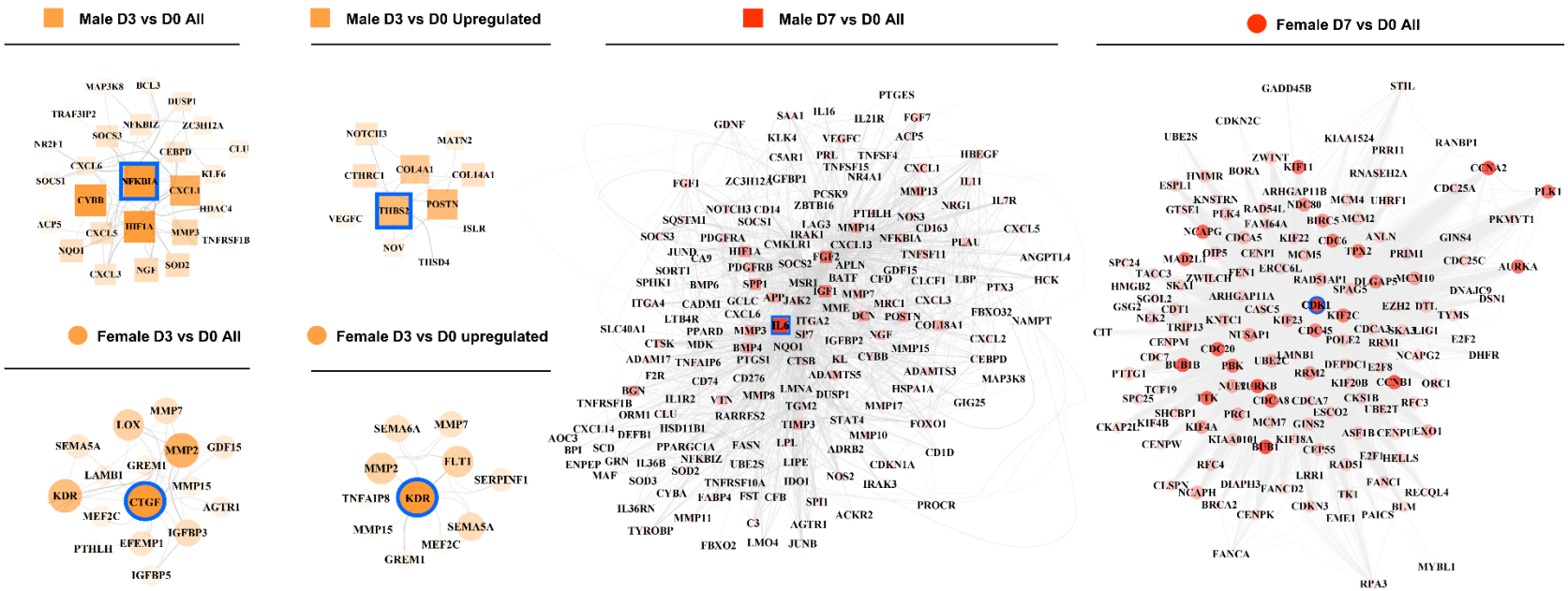

Supplementary Table 2.1-2.5 are deposited and available at figshare (https://figshare.com/s/88f0e99232978ea3ce45).

Supplementary Table 2.6 CT value for the selected housekeeping genes

Donor	Time (day)	*B2M*		*β-Actin*		*YWHAZ*	
		Static	SMG	Static	SMG	Static	SMG
F1	0	20.44		18.77		24.08	
	1	20.27	20.51	18.78	18.78	24.33	24.17
	3	20.48	20.45	19.26	18.98	24.57	24.38
	7	20.21	20.10	19.05	19.33	24.70	24.52
F2	0	21.65		19.11		24.97	
	1	21.71	21.68	19.09	18.93	25.34	24.93
	3	21.78	21.30	19.44	19.42	25.63	25.54
	7	21.20	20.72	19.74	19.23	25.82	25.57
F3	0	21.48		18.85		24.91	
	1	21.71	21.43	19.27	19.05	25.33	25.13
	3	22.01	21.28	19.78	19.51	26.00	25.40
	7	21.32	19.89	19.89	19.41	25.89	25.56
M1	0	19.89		19.09		24.93	
	1	20.73	20.30	18.57	18.46	24.81	24.54
	3	20.62	20.52	19.09	18.83	25.06	24.40
	7	20.86	19.39	19.54	19.14	26.02	24.69
M2	0	19.70		19.75		26.79	
	1	19.75	19.99	18.47	18.63	24.57	24.46
	3	20.25	20.05	19.12	19.06	25.35	24.58
	7	20.40	20.19	19.39	19.30	25.69	24.97
M3	0	19.17		18.72		24.59	
	1	20.64	20.32	18.85	18.85	25.25	25.10
	3	20.91	20.76	19.36	19.56	25.79	25.64
	7	20.59	19.87	19.26	19.10	25.88	25.30

2.8 Fundings and acknowledgement

The project was supported by Canadian Space Agency (CSA FAST 21FAALBA04), Natural Sciences and Engineering Research Council (NSERC RGPIN-2018-06290 Adesida), the Alberta Women's Health Foundation through the Women and Children's Health Research Institute (UOFAB WCHRIIG 3126 Adesida), the Cliff Lede Family Charitable Foundation through the University Hospital Foundation (RES00045921 Adesida), and Women and Children's Health Research Institute (WCHRI) graduate studentship.

2.9 Competing interests

The authors declare no competing interests.

2.10 Availability of Data and Materials

RNA-Seq data was deposited into the Gene Omnibus Database (GEO) under accession number GSE231848.

Chapter 3

Engineered Human Meniscus in Modeling Sex Differences of Knee Osteoarthritis in Vitro

This Chapter has been previously published as:

Ma Z, Li DX, Kunze M, Mulet-Sierra A, Westover L, Adesida AB. Engineered Human Meniscus in Modeling Sex Differences of Knee Osteoarthritis in Vitro. *Front Bioeng Biotechnol*. 2022;10:823679.

3.1 Introduction

Osteoarthritis (OA) is the most common form of degenerative disease and primarily affects loading-bearing joints, with the knee joint being the most prevalent (98, 102). A hallmark feature of knee osteoarthritis (KOA) is the atrophy of articular cartilage. Surrounding joint tissues, including the menisci, will also undergo breakdown (140, 141). These abnormal changes can lead to rapid loss of the knee joint's function and mobility, making KOA a leading cause of physical disability (142). Although KOA occurs in almost all demographic groups, the prevalence and severity of KOA increases with age and is disproportionately higher in females than males (7, 103, 143-145). It has been reported by the World Health Organization that 9.6% of males and 18% of females above the age of 60 years have symptomatic OA (6).

The molecular mechanisms and cellular events underlying the pathogenesis and progression of KOA are not well understood. As well, the molecular basis of biological sex matters has not been previously investigated. Currently, there is no consensus model to reflect the pathophysiology of KOA holistically. However, the molecular and cellular characteristics of KOA resemble the hypertrophic differentiation of chondrocytes as they progress to the bone during endochondral ossification (146). Conveniently, this process includes the upregulation of hypertrophic markers *COL10A1* and *MMP13*, which can be

indicators for the KOA phenotype (147, 148). Healthy chondrocytes, on the other hand, resist hypertrophic differentiation and lack expression of these hypertrophic markers (149). Given the disproportionate incidence of KOA in females as compared to males, we reasonably expect the cellular and molecular characteristics of KOA to show sex-dependent differences.

Mechanical stimulation was reported by an abundance of studies to play a critical role in modulating OA-related responses of loading-bearing tissues. Applying mechanical loading to joints through regular exercise is essential to maintaining healthy cartilage and preventing breakdown from prolonged disuse (81). Cyclic hydrostatic pressure (CHP) as a loading modality mimics physiological loading patterns and can be easily recreated in-vitro using specialized bioreactors (59) (150). Studies have shown that CHP applied to engineered tissue constructs has induced a mostly prochondrogenic effect. For example, Zellner et al. applied dynamic hydrostatic pressure (cyclic at 1 Hz for 4 h per day, 0.55–5.03 MPa) for 7 days to cellular aggregates generated from inner and outer meniscus fibrochondrocytes (MFCs) (60). After 14 additional days of static culture, aggregates loaded initially for the 7 days showed immunohistochemically enhanced chondrogenesis compared to unloaded controls (60). Further, Gunja et al. applied dynamic hydrostatic pressure (0.1 Hz for 1 h every 3 days, 10 MPa) for 28 days to engineered tissue constructs using MFCs with added TGF-β1 growth factors (151). Loaded tissue constructs with growth factors showed additive and synergistic increases in collagen deposition (approximately 2.5-fold), GAG deposition (2-fold), and enhanced compressive properties compared to unloaded controls without growth factors (151).

Mechanical unloading of joints from long-term immobilization has been shown to induce cartilage atrophy that resembles characteristics of KOA. In a case study by Souza et al., joint immobilization of healthy individuals without prior history of OA resulted in magnetic resonance imaging (MRI) parameters of their knee articular cartilage that resemble KOA (109). When returning to standard weight-bearing, the MRI parameters for the joints were restored to baseline values consistent with healthy articular cartilage (109). Mechanical unloading has also been modelled by simulated microgravity (SMG) using rotating wall vessel bioreactors (59, 64, 92, 152, 153). Mayer-Wagner et al. applied

simulated microgravity for 21 days to human mesenchymal stem cell (hMSC) pellets and found a decrease in histological staining of proteoglycans and collagen type-II compared to normal gravity controls (64). SMG pellets also showed a lower *COL2A1/COL10A1* expression ratio suggesting that mechanical unloading via SMG reduced the chondrogenic differentiation of hMSCs (64). Finally, in a comparative study, CHP-loaded pellets from human adipose-derived stem cells showed increased expression of *ACAN*, *SOX9*, and *COL2A1*, and a 3-fold increase in GAG productions compared to unloaded SMG groups (59). However, none of the above studies investigated the sex-dependent differences in the magnitude of differential modulation by mechanical loading and unloading via CHP and SMG, respectively.

A recent definition of OA from the Osteoarthritis Research Society International includes the menisci of the knee joint as a tissue undergoing breakdown and abnormal changes from the disease (141). Knee menisci undergoing OA has also been shown to have similar characteristics as knee articular cartilage undergoing OA, such as focal calcification and the increased expression of hypertrophic markers *COL10A1* and *MMP13* (140, 154). This suggests that MFC may play an active role in the pathogenesis of KOA alongside knee articular chondrocytes, making MFC a reasonable cell option to model OA *in vitro*.

Taken together, the goal of this study was to evaluate the effects of mechanical loading and unloading via CHP and SMG, respectively, and determine sex-dependent differences in the modulation of OA-related characteristics in bioengineered human meniscus tissues. This would serve as an OA disease model in-vitro to determine the cellular and molecular profiles responsible for the sex-dependent incidence of the disease.

3.2 Methods

The experiment is outlined in Figure 3.1. Most culture methods and assays were performed identically to those described in previous work (54, 55, 155).

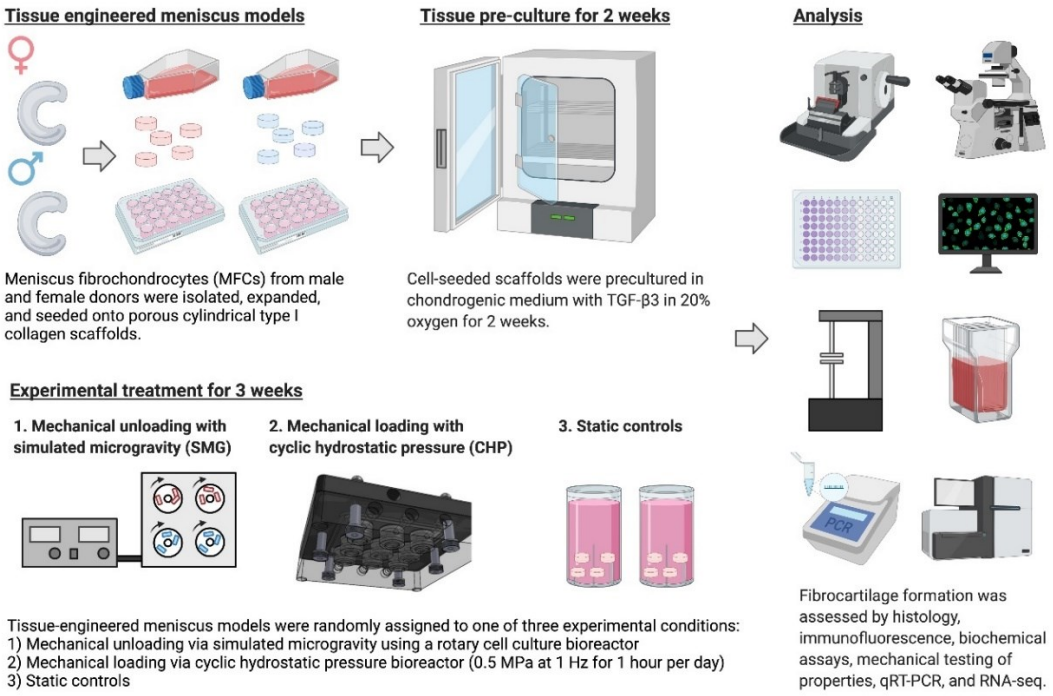

Figure 3.1 Experiment outlines.

3.2.1 Ethics statement

Human non-osteoarthritic inner meniscus samples were collected from patients undergoing partial meniscectomies at the University of Alberta Hospital and Grey Nuns Community Hospital in Edmonton. The ethics of this study was approved by the Health Research Ethics Board of the University of Alberta. Non-identifying donor information is listed in Table 3.1.

Table 3.1 Non-identifying donor information.

Sex	Donor Number	Age	Population Doubling (PD)
Female	F1	33	2.687
	F2	44	2.380
	F3	30	2.774
	F4	28	3.860
Male	M1	19	3.349
	M2	45	2.699
	M3	22	3.247
	M4	35	2.149

3.2.2 Cell and tissue culture

Meniscus fibrochondrocytes (MFCs) were isolated from inner meniscus tissue samples by type II collagenase (0.15% w/v of 300 units/mg; Worthington) mediated digestion, followed by 48 h recovery. After recovery, cells were replated in tissue culture flasks at the density of 1×10^4 cells/cm^2 and expanded for 1 week in high glucose Dulbecco's modified Eagle's medium (HG-DMEM) supplemented with 10% v/v heat-inactivated fetal bovine serum (FBS), 10mM 4-(2-hydroxyethyl)-1-piperazineethanesulfonic acid (HEPES), 100 U/mL penicillin, 100 µg/mL streptomycin and 2 mML-glutamine (PSG; Life Technologies, ON, Canada), 5 ng/mL of FGF-2 (Neuromics, MH, United States, catalogue #: PR80001) and 1 ng/mL of TGF-β1 (ProSpec, catalogue #: CYT- 716) for 1 week.

Expanded MFCs were resuspended in defined chondrogenic medium (HG-DMEM supplemented with HEPES, PSG, ITS+ premix (Corning, Discovery Labware, Inc, MA, United States), 125 µg/mL of human serum albumin, 100 nM of dexamethasone, 365 µg/mL ascorbic acid 2-phosphate, 40 µg/mL of L-proline, and 10 ng/mL of TGF-β3) and seeded onto bovine type I collagen scaffolds (dimensions: 6 mm diameter, 3.5 mm height; Integra LifeSciences, NJ, United States) at the density of 5×10^6 cells/cm^3. The cell-containing constructs were precultured statically in standard 24-well plates with 2.5 mL/construct of the chondrogenic medium described above for 2 weeks; media changes occurred once per week.

3.2.3 Mechanical stimulation

After the 2-weeks preculture, tissue constructs were randomly assigned to a mechanical stimulation group. For the static control group, constructs were placed in a tissue culture tube (Sarstedt, Germany). For the mechanical unloading group, a commercially available bioreactor (RCCS-4; Synthecon Inc.) was used to culture tissue constructs in a simulated microgravity (SMG) environment. The rotation speed was adjusted over time to maintain constructs in suspension (30 rpm from day 1–2; 34 rpm from day 3–7; 37 rpm from day 8–13; 40 rpm from day 14–21). For the mechanical loading group, cyclic hydrostatic pressure (CHP) was applied to tissue constructs using a MechanoCulture TR (CellScale,

Canada). Constructs were loaded 1 h per day and daily with 0.9 MPa cyclic hydrostatic pressure at the frequency of 1 Hz. When not loaded, tissue constructs were cultured in 6-well plates under static conditions. All experimental groups were cultured with chondrogenic medium with supplemented TGF-β3 growth factor, and the volume of medium per tissue construct (approximately 6.5 mL per tissue construct per week) was equivalent among the different groups. Mechanical stimulation was applied for 3 weeks, and medium change was performed once a week. At the end of the 3-weeks treatment, the CHP group was allowed 30 min of rest following the last loading event for gene expression changes to occur. Tissue replicates for RNA extraction were placed in TRIzol reagent and frozen at −80°C. Constructs from SMG and static control groups were harvested at approximately the same time.

3.2.4 Histology, immunofluorescence and biochemical analysis

The wet weight of tissue constructs (n = 5–8 replicates) intended for histology and biochemical analysis was recorded at the end of the experiment. Constructs (n = 2 replicates, only one replicate is presented) were then fixed in 1 mL of 10% v/v buffered formalin (Fisher Scientific, MA, United States) overnight at 4°C, dehydrated, embedded in paraffin wax, and sectioned at 5 μm thickness. Tissue sections approximately from the middle region of the constructs were stained with Safranin- O (Sigma-Aldrich, United States, #S2255-25G), Fast Green FGF (Sigma-Aldrich, United States, #F7258-25G), and Haematoxylin (Sigma-Aldrich, United States, #MHS32-1L) for histological examination of cell morphology and extracellular matrix deposition. Briefly, for immunofluorescence staining, tissue sections were labelled with primary antibody against human type I, type II, and type X collagen (1:200 dilution of anti-human rabbit type I collagen, Cedarlane, Canada, #CL50111AP-1; 1:200 dilution of mouse anti-human type II collagen, Developmental Studies Hybridoma Bank, United States, #II-II6B3; 1:100 dilution of rabbit anti-human type X collagen, Abcam, UK, #ab58632) and incubated overnight at 4°C (156). On the next day, the secondary antibody (1:200 dilution of goat anti-rabbit, Abcam, UK, #ab150080; 1:200 dilution of goat anti-mouse, Abcam, UK, #ab150117) and DAPI (Cedarlane, Canada) was applied to visualize the stained components.

Biochemical assays quantified the total content of glycosaminoglycan (GAG) and DNA. Tissue constructs (n = 4 replicates for donors F1-3 and M1-3; n = 3 replicates for donors F4 and M4) were digested overnight with proteinase K (Sigma- Aldrich, United States, #P2308) at 56°C. GAG content was measured with a 1,9-dimethyl methylene blue assay (DMMB, Sigma-Aldrich, United States, #341088). Chondroitin sulphate (Sigma-Aldrich, United States, #C8529) was used to generate the standard curve. DNA content was measured with a CyQuant cell proliferation assay kit (ThermoFisher Scientific, United States, #C7026) with different dilutions of supplied bacteriophage λ DNA as the standard.

3.2.5 Mechanical property assessment

Detailed sequence of the mechanical testing protocol is included in Supplementary Material 3.3. A stepwise stress relaxation test (Supplementary Figure 3.1) was used to assess the mechanical properties of tissue constructs (n = 2 replicates for donor F1-3 and M1-3) with the BioDynamic 5210 system (TA Instruments, United States). The cross-section areas of tissue constructs were measured before mechanical tests. For the test, constructs were placed between two platens and the initial height was determined by bringing tissue to near contact with platens. Constructs were first preconditioned by 15 cycles of sine wave dynamic loading with the amplitude of 5% tissue height at the frequency of 1 Hz. The following stress relaxation test consisted of 3 incremental strain steps. In the first two steps, the constructs were subjected to a 10% strain ramp at the rate of 50% strain/sec followed by 5 min relaxation under constant strain. In the third step, the relaxation time was adjusted to 10 min. All tested constructs were able to reach equilibrium within the given relaxation period. Force was recorded as a function of time, and stress was calculated by normalizing force to construct's cross-section area. The peak modulus was calculated by dividing the maximum stress measured immediately after each strain increment by the strain increment. The strain was applied in 10% increments up to a maximum of 30% strain.

3.2.6 RNA extraction, RT-qPCR and RNA sequencing

Tissue constructs (n = 2 for donors F1-3 and M1-3; n = 3 replicates for donors F4 and M4) intended for transcriptome analysis were preserved in Trizol (Life Technologies, United States) immediately upon harvesting and stored at −80°C until RNA extraction. RNA was extracted and purified from ground constructs using PuroSPIN Total DNA Purification KIT (Luna Nanotech, Canada) following the manufacturer's protocol. RNA was reversely transcribed into cDNA, and genes of interest were amplified by reverse transcription-quantitative polymerase chain reaction (RT-qPCR) using specific primers (Supplementary Table 3.1). The expression level of genes of interest was normalized to chosen housekeeping genes (i.e., *β-actin*, *B2M*, and *YWHAZ*) based on the coefficient of variation (CV) and M-value as measures of reference gene stability (157), and the data was presented using the $2^{-\Delta\Delta CT}$ method (158, 159). RNA sequencing was performed on the Illumina NextSeq 500 platform with paired-end 42 bp × 42 bp reads, and FastQ files were obtained for further bioinformatics analysis.

3.2.7 Bioinformatics

RNA sequencing data were analyzed with Partek® Flow® software (Version 10.0.21.0302, Copyright© 2021, Partek Inc, St. Louis, MO, United States). Raw input reads were first trimmed from the 3′ end to achieve a quality score beyond 20 and then aligned to the reference human genome hg38 using the STAR 2.7.3a aligner. Aligned data were quantified to a transcript model (hg38-RefSeq Transcripts 94–2020–05–01) using the Partek E/M algorithm. Genes with maximum read counts below 50 were filtered out to reduce noise. Quantified and filtered reads were normalized in sequential order using the Add: 1.0, TMM, and Log 2.0 methods. Statistical analysis was performed using analysis of variance (ANOVA) for biological sex and treatment. Within each sex, the donors were assigned as a random variable. Differentially expressed genes (DEGs) for each comparison were determined by p-values, adjusted p-values (q-values), and fold change (FC). Gene ontology enrichment, pathway enrichment, and the visualization of DEGs using Venn diagrams were all conducted in Partek.

3.2.8 Statistical analysis

Statistical analyses were performed in Prism 9 (GraphPad) and Partek® Flow® software. The statistical test used, and p-values and q-values are indicated in the respective Figure legends. For analysis in Figure 3.3B, paired t-test were used between SMG and CHP groups within each sex and unpaired t-test were used between female and male groups within each mechanical treatment. For analysis in Figure 3.4A, a repeated measurement one-way ANOVA with Geisser-Greenhouse correction was used to compare mechanical treatment groups within each sex and a Tukey'smultiple comparison test was used to find the adjusted p-value between each comparison. Within each mechanical treatment, unpaired t-tests between female and male groups were used. For the male cohort, no statistical analysis was conducted for the SMG group in contraction due to limited data points. For analysis in Figure 3.4B, repeated measurement one-way ANOVA with Geisser- Greenhouse correction was used to compare different strain levels within each mechanical treatment group and a Tukey's multiple comparison test was used to find the adjusted p-value between each comparison. Within each strain level, paired t-tests were used to compare CHP and SMG groups. For the male cohort, no statistical analysis was conducted for the SMG group due to limited data points.

3.3 Results

3.3.1 Dataset overview

Transcriptome analysis included the expression profiles of 8 donors (4 females and 4 males), each individually exposed to static, mechanical loading (CHP), and mechanical unloading (SMG) conditions. After preprocessing as described in the methods, 13,361 genes were preserved for downstream analysis.

3.3.2 Transcriptome profiles of the engineered meniscus to CHP and SMG

We first analyzed the overall effect of mechanical loading and unloading on the transcriptome profiles of all donors combined. Summarized results are shown in Figure 3.2. Fold-change of gene expression levels in the CHP and SMG groups were calculated by normalizing to its corresponding static group. Differentially expressed genes (DEGs)

were defined as genes with expression fold-change over 2 and q-value less than 0.05. Mechanical loading from CHP significantly modulated 236 genes, while mechanical unloading from SMG significantly modulated 388 genes. The overlay of DEGs between the two mechanical stimulation groups showed only a small proportion of common DEGs (52 genes), whereas the majority of DEGs were uniquely modulated by CHP (184 genes) and SMG (336 genes) (Figure 3.2A). These results indicated that CHP and SMG distinctly modulate the transcriptome profile of donors in this study.

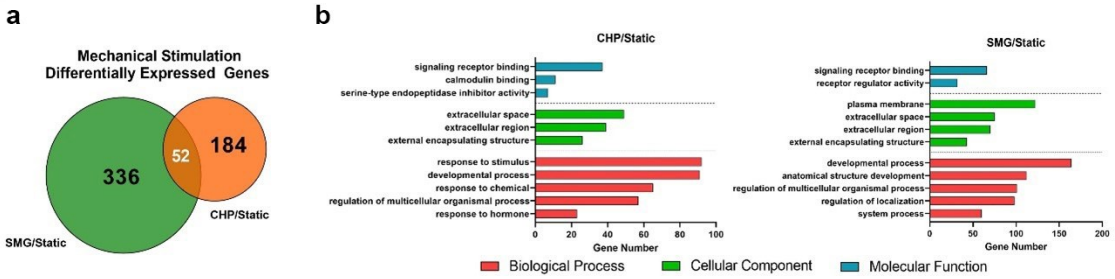

Figure 3.2 Effect of CHP and SMG on the transcriptome profile alteration of engineered meniscus tissues.

a. Overlap of differentially expressed genes (DEGs) by CHP and SMG. b. Top non-redundant Gene Ontology (GO) terms enriched by DEGs of CHP and SMG. DEGs were identified based on all 8 donors. Top significant enriched GO terms were selected by p-value and plotted to the number of genes included in each term.

The most significant Gene Ontology (GO) terms enriched by the DEGs for CHP and SMG were examined next (Figure 3.2B). Although the top 3 most significantly enriched Gene Ontology (GO) in biological components were identical for CHP and SMG ("extracellular space," "extracellular region," and "extracellular matrix"), the included gene expression profiles were different between the treatment groups. The top 20 genes with the highest absolute fold change participating in the ECM relevant activities in CHP and SMG groups are listed in Table 3.2. For CHP, most of the genes are signaling molecules or proteins associated with ECM structure remodeling. For SMG, many of the strongly regulated genes played a more general role, such as various growth factors coding genes: *IGFBP1*, *TGFA*, and *NGF*. Among the top regulated genes, only *NETO1* and *OLFML2A* were common between CHP and SMG; these two genes were upregulated in both treatment groups.

Table 3.2 Top 20 genes with the highest absolute fold change participating in the ECM relevant activities in CHP and SMG groups as compared to static controls.

Gene	Description	P-value: CHP vs Static	Fold Change: CHP vs Static
EREG	Epiregulin	1.20E-06	19.10
NETO1	Neuropilin And Tolloid Like 1	2.53E-08	7.98
MMP3	Matrix Metallopeptidase 3	1.22E-06	6.47
MMP10	Matrix Metallopeptidase 10	1.14E-03	4.54
SBSPON	Somatomedin B And Thrombospondin Type 1 Domain Containing	7.88E-04	3.97
CCL2	C-C Motif Chemokine Ligand 2	8.18E-07	3.62
UCN2	Urocortin 2	5.86E-05	3.61
PLA2G2A	Phospholipase A2 Group IIA	7.00E-04	3.60
OLFML2A	Olfactomedin Like 2A	1.15E-03	3.45
CXCL13	C-X-C Motif Chemokine Ligand 13	1.00E-03	3.40
SFRP2	Secreted Frizzled Related Protein 2	1.17E-05	-4.07
ADM	Adrenomedullin	1.34E-06	-4.49
CPXM1	Carboxypeptidase X, M14 Family Member 1	1.95E-04	-4.53
SELENOP	Selenoprotein P	3.90E-03	-5.82
FAM20A	FAM20A Golgi Associated Secretory Pathway Pseudokinase	2.24E-03	-5.92
MNDA	Myeloid Cell Nuclear Differentiation Antigen	4.02E-03	-5.99
SCUBE1	Signal Peptide, CUB Domain And EGF Like Domain Containing 1	3.28E-03	-7.06
SFRP4	Secreted Frizzled Related Protein 4	6.83E-04	-8.17
ODAPH	Odontogenesis Associated Phosphoprotein	3.30E-03	-9.07
APOE	Apolipoprotein E	3.30E-07	-14.78
Gene	**Description**	**P-value SMG vs Static**	**Fold Change: SMG vs Static**
IGFBP1	Insulin Like Growth Factor Binding Protein 1	5.49E-04	15.94
OLFML2A	Olfactomedin Like 2A	2.34E-05	6.34
NETO1	Neuropilin And Tolloid Like 1	1.26E-06	5.00
ADAMTS14	ADAM Metallopeptidase With Thrombospondin Type 1 Motif 14	8.34E-04	3.72
PCSK9	Proprotein Convertase Subtilisin/Kexin Type 9	2.20E-03	3.48
VSTM2L	V-Set And Transmembrane Domain Containing 2 Like	3.03E-04	3.47
BMPER	BMP Binding Endothelial Regulator	1.91E-04	3.45
NTM	Neurotrimin	1.30E-04	3.40
HMOX1	Heme Oxygenase 1	5.06E-08	3.38
CAPG	Capping Actin Protein, Gelsolin Like	2.94E-07	3.22
LEP	Leptin	8.50E-04	-4.81
R3HDML	R3H Domain Containing Like	8.67E-04	-4.93
APLN	Apelin	8.68E-07	-4.94
STC1	Stanniocalcin 1	8.99E-05	-5.41
NGF	Nerve Growth Factor	7.68E-05	-5.42
TGFA	Transforming Growth Factor Alpha	8.23E-04	-5.47
VEGFA	Vascular Endothelial Growth Factor A	6.33E-06	-5.68
DSCAML1	DS Cell Adhesion Molecule Like 1	3.09E-03	-6.17
ADAMTSL2	ADAMTS Like 2	4.74E-04	-7.23
PDE4C	Phosphodiesterase 4C	2.48E-04	-8.73

3.3.3 Sex-dependent response of engineered meniscus to CHP and SMG

Next, we sought to explore the sex-dependent differences in the engineered meniscus responses to CHP and SMG. Therefore, we separated donors into female and male cohorts and evaluated several factors involved in normal cartilage physiology and OA-related alterations. The GAG and type II collagen content are often used to characterize the degree of chondrogenesis for cartilage tissues, and higher content is linked to higher chondrogenic capacity. Type X collagen, on the other hand, is a hypertrophic marker that suggests an OA-like phenotype. The histological staining for GAG by Safranin-O and immunofluorescence labelled type II collagen (Figure 3.3A) showed highly variable chondrogenic capacities within the female and male cohorts in the baseline static control group. Regardless, tissue constructs exposed to CHP and SMG showed an increase in type II collagen content, with CHP having a generally more pronounced effect. Type X collagen staining intensity was also modulated by mechanical stimulations compared to baseline. A clear increase in type X collagen content was observed in the SMG group, while the CHP group showed comparable type X collagen intensity as the baseline.

To further pursue sex matters in responses to CHP and SMG, the gene expression of selected markers was examined by RT-qPCR (Figure 3.3B). In addition to *COL1A2*, *COL2A1*, and *COL10A1*, the transcription factor *SOX9* and cartilage-specific proteoglycan core protein *ACAN* were also quantified. The observed increase of type II collagen level in the CHP group was confirmed quantitatively by gene expression results. The average *COL2A1* expression level was upregulated 215.9-fold in the CHP group for the female cohort compared to a 21.4-fold increase in CHP for the male cohort. For *ACAN*, *SOX9*, and *COL1A2*, the CHP group had a higher average fold-change than the SMG group, but the differences between the sexes were not significant. For *COL10A1*, the average fold-change of expression level was comparable between the CHP and SMG groups for both females and males. However, when taking individual female donors into account, only female donor 2 showed a significant increase in *COL10A1* expression level in CHP (8.9-fold) compared to SMG (5.7-fold) group. Generally, CHP, as compared to SMG, reduced *COL10A1* expression level for the female cohort. The RT-qPCR data were consistent with the histological observations, providing additional evidence on the

cellular and molecular influence of CHP and SMG. The RT-qPCR data also agreed with the RNA sequencing data, thereby providing additional validation for the observed trends (Supplementary Figure 3.2).

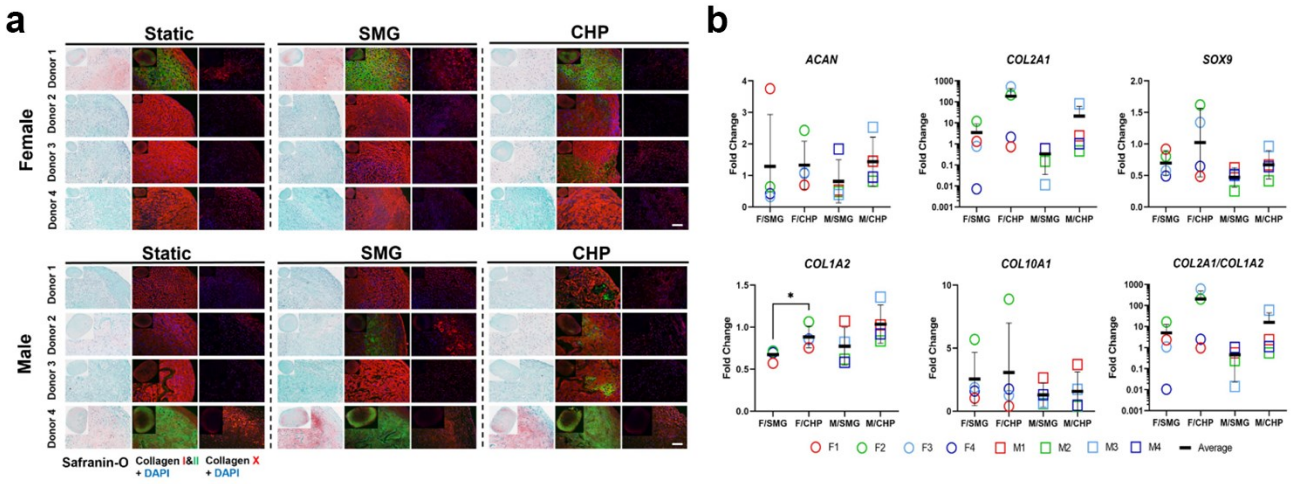

Figure 3.3 Effect of CHP and SMG on the chondrogenic and hypertrophic differentiation potential of female and male donors.

a. Histological and immunofluorescent staining analysis. b. Regulation of selected genes expression level. Gene expression level of individual samples was measured by RT-qPCR. Fold change of expression level was calculated by normalizing expression level in the CHP or SMG group to its corresponding static group. Scale bar: 100 μm *$p < 0.05$.

Sex-dependent differences were also assessed in other related aspects (Figure 3.4A). Quantitative GAG/DNA measurements showed that CHP increased while SMG decreased the GAG production per MFC. The tissue wet weights showed similar trends as the GAG/DNA ratios; CHP tissues weighed more, and SMG tissues weighed less on average than the static control groups. This difference in tissue wet weight was significant in only the female cohort between treatments. Further, at the end of the mechanical stimulation period, tissue constructs from all three experimental groups contracted to certain degrees. The percentage of contraction (percentage reduction in area) was quantified, and comparison among groups showed that SMG tissues had increased contraction compared to the CHP tissues. The contraction plot is presented as the percentage contracted in Supplementary Figure 3.4.

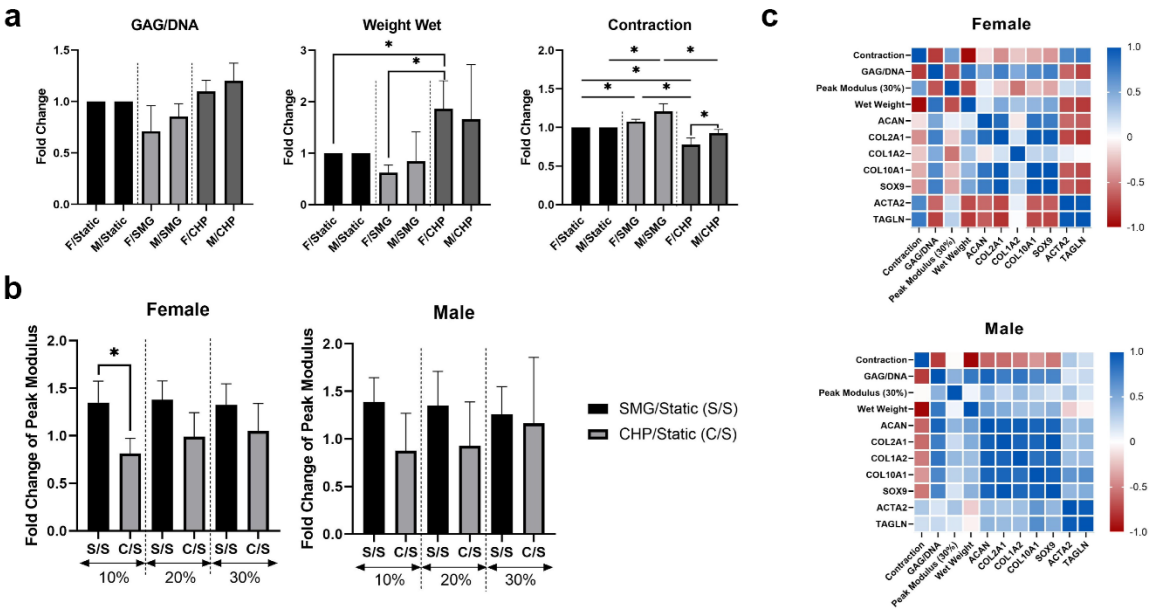

Figure 3.4 Effect of CHP and SMG on chondrogenesis related factors of female and male donors.

a. Biochemical and morphological analysis; contraction is calculated as the %of area lost as compared to the original area. No statistical analysis was conducted for the contraction data with the male SMG group due to limited data points b. Mechanical property analysis. No statistical analysis was conducted for the mechanical property data with the male SMG group due to limited data points c. Pearson correlation heatmap of analyzed factors. Fold change value of characterized factors was calculated by normalizing the CHP or SMG group to its corresponding static group. Heatmap was generated by calculating the pairwise Pearson correlation coefficient of included factors. *$p < 0.05$.

The differences among stimulation groups were significant within the female and male cohorts while also significant between female CHP and male CHP groups. For the mechanical properties of tissue constructs, SMG groups showed higher peak modulus at all tested strain levels for both sexes as expected based on contraction results, and the differences of the average fold-change decreased with increasing strain level. No significant differences were observed between female and male cohorts (Figure 3.4B).

To better understand the relationship among all factors of interest and the sex-dependent differences, a Pearson correlation network (Figure 3.4C) was generated for both the

female and male cohorts with data from all three treatment groups. Some observations mentioned above were further confirmed with correlation coefficients, such as the positive correlation between GAG/DNA and wet weight, the negative correlation between GAG/DNA and contraction, and the positive correlation between *SOX9* and *COL2A1* expression levels. Overall, the correlation analysis yielded different patterns between the female and male cohorts, especially for two examined genes, *ACTA2* and *TAGLN*, that are characteristic of the contractile phenotype in dedifferentiated articular chondrocytes compared to the other factors (160). The level of contraction was positively correlated with *ACTA2* and *TAGLN* expression levels in both female and male groups, confirming their indication for contraction levels. However, the female cohort showed differently a mostly strong negative correlation between the contractile genes and the rest of the factors compared to the male cohort. *ACTA2* and *TAGLN* activity is associated with cytoskeletal composition and structure (161, 162), and thus results may suggest sex-dependent differences of cytoskeletal activity in response to mechanical stimulation.

3.3.4 Comparison of female and male transcriptome response to CHP and SMG

Finally, we investigated the sex-dependent difference in the global transcriptome profile in response to mechanical loading and unloading. Consistent with the DEGs analysis for all donors combined, CHP and SMG uniquely regulated a large proportion of genes within each sex group (Figure 3.5A). We identified the top 25 enriched KEGG pathways for female and male tissues under CHP and SMG using the corresponding DEG sets (Figure 3.5B). For CHP, the most enriched KEGG pathway for both female and male groups was “mineral absorption.” Other relevant terms, such as “IL-17 signalling pathway”, “HIF-1 signalling pathway”, and “glycosaminoglycan biosynthesis,” were also observed for both sex groups. Although some of the enriched pathways were shared, a distinct gene profile with different magnitudes and sometimes the direction of modulation was observed for each sex group (Table 3.3). For example, the *NOTUM* gene in the Wnt-signalling pathway was significantly upregulated by 6.7-fold in CHP for the female cohort and only 1.8-fold in CHP for the male cohort. A large proportion of the top 25 KEGG pathways enriched by SMG overlapped with the pathways in CHP, but the

corresponding gene profiles were different. For example, SMG did not significantly regulate the *NOTUM*, and it showed the opposite direction between female and male cohorts. The *MMP3* gene was downregulated by SMG but upregulated by CHP. Interestingly, in addition to the OA-related KEGG pathways, the "fluid shear stress and atherosclerosis" pathway was enriched for both female and male cohorts, suggesting an effect of mechanical stimulation from CHP and SMG on engineered meniscus constructs.

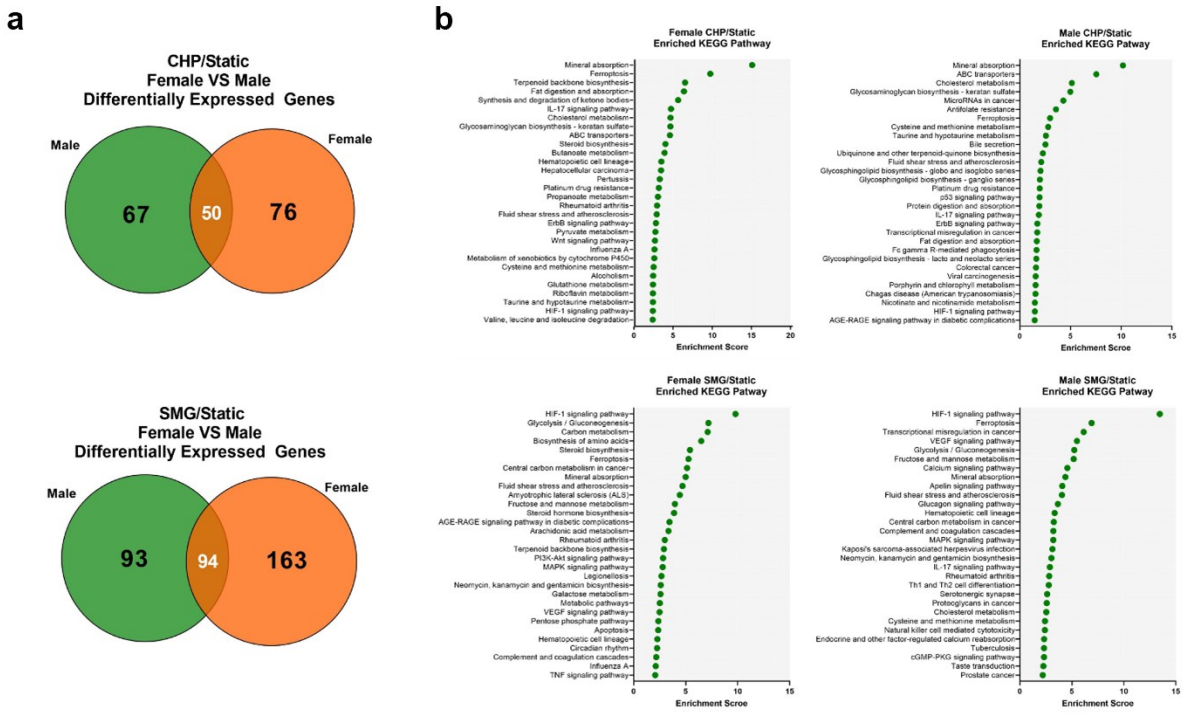

Figure 3.5 Transcriptome response of female and male donors to CHP and SMG.

a. Overlap of DEGs of female and male donors exposed to CHP and SMG. b. Top enriched KEGG pathways by identified DEGs. KEGG terms were selected by p-value and plotted to the enrichment score.

In relation to mechanobiology of the meniscus, we investigated the transcriptome profile changes of various mechanosensitive molecules such as *TRPV1/4*, *PIEZO1*, *TMEM63A/B/C*, and *RUNX2* (163-167). Furthermore, the mechanotransduction function of *FOSB* in MFCs (54) was reported by Szojka et al., and its function in the IL-17 signaling pathway was well demonstrated (168). Finally, Vyhlidal et al. recognized the

potential of caveolae molecules such as *CAV1/2* in the mechanotransductive mechanism of the meniscus, but this needs to be further verified in future studies (41). The transcriptome changes are summarized in Table 3.4. Within our dataset, only *CAV1*, *CAV2*, and *FOSB* are significant by q-value for loading regime comparison and sex-based comparison. *CAV2* was regulated in the opposite direction by CHP and SMG. CHP upregulated *FOSB* by 49.5-fold compared to 3.4-fold by SMG. The difference was even larger in female tissues (137.8-fold by CHP and 2.8-fold by SMG), and in comparison, the fold change of *FOSB* expression was similar by CHP and SMG for male tissues (9.7-fold and 3.7-fold). Other mechanosensitive molecules were not significantly modulated from the treatments. The transcriptome profile changes suggest sex-dependent differences in the mechanotransduction mechanisms as well as varying capabilities to sense cytoskeletal structural changes

Table 3.3 Key enriched KEGG pathways and associated differentially expressed genes (DEGs) in CHP and SMG groups as compared to static controls within female and male donor cohorts.

Gene	**Description**	**Fold Change: CHP/Static**			**Fold Change: SMG/Static**		
		Female	Male	Combined	Female	Male	Combined
KEGG: Mineral absorption							
FTH1	Ferritin Heavy Chain 1	2.18*	3.47*	1.70*	3.47*	2.32*	2.77***
HMOX1	Heme Oxygenase 1	2.94*	3.51**	2.83***	3.51**	3.28**	3.38***
MT1E	Metallothionein 1E	2.79**	1.96*	2.48***	1.96*	-1.09	1.32
MT1G	Metallothionein 1G	8.25*	3.29	9.38**	3.29	1.11	2.21
MT1M	Metallothionein 1M	2.59**	1.89*	2.20***	1.89*	-1.35	1.14
MT2A	Metallothionein 2A	2.59*	1.57	2.79***	1.57	1.18	1.35
SLC30A1	Solute Carrier Family 30 Member 1	2.21**	2.03*	1.70**	2.03*	1.23	1.57**
SLC8A1	Solute Carrier Family 8 Member A1	-2.13	1.15*	-1.44	1.15*	-3.13*	-2.91**
KEGG: Wnt signaling pathway							
FOSL1	FOS Like 1, AP-1 Transcription Factor Subunit	2.99*	3.88**	3.44***	1.16	1.88	1.53
FZD2	Frizzled Class Receptor 2	-2.22*	-1.25	-1.68*	-1.48	-1.12	-1.30
NOTUM	Notum, Palmitoleoyl-Protein Carboxylesterase	6.71*	1.77	2.97*	1.17	-1.94	-1.48
SFRP2	Secreted Frizzled Related Protein 2	-6.22*	-3.03*	-4.07**	-2.55	-3.15	-2.82*
KEGG: HIF-1 signaling pathway							
EGLN3	Egl-9 Family Hypoxia Inducible Factor 3	1.00	2.49	1.58	-4.24*	-5.75*	-4.72***

ENO2	Enolase 2	-1.24	1.48	1.11	-2.96*	-2.51	-2.74**
GAPDH	Glyceraldehyde-3-Phosphate Dehydrogenase	-1.14	1.24	1.06	-2.27*	-2.21	-2.24**
HK2	Hexokinase 2	-1.61	1.03	-1.21	-2.20*	-2.66*	-2.41**
HMOX1	Heme Oxygenase 1	2.94*	2.74*	2.83***	3.51**	3.28**	3.38***
LDHA	Lactate Dehydrogenase A	1.21	1.31	1.26	-1.94*	-2.04*	-1.98***
PDK1	Pyruvate Dehydrogenase Kinase 1	-1.28	-1.13	-1.20	-2.89**	-3.43**	-3.11***
PFKFB3	6-Phosphofructo-2-Kinase/Fructose-2,6-Biphosphatase 3	-1.80	-1.15	-1.44	-2.33*	-2.34*	-2.33**
PGK1	Phosphoglycerate Kinase 1	1.17	1.23	1.20	-2.04*	-2.24*	-2.13***
TFRC	Transferrin Receptor	2.80**	1.36	1.92**	2.55**	2.22*	2.35***
VEGFA	Vascular Endothelial Growth Factor A	-1.57	-1.11	-1.33	-5.48**	-5.95*	-5.68***
KEGG: IL-17 signaling pathway							
CCL2	C-C Motif Chemokine Ligand 2	3.85*	3.48**	3.62***	3.51**	1.41	2.17**
FOSB	FosB Proto-Oncogene, AP-1 Transcription Factor Subunit	137.8*	9.70	49.48**	2.82	3.66	3.40
FOSL1	FOS Like 1, AP-1 Transcription Factor Subunit	2.99*	3.88**	3.44***	1.16	1.88	1.53
MAPK13	Mitogen-Activated Protein Kinase 13	-1.51	1.31	-1.07	-3.05*	-3.01*	-3.03***
MMP13	Matrix Metallopeptidase 13	1.56*	1.38	1.51	1.64	2.57*	1.89**
MMP3	Matrix Metallopeptidase 3	10.5**	4.36	6.47***	-1.80	-3.99*	-2.82**
KEGG: Fluid Shear stress and atherosclerosis							
CCL2	C-C Motif Chemokine Ligand 2	3.85*	3.48**	3.62***	3.51**	1.41	2.17**
HMOX1	Heme Oxygenase 1	2.94**	2.74**	2.83***	3.51**	3.28**	3.38***
MAP3K5	Mitogen-Activated Protein Kinase Kinase Kinase 5	-1.37	-1.39	-1.38	2.38*	1.49	1.87**
MAPK13	Mitogen-Activated Protein Kinase 13	-1.51	1.31	-1.07	-3.05*	-3.01*	-3.03***
MGST1	Microsomal Glutathione S-Transferase 1	2.21**	1.40	1.65**	1.86*	1.25	1.43**
NQO1	NAD(P)H Quinone Dehydrogenase 1	3.83***	2.40**	2.88***	4.04***	2.42**	2.97***
PLAT	Plasminogen Activator, Tissue Type	1.51	2.27	1.88*	2.51*	2.43*	2.47**
PRKAA2	Protein Kinase AMP-Activated Catalytic Subunit Alpha 2	-1.37	1.44	1.03	-4.63*	-2.90	-3.70**
VEGFA	Vascular Endothelial Growth Factor A	-1.57	-1.11	-1.33	-5.48**	-5.95*	-5.68***

*q<0.05, **q<0.01, ***q<0.001 represent statistical difference of the two groups in each fold change value.

3.4 Discussion

Currently, there is no existing model to reflect the physiological mechanism of OA holistically, but several *in vitro* and *in vivo* models have been developed to answer questions regarding the mechanisms of OA (169). This study aimed to evaluate the effects of mechanical loading and unloading via CHP and SMG, respectively, on the OA-related profile changes of engineered meniscus tissues and explore biological sex-related differences. This can serve as an *in vitro* model to investigate the cellular and molecular profiles responsible for the sex-dependent incidence of OA disease.

Cartilage is a highly mechanosensitive tissue, and appropriate levels of mechanical stimulation are crucial for homeostasis and healthy cartilage development. Mechanical stimuli are transmitted by the pericellular matrix (PCM) (133, 170) to the chondrocyte surface and sensed by mechano-receptors, triggering a cascade of downstream activities (71). The importance of mechanical loading under normal gravity environments has been demonstrated by studies examining the protective effects of moderate loading against tissue degradation as well as investigating the unwanted consequences from unloading. From several *in vitro* and *in vivo* models, mechanical loading has been shown to attenuate inflammatory cytokine-induced expression of matrix-degrading enzyme (171), upregulating the content of sulphated glycosaminoglycan (GAG), aggrecan, cartilage oligomeric matrix protein, type II collagen, and lubricin (PRG4) (172), and modulating relevant pathways such as the HIF-1 (173) and IL-4 (174) signaling pathways. On the contrary, prolonged mechanical unloading by space flight has been shown to accelerate cartilage degeneration (95, 111, 175). Although several studies suggested that SMG was beneficial for preserving a chondrogenic phenotype through induction of 3D aggregates from monolayer cultures (93, 96, 176) and promoted cartilaginous components deposition for scaffold cultures (177), the degree of hypertrophic differentiation was not investigated in these studies. Through regulation of key genes and molecular pathways, SMG was also reported to increase activities associated with cartilage catabolism (91, 97, 110) and promoted hypertrophic differentiation of chondrocytes (65, 92).

In addition to cartilage, the meniscus also plays a critical role in the biomechanics of the knee joint. Evidence has shown that the role of meniscus fibrochondrocytes (MFCs) in

response to mechanical signals affects the physiological, pathological, and repair response of the meniscus (165). The PCM of MFCs is also involved in mechanotransduction, although it may play a protective role against larger stresses and strains (178). Various *in vivo* studies have documented that mechanical stimulation can drive both anti- and pro-inflammatory responses in MFCs (179, 180), as well as the detrimental effects of mechanical unloading from joint immobilization on meniscus development, function, and repair (181-186). Additionally, several *in vitro* studies have shown the anabolic effect of mechanical loading on MFCs with enhanced meniscus ECM components like *ACAN* expression and collagens and mechanical properties (62, 187). Finally, there have been various *in vitro* meniscus repair models that utilized mechanical loading to suppress IL-1 mediated increases in MMP activity, enhance GAG production, and increase integrative strength of the engineered tissue constructs (165, 188-191).

Consistent with these previous reports, our results showed that mechanical loading via CHP increased the deposition of type II collagen and aggrecan, supported by immunofluorescence staining and gene expression analysis. In addition, the Safranin-O staining and biochemical quantification of GAG production per cell confirmed that CHP increased the chondrogenic potential of meniscus MFCs. As expected, the wet weight of engineered constructs in the CHP group was the highest among the three treatment groups since the GAG is a major water-binding component of cartilage (192). The ratio of *COL2A1* to *COL1A2* has also been used to evaluate chondrogenic capacity (96, 176), and in our results, CHP substantially increased the *COL2A1/ COL1A2* ratio compared to SMG groups. Although upregulation of type II collagen deposition and *COL2A1* expression was observed in the SMG groups compared to static controls, the magnitude of upregulation was not less than in the CHP groups. The GAG/DNA ratio of the SMG group was also lower than static controls in addition to a stronger intensity of type X collagen staining. Taken together, our data highlights the detrimental effect of SMG on the chondrogenic capacity of the engineered meniscus and suggests that mechanical unloading increases the hypertrophic differentiation of MFCs, driving them to display OA-like characteristics.

To the best of our knowledge, this is one of the first studies to investigate the effect of mechanical loading and unloading on cartilage models by examining global transcriptome profile alterations. The ECM of chondrocytes is crucial for regulating key functions through receptor-mediated matrix-cell interactions. The composition of the ECM and the bound signaling molecules largely influences the chondrogenic capacity of embedded chondrocytes (193). By overlaying the DEGs, we found that CHP and SMG regulated MFC functions through largely different mechanisms. As listed in Table 3.2, several Wnt-signaling pathway-related genes were strongly regulated by CHP, in addition to various matrix remodeling enzymes. But for SMG, the genes with the highest fold-change functioned in more general ways, such as the several growth factors encoding genes identified to regulate general development processes. The KEGG pathway analysis also showed that several chondrogenesis- and OA-related pathways such as mineral absorption, Wnt-signalling pathway, HIF-1 signalling pathways, and IL-17 signalling pathway were enriched by both CHP and SMG. However, the expression profile of related genes in terms of magnitude and direction was quite different (Table 3.3). It is worth mentioning that no sex hormone-related pathways were present in the top enriched pathways. Thus, the observed sex-dependent differences are independent of differences between sex-related hormones. Taken together, the comparative transcriptome analysis suggested a distinct effect of CHP and SMG on regulating chondrogenesis, but further investigations are needed to determine the specific underlying mechanisms.

The cellular and molecular mechanisms behind the well documented sex discrepancy in OA incident rates are poorly understood. Many factors are believed to contribute to the higher incidence and severity of OA in females, such as age, psychosocial status, metabolic variables, hormonal differences, anatomical variations, and inflammatory disease (194). While the focus of many previous studies was mainly on bone shape (195-197), gait kinematics (198-200), and sex hormones (98, 201-204), little effort was invested into determining differences in the global transcriptome profile. Two studies reported that female OA patients have higher levels of inflammatory cytokines in the synovial fluid than males (205, 206), but the underlying signaling mechanism was not investigated. To explore the sex-dependent differences in OA pathogenesis, we separated our donor cohort based on sex and compared the OA-related characteristics.

Although the female and male donor cohorts included in this study showed highly variable trends in terms of histological and immunofluorescence staining for cartilage markers like aggrecan and type II collagen, an expected similar trend was observed for *COL2A1*, *SOX9*, *ACAN*, and *COL2A1/COL1A2* average foldchange levels across donor and treatment groups. The average fold change level for *COL10A1* was comparable between the CHP and SMG groups for both sexes. However, one female donor showed significantly higher fold-changes for *COL10A1* while the remaining female cohort showed a generally reduced expression of *COL10A1* in CHP compared to SMG, but not significant. The observed deposition of type X collagen in immunofluorescence staining shows high variability, and sex-dependent differences are difficult to elucidate. Our results suggest overall that at the protein level, the effect of mechanical stimulation is more dominant than sex differences for the deposition of cartilaginous components.

A significant sex-dependent difference was observed for tissue contraction between female and male CHP groups. Additionally, the Pearson correlation network generated for the female and male donor cohorts shows clear sex-dependent differences in expression trends between contractile genes *ACTA2* and *TAGLN* in relation to the other factors investigated in this study. Firstly, the measured contraction based on the percentage of reduction in tissue area positively correlated with *ACTA2* and *TAGLN* expression levels in both female and male cohorts. This suggests that these contractile genes are indeed correlated with physical contraction levels in our study. Interestingly, *ACTA2* and *TAGLN* expression levels in relation to other factors show distinct sex-dependent differences. Among the female cohort, the contractile genes showed a mostly strong negative correlation with the other factors, while the genes in the male cohort showed a generally positive correlation. Mechanical loading has been suggested to mediate the function of chondrocytes by stimulating the reorganization of cytoskeleton (161, 162). And simulated microgravity was also reported to alter the structure of cytoskeleton components (176) and regulate the expression of several cytoskeletal genes (93). Since *ACTA2* and *TAGLN* activity is associated with cytoskeletal composition and structure, the opposite trend in correlation with other factors between the female and male cohort may suggest sex-dependent differences from cytoskeletal activity in response to varying levels of mechanical stimulation. Furthermore, the mechano-sensitive gene

FOSB in the IL-17 signaling pathway was identified in our dataset to show a 137.8-fold upregulation from CHP in the female cohort while only observing a 9.7-fold increase in the male cohort. This may suggest sex-dependent differences in the mechanotransduction mechanisms as well as varying capabilities to sense cytoskeletal structural changes arising from mechanical stimulation.

There are several limitations to our model explored in this study. Firstly, we did not have any tissue samples from OA patients to confirm the OA-phenotype observed in our model. However, the modulation of several OA markers (154) from SMG such as the upregulation of *MMP13* and the increased staining of collagen type X, reasonably suggest that the SMG treatment is pushing the engineered tissues constructs towards an OA-phenotype, and this effect is likely to increase with longer treatment periods. Another limitation is that even prolonged joint mobility under normal gravity can induce an OA-phenotype, and thus the static group in this study may also serve as an alternate condition for simulating OA. However, the static group here is meant as a baseline control between the two mechanical treatments and serves to reduce donor-to-donor variability by normalizing measurements to the static control within each donor. Finally, a limitation in our model is that although the engineered meniscus constructs contain the necessary component of fibrocartilage, the tissue microenvironment experienced by the cells is likely different from that of the native meniscus. In particular, the cells in the native meniscus may respond differently to receptor-mediated cell- ECM interactions from mechanical load than in the engineered meniscus models, especially due to differences in the matrix stiffness. We hope to address this limitation in our future studies by evaluating cytoskeleton factors and measurements and using substrates with tunable stiffnesses such as hydrogels.

3.5 Conclusion

Taken together, our data suggest that engineered meniscus tissues responded to mechanical loading and unloading via CHP and SMG in a sex-dependent manner. Mechanical unloading via SMG was shown to induce an OA-like profile, while mechanical loading via CHP promotes elements of chondrogenesis. Within each mechanical stimulation group, female and male donor cohorts show sex-dependent

differences in the magnitude and direction of many differentially expressed genes, as well as tissue contraction and correlation of contractile genes with the other factors investigated in this study. The combination of CHP and SMG can feasibly serve as an *in vitro* model to study the cellular and molecular mechanisms of KOA and provide a platform for exploring potential drug-targetable pathways as therapeutics.

3.6 Data availability statement

The datasets presented in this study can be found in online repositories. The names of the repository/repositories and accession number can be found below: GEO and GSE192982.

3.7 Funding

NSERC (NSERC RGPIN-2018-06290 Adesida) DL: NSERC Undergraduate Student Research Awards MK: Alberta Cancer Foundation-Mickleborough Interfacial Biosciences Research Program (ACF-MIBRP 27128 Adesida) AM-S: Canadian Institutes of Health Research (CIHR MOP 125921 Adesida) LW: University of Alberta Pilot Seed Grant Program (UOFAB PSGP); University of Alberta Women and Children's Health Research Institute Innovation Grant (UOFAB WCHRIIG 3126) AA: Natural Sciences and Engineering Research Council (NSERC RGPIN-2018-06290); Canadian Institutes of Health Research (CIHR MOP 125921 Adesida); Canada Foundation for Innovation (CFI 33786); University Hospital of Alberta Foundation (UHF; RES0028185 Adesida); Edmonton Orthopaedic Research Committee, Cliff Lede Family Charitable Foundation (RES00045921 Adesida); University of Alberta Pilot Seed Grant Program (UOFAB PSGP); University of Alberta Women and Children's Health Research Institute Innovation Grant (UOFAB WCHRIIG 3126); the Alberta Cancer Foundation-Mickleborough Interfacial Biosciences Research Program (ACF-MIBRP 27128 Adesida). Research grant funding for the work was provided by Natural Sciences and Engineering Research Council (NSERC RGPIN-2018-06290 Adesida), NSERC RTI-2019-00310 Adesida; Canada Foundation for Innovation (CFI 33786); University Hospital of Alberta Foundation (UHF; RES0028185 Adesida); Edmonton Orthopaedic Research Committee, Cliff Lede Family Charitable Foundation (RES00045921 Adesida); University of Alberta Pilot Seed Grant Program (UOFAB PSGP); University of Alberta Women and Children's

Health Research Institute Innovation Grant (UOFAB WCHRIIG 3126); the Alberta Cancer Foundation-Mickleborough Interfacial Biosciences Research Program (ACF-MIBRP 27128 Adesida).

3.8 Acknowledgement

We thank Tara Stach and the team at the Biomedical Research Centre from the University of British Columbia for their help with RNA sequencing.

3.9 Supplementary materials

Supplementary Figure 3.1 Strain-controlled undefined compression test was used to measure the peak modulus of samples at three indicated strain levels.

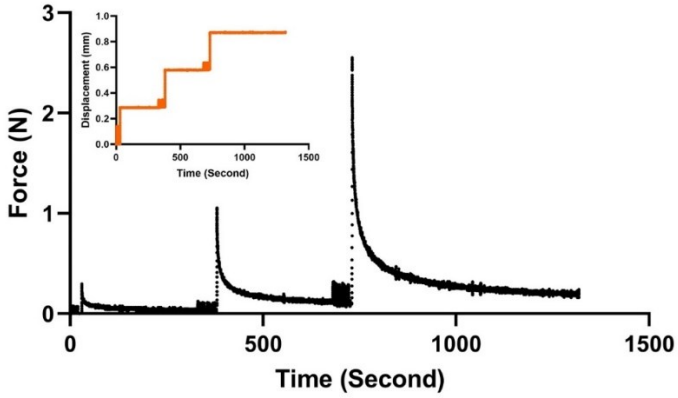

Supplementary Figure 3.2 Linear regression was used to evaluation to correlation between gene expression value measured by qRT-PCR and RNA-Seq.

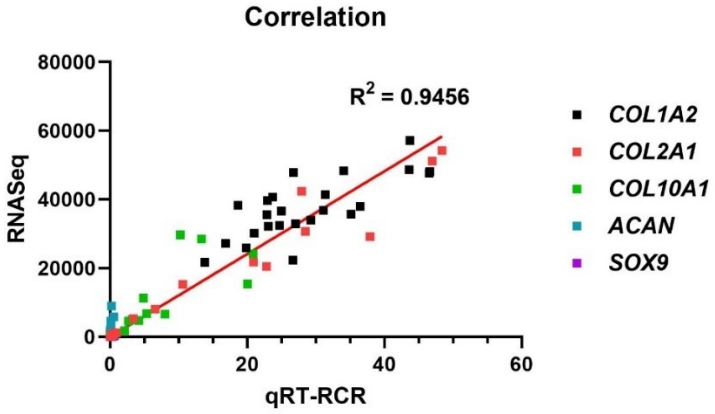

Supplementary Material 3.3 Detailed sequence of mechanical testing protocol.

1. Dwell (wait): 5s
2. Sine (cyclic compression): -5% strain amplitude at 1 Hz for 15 cycles
3. Dwell: 10s
4. Ramp (increase compression): at a speed of -50% strain/s to -10% strain
5. Dwell: 300s
6. Sine: -2% strain amplitude at 0.5 Hz for 10 cycles
7. Dwell: 5s
8. Sine: -2% strain amplitude at 1 Hz for 10 cycles
9. Dwell: 5s
10. Sine: -2% strain amplitude at 2 Hz for 10 cycles
11. Dwell: 5s
12. Ramp: at a speed of -50% strain/s to -20% strain
13. Dwell: 300s
14. Sine: -2% strain amplitude at 0.5 Hz for 10 cycles
15. Dwell: 5s
16. Sine: -2% strain amplitude at 1 Hz for 10 cycles
17. Dwell: 5s
18. Sine: -2% strain amplitude at 2 Hz for 10 cycles
19. Dwell: 5s
20. Ramp: at a speed of -50% strain/s to -30% strain
21. Dwell: 600s
22. Sine: -2% strain amplitude at 0.5 Hz for 10 cycles
23. Dwell: 5s
24. Sine: -2% strain amplitude at 1 Hz for 10 cycles
25. Dwell: 5s
26. Sine: -2% strain amplitude at 2 Hz for 10 cycles
27. Dwell: 5s
28. Ramp: release compression

Supplementary Figure 3.4 Effect of CHP and SMG on tissue contraction; contraction is calculated as the % of area lost as compared to the original area. No statistical analysis was conducted for the contraction data with the male SMG group due to limited data points

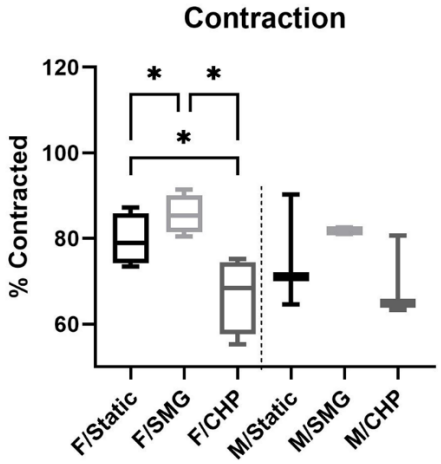

Supplementary Table 3.1 Real-time qPCR Primer Sequences.

Gene	Forward	Reverse	GenBank Accession
ACAN	AGGGCGAGTGGAATGATGTT	GGTGGCTGTGCCCTTTTTAC	NM_001135.3
B-actin	AAGCCACCCCACTTCTCTCTAA	AATGCTATCACCTCCCCTGTGT	NM_001101.4
B2M	TGCTGTCTCCATGTTTGATGTATCT	TCTCTGCTCCCCACCTCTAAGT	NM_004048.3
COL1A2	GCTACCCAACTTGCCTTCATG	GCAGTGGTAGGTGATGTTCTGAGA	NM_00008 9.3
COL2A1	CTGCAAAATAAAATCTCGGTGTTCT	GGGCATTTGACTCACACCAGT	NM_001844.5
COL10A1	GAAGTTATAATTTACACTGAGGGTTTCAAA	GAGGCACAGCTTAAAAGTTTTAAACA	NM_000493.3
SOX9	CTTTGGTTTGTGTTCGTGTTTTG	AGAGAAAGAAAAAGGGAAAGGTAAGTTT	NM_000346.3
YWHAZ	TCTGTCTTGTCACCAACCATTCTT	TCATGCGGCCTTTTTCCA	NM_003406.3

Chapter 4

Mechanical Unloading of Engineered Human Meniscus Models Under Simulated Microgravity: A Transcriptomic Study

Chapter 4.1 and 4.2 have been previously published as:

Ma Z, Li DX, Chee RKW, Kunze M, Mulet-Sierra A, Sommerfeldt M, Westover L, Graf D, Adesida AB. Mechanical Unloading of Engineered Human Meniscus Models Under Simulated Microgravity: A Transcriptomic Study. *Sci Data*. 2022; 9(1):736.

4.1 Introduction

Osteoarthritis (OA) is a degenerative joint disease that primarily affects mechanical load-bearing joints, with the knee being the most common (98, 102). Much of the focus of OA is on knee osteoarthritis (KOA) due to its 83% prevalence among cases of OA (142, 207). Most demographic groups are affected by OA, but the prevalence and burden are disproportionately higher in females (6, 7, 98, 103, 143-145). While sex hormones regulate joints' cartilage and bone development and homeostasis in a sex-dependent manner, hormonal differences alone do not fully account for the higher incidence of OA in females (143). Kinney et al. reported that sex-specific variations in the response of human articular chondrocytes to estrogen are due to differences in receptor number and the mechanisms of estrogen action (104).

The molecular basis for sex differences in the burden of KOA is not well understood, and questions remain for the cellular and molecular events underlying the pathogenesis and progression of KOA. However, some cellular and molecular characteristics of KOA resemble chondrocyte hypertrophy before endochondral ossification during skeletogenesis (146). This includes chondrocyte proliferation, chondrocyte hypertrophy along with upregulation of hypertrophy markers *COL10A1* (147) and *MMP13* (148),

remodeling of the cartilage matrix by proteases, vascularization, and focal calcification of cartilage with hydroxyapatite crystals.

A plethora of *in vitro* and *in vivo* studies show joint cartilage atrophy after long-term mechanical unloading (i.e., joint immobilization) (59, 64, 92, 109, 208-213). For example, in a case study involving ten healthy young individuals (4 males and 6 females), with no history of KOA requiring 6 to 8 weeks of non-weight bearing for injuries affecting the distal lower extremity, the axial mechanical unloading of the joint resulted in increased magnetic resonance imaging (MRI) parameters, T1rho and T2 relaxation times, of the knee articular cartilage that resembled signs of KOA. After four weeks of returning to axial mechanical loading, the T1rho and T2 relaxation times were restored to baseline values of normal healthy articular cartilage (109). However, it is unknown if the magnitude or rate of cartilage atrophy was disproportionate between the male and female participants after mechanical unloading. And neither were knee menisci investigated despite their functional importance for load distribution across the knee joint.

The effects of mechanical unloading on cartilage have been studied via simulated microgravity (SMG) (59, 61, 64, 65, 152). Microgravity, both real and simulated, as well as reduced weight-bearing, have been shown to induce detrimental effects on cartilage, and in some cases, promote an OA-like phenotype (64, 92, 111, 175, 208, 209, 213). This makes SMG a relevant model to study OA-related changes in chondrocytes from mechanical unloading conditions (64, 152). SMG can be produced by rotating wall vessel (RWV) bioreactors developed by the National Aeronautics Space Administration (NASA). RWV rotates at a constant speed to maintain tissues in a suspended free-fall, resulting in a randomized gravitational vector (92, 153). Our group has demonstrated that four weeks of SMG using a RWV bioreactor could enhance KOA-like gene modulations in bioengineered cartilage (65). Specifically, *COL10A1* and *MMP13* as markers of chondrocyte hypertrophy were significantly increased by SMG (65). However, the potential of mechanical unloading and molecular profiling techniques to explore the molecular basis of the disproportionate incidence of KOA in females is yet to be explored. Menisci from KOA joints have been reported to exhibit similar molecular characteristics found in osteoarthritic articular cartilage (140, 154). Osteoarthritic

meniscus fibrochondrocytes (MFC) produced more calcium deposits than normal MFC (140, 214). Moreover, osteoarthritic MFC expressed aggrecan (*ACAN*) at a significantly higher level than normal MFC (214). More recently, type X collagen and MMP13 were shown to be highly expressed in osteoarthritic meniscus relative to the normal meniscus (154). As both proteins are markers of chondrocyte hypertrophy, these findings suggested that MFC undergoes hypertrophic differentiation like osteoarthritic articular chondrocytes and that the knee menisci maybe actively involved in the pathogenesis of OA. The potential impact of OA on meniscus tissue was also explored in a mice model that was exposed to either microgravity on the International Space Station or hind limb unloading (208). Prolonged unloading in both treatments resulted in cartilage degradation, meniscal volume decline, and elevated catabolic enzymes such as MMPs (208).

In this study, meniscus models were generated from healthy human meniscus MFC seeded onto a type I collagen scaffold and cultured under SMG condition in RWV bioreactor with static normal gravity as controls. Full transcriptome RNA sequencing of 4 female and 4 male donors were conducted, along with the analysis of phenotypic characteristics. Data from this study could be used to further explore the mechanism of the early onset of KOA and to investigate the molecular basis of observed sex differences in KOA.

4.2 Methods

The experiment is outlined in Figure 4.1. Most culture methods and assays were performed identically to those described in previous work (54, 55, 155).

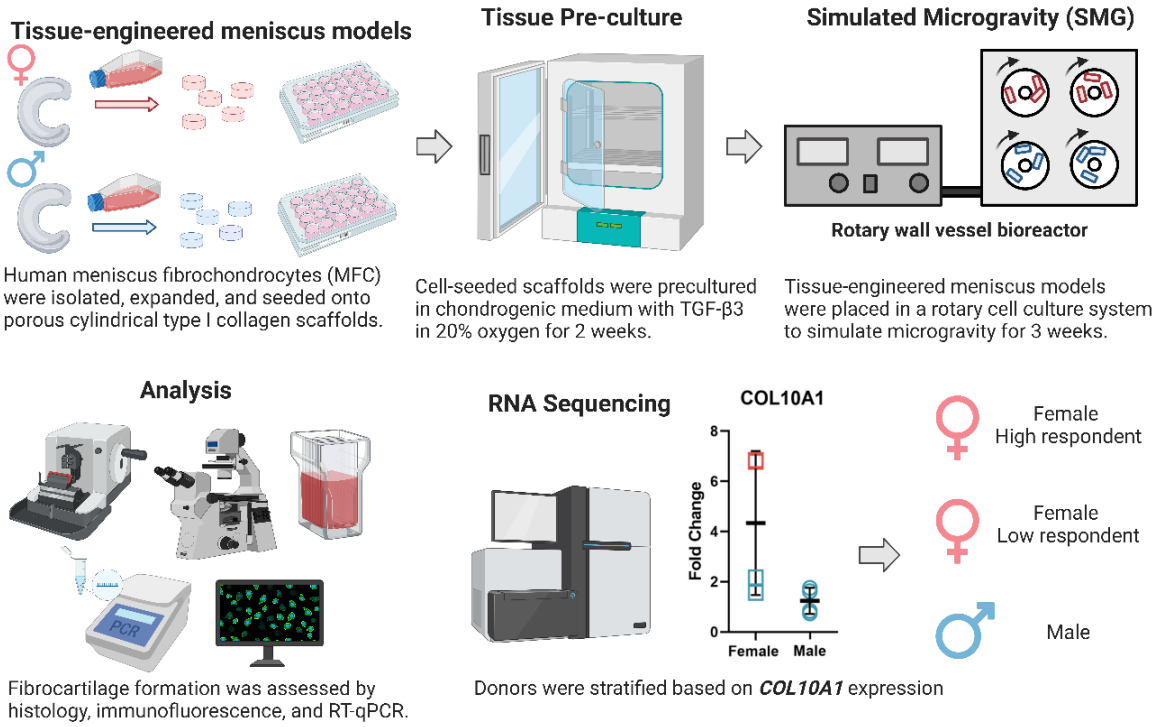

Figure 4.1 Experiment overview.

Human meniscus fibrochondrocytes (MFC) were isolated from 4 males and 4 females. Complete treatment was repeated for each donor. Created with BioRender.com.

4.2.1 Ethics statement

Human non-osteoarthritic inner meniscus samples were obtained from patients undergoing arthroscopic partial meniscectomies because of traumatic meniscal tears at the Grey Nuns Community Hospital in Edmonton. Experimental methods and tissue collection were with the approval of and in accordance with the University of Alberta's Health Research Ethics Board-Biomedical Panel (Study ID: Pro00018778). The ethics

board waived the need for written informed consent of patients, as specimens used in the study were intended for discard in the normal course of the surgical procedure. Extensive precautions were taken to preserve the privacy of the participants donating specimens such that only patient sex, age, weight, height, and underlying health conditions were provided.

4.2.2 Cell isolation

Meniscus fibrochondrocytes (MFC) were isolated from inner meniscus specimens by digestion with type II collagenase (0.15% w/v of 300 units/mg; Worthington). For this, the inner meniscus specimens were first cut into smaller pieces. The type II collagenase solution in high glucose Dulbecco's modified Eagle's medium (HG-DMEM) supplemented with 5% (v/v) fetal bovine serum (FBS) was added to pieces at a ratio of 10 mL per 1 g of the meniscus and left to incubate at 37 °C for 22 hours in an orbital shaker set at 250 rpm. After digestion, the cell suspension was filtered through a 100 μm nylon mesh filter (Corning Falcon, NY, USA), and MFC were isolated by centrifuge. The isolated MFC were plated for 48 hours to recovery before cell expansion.

4.2.3 Cell expansion

After 48 hours, the MFC were detached by 0.05% w/v trypsin-EDTA in Hank's buffered saline solution (Invitrogen, CA, USA) and plated in a tissue culture flask (Sarstedt, Germany) at 1×10^4 cells/cm^2 in HG-DMEM supplemented with 10% v/v heat-inactivated fetal bovine serum (FBS), 100 mM 4-(2-hydroxyethyl)-1- piperazineethanesulfonic acid (HEPES), 1 mM sodium pyruvate (all from Sigma-Aldrich Co., MO, USA), and 100 U/mL penicillin, 100 μg/mL streptomycin and 0.29 mg/mL glutamine (PSG; Life Technologies, ON, Canada), and 5 ng/mL of FGF-2 (Neuromics, MH, USA, catalog #: PR80001) and 1 ng/mL of TGF-β1 (ProSpec, catalog #: CYT-716) for 1 week. Cell population doubling (PD) was calculated as log2(N/NO), where NO and N are the number of MFC respectively at the beginning and the end of the cell amplification period.

4.2.4 3D Cell culture in porous type I collagen scaffold

The expanded MFC were resuspended in a defined serum-free chondrogenic medium HG-DMEM supplemented with HEPES, PSG, ITS+ premix, 125 μg/mL of human serum albumin, 100 nM of dexamethasone, 365 μg/mL ascorbic acid 2-phosphate, 40 μ/mL of L-proline, and 10 ng/mL of TGF-β3, followed by seeding onto type I collagen scaffolds (diameter: 6 mm or 10 mm; height: 3.5 mm; pore size: 115 ± 20 μm, Integra LifeSciences, NJ, USA) at the density of 5×10^6 cells/cm`. The cell-seeded scaffolds were cultured in a 24-well plate (12-well plate for 10 mm scaffolds) with serum-free chondrogenic medium for 2 weeks for initial extracellular matrix formation. Medium change was performed once per week.

4.2.5 Mechanical stimulation

After 2 weeks of preculture, engineered meniscus tissues of each donor were randomly assigned to two mechanical stimulation groups: static control under normal gravity and simulated microgravity (SMG). Each experimental group had 8 technical replicates of engineered tissue constructs. For the static control group, engineered constructs were cultured in a tissue culture tube (Sarstedt, Germany) with 55 mL serum-free chondrogenic medium for 3 weeks. For the SMG group, the same number of constructs were cultured in the slow turning lateral vessels (STLV; Synthecon, Inc., TX, USA) on a rotary cell culture system (RCCS-4; Synthecon, Inc.) with 55 mL of serum-free chondrogenic medium for 3 weeks. The rotation speed of the STLV was adjusted during the 3-week treatment to account for the increasing weight of the tissues and to maintain a stable free-falling position (30 rpm from day 1 to day 2, 34 rpm from day 3 to day 7, 37 rpm day from 8 to day 13, 40 rpm day from 14 to day 21). Medium change was performed for both groups once per week.

4.2.6 Histology and immunofluorescence

After 3 weeks of mechanical stimulation, constructs intended for histology and immunofluorescence were fixed in 1 mL of 10% v/v buffered formalin (Fisher Scientific, MA, USA) overnight at 4 °C, dehydrated, and embedded in paraffin wax. The embedded

tissues were sectioned at 5 μm thickness and stained for Safranin O, Fast Green, Haematoxylin, collagen type I, collagen type II, and collagen type X.

For immunofluorescence staining, the sections were first deparaffinized and rehydrated. Protease XXV (Thermo Scientific) and hyaluronidase (Sigma-Aldrich) were then applied for 30 min each to improve antigen accessibility. Blocking was performed with 5% w/v bovine serum albumin in PBS for 30 min before staining for the primary antibody. Collagen type I, type II, and type X were stained with a 1:200 dilution of rabbit anti-collagen I antibody (CL50111AP-1; Cedarlane Labs, ON, Canada), a 1:200 dilution of mouse anti-collagen II antibody (II-II6B3, Developmental Studies Hybridoma Bank, IA, USA), and a 1:100 dilution of rabbit anti-collagen X antibody (ab58632; Abcam, UK), respectively. The sections were incubated with primary antibodies overnight at 4 °C. Secondary antibody labelling was applied on the second day. A 1:200 goat anti-rabbit IgG (H&L Alexa Fluor 594; Abcam) was used for collagen I and X. A 1:200 goat anti-mouse IgG (H&L Alexa Fluor 488; Abcam) was used for collagen II. Cell nuclei were stained with DAPI (4′, 6-diamidino-2-phenylindole; Cedarlane) after secondary antibody staining. The slides were finally mounted with a 1:1 ratio of glycerol and PBS. The Eclipse Ti-S microscope (Nikon Canada; ON, Canada) was used for immunofluorescence images.

4.2.7 RNA extraction, RT-qPCR and RNA sequencing

Constructs intended for transcriptome analysis were preserved in Trizol (Life Technologies) immediately upon harvesting and stored at −80 °C until RNA extraction. For female and male donors # 1, 2, and 3, RNA was extracted and purified from ground samples using PuroSPIN Total DNA Purification KIT (Luna Nanotech, Canada) following the manufacturer's protocol. For female and male donors # 4, RNA was extracted and purified from ground samples using RNeasy Minikits (Qiagen, ON, Canada) following the manufacturer's protocol. The quality of purified RNA was assessed by Nanodrop One (Thermo Scientific, USA), and fixed mass of RNA were sent for RNA sequencing at the University of British Columbia Biomedical Research Centre (UBC-BRC). A standard quality control assessment was conducted on the RNA samples prior to sequencing. All RNA samples showed reasonable quality, and no noticeable

differences were observed in quality between the two isolation methods. RNA sequencing was performed on the Illumina NextSeq. 500 with paired-end 42 bp × 42 bp reads and FastQ files were obtained from sequenced donors for further bioinformatics analysis.

Extracted RNA was reverse transcribed into cDNA with GoScript reverse transcriptase (Fisher Scientific) and amplified by reverse transcription-quantitative polymerase chain reaction (RT-qPCR) for chosen genes with specific primers (Table 4.1). The expression level of selected genes was normalized to chosen housekeeping genes (Table 4.1; *β-actin*, *B2M*, and *YWHAZ*) based on the coefficient of variation (CV) and M-value as measures of reference gene stability (157), and the data was presented using the $2^{-\Delta\Delta CT}$ method (158, 159). An unpaired t-test was performed between treatment groups.

Table 4.1 RT-qPCR Primer Sequences.

Gene	Forward	Reverse	GenBank Accession
ACAN	AGGGCGAGTGGAATGATGTT	GGTGGCTGTGCCCTTTTTAC	NM_001135.3
B-actin	AAGCCACCCCACTTCTCTCTAA	AATGCTATCACCTCCCCTGTGT	NM_001101.4
B2M	TGCTGTCTCCATGTTTGATGTATCT	TCTCTGCTCCCCACCTCTAAGT	NM_004048.3
COL1A2	GCTACCCAACTTGCCTTCATG	GCAGTGGTAGGTGATGTTCTGAGA	NM_00008 9.3
COL2A1	CTGCAAAATAAAATCTCGGTGTTCT	GGGCATTTGACTCACACCAGT	NM_001844.5
COL10A1	GAAGTTATAATTTACACTGAGGGTTTCAAA	GAGGCACAGCTTAAAAGTTTTAAACA	NM_000493.3
SOX9	CTTTGGTTTGTGTTCGTGTTTTG	AGAGAAAGAAAAAGGGAAAGGTAAGTTT	NM_000346.3
YWHAZ	TCTGTCTTGTCACCAACCATTCTT	TCATGCGGCCTTTTTCCA	NM_003406.3

4.2.8 Bioinformatics and donor stratification

RNA sequencing data were analyzed with Partek® Flow® software (Version 10.0.21.0302, Copyright © 2021, Partek Inc., St. Louis, MO, USA). A quality score threshold of 20 was set to trim the raw input reads from the 3′ end. Trimmed data were then aligned to the reference human genome hg38 using the STAR 2.7.3a aligner and followed by the quantification to a transcript model (hg38-RefSeq Transcripts 94 - 2020-05-01) using the Partek E/M algorithm. A noise reduction filter was applied to exclude genes whose maximum read count was below 50. Quantified and filtered reads were then normalized using the Add: 1.0, TMM, and Log 2.0 methods in sequential order. Based on

the fold change of *COL10A1* expression level (SMG to static), sequenced female donors were stratified into a high-response group and a low-response group, while male donors remained in one group for further analysis. Statistical analysis was performed using analysis of variance (ANOVA) for sex and treatment. Differentially expressed genes (DEGs) for each comparison were determined by p-value and fold change (FC). Principal component analysis (PCA) and the visualization of DEGs using Venn diagrams were all conducted in Partek® Flow® software.

4.2.9 Data records

All data generated during this study are deposited in the National Centre for Biotechnology Information (NCBI) Gene Expression Omnibus (GEO) with accession number GSE192983. The deposited data includes the raw FastQ files and.txt files containing normalized counts generated as described in the method section. The raw RNA sequencing dataset can be found in the online repository (https://identifiers.org/geo/GSE192983). The histology and immunofluorescence figures of each treatment group for all donors can be accessed at Figshare (215).

4.2.10 Technical validation

The non-identifiable information of the donors of meniscal specimens is listed in Table 4.2. After the 2-week preculture and 3-week mechanical stimulation periods, engineered meniscus constructs' chondrogenic and hypertrophic differentiation potential was qualitatively assessed with Safranin O staining and collagen type I, II, and X immunofluorescence staining (Figure 4.2). Donors from both biological sexes exhibited cartilage-like phenotype with a wide range of chondrogenic capacity at the static baseline. Tissues that intensively stained for Safranin O and collagen type II showed more hyaline cartilage-like phenotype, while the rest with strong collagen type I staining showed more fibrous cartilage-like phenotype. The expression levels of collagen type X were comparable for all donors under static conditions. SMG upregulated collagen type X expression in nearly all donors, but the highly variable staining between donors makes it difficult to determine sex differences.

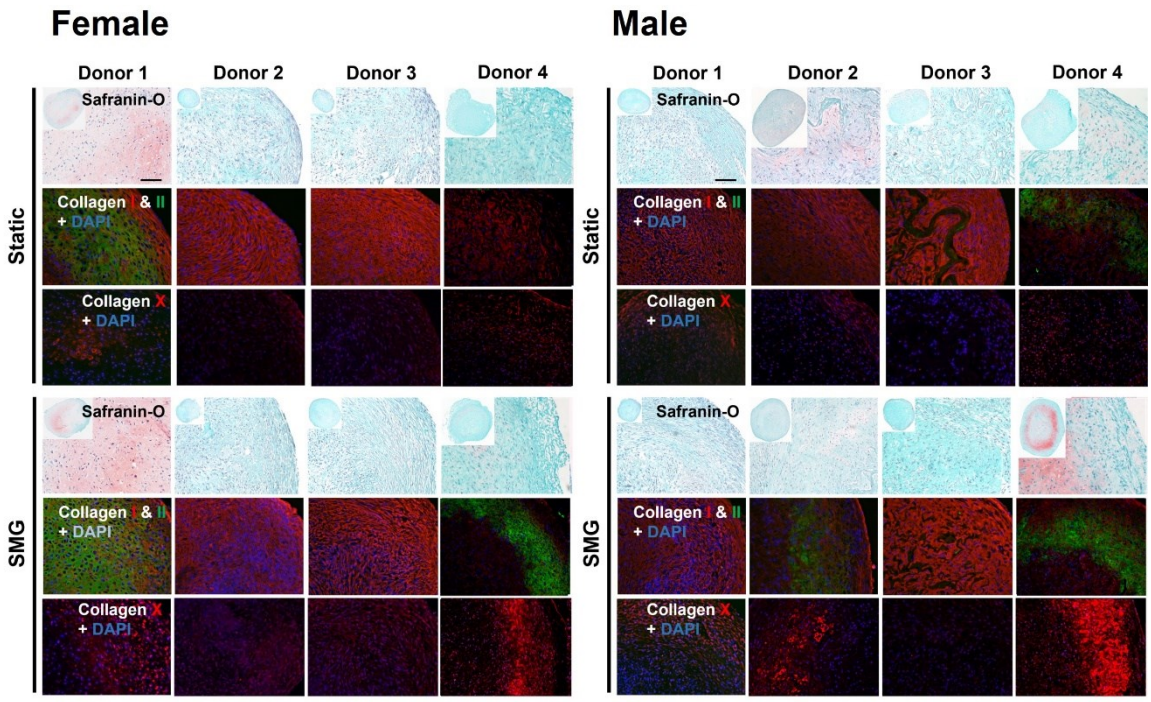

Figure 4.2 Impact of SMG in the chondrogenic and hypertrophic differentiation potential of engineered meniscus tissues.

For each treatment group (static or SMG), top panel: safranin O staining, middle panel: collagen types I, II immunofluorescence staining, bottom panel: collagen type X immunofluorescence staining. Scale bar: 100 μm

Table 4.2 Meniscal specimen non-identifying donor information.

Sex	Donor Number	Age	Population Doubling (PD)	Sample Code
Female	Donor 1	33	2.687	ScACS1.1, ScACS1.2
	Donor 2	44	2.38	ScACS3.1, ScACS3.2
	Donor 3	30	2.774	ScACS4.1, ScACS4.2
	Donor 4	31	1.599	ScAAK9, ScAAK10
Male	Donor 1	19	3.349	ScACS2.1, ScACS2.2
	Donor 2	45	2.699	ScACS5.1, ScACS5.2
	Donor 3	22	3.247	ScACS6.1, ScACS6.2
	Donor 4	59	2.263	ScAAK7, ScAAK8

The summary information of the generated RNA sequencing and processing quality data of each sample is listed in Table 4.3. The RNA Integrity Number (RIN) of all sequenced samples were close to 10 (10 is the highest possible RNA quality), and the average pre-alignment read quality had Phred scores above 30, indicating high-quality reads. The trimming and alignment algorithm used resulted in an average of at least 95% alignment as well as having the read quality Phred scores maintained. The authenticity of the RNA-sequencing data is also validated by calculating the degree of correlation with the RT-qPCR data of selected genes (Supplementary Figure 4.1). An R2 value of 0.828 was achieved, showing a strong correlation between the two transcription measurement methods.

Table 4.3 Quality data of RNA sequencing and bioinformatics processing.

* Phred Quality Score (-10log$_{10}$Prob) 30: Base call accuracy 99.9%, 40: Base call accuracy 99.99%.

					Pre-alignment			***Post-alignment***			
Sample Name	***Group***	***RNA extract. method***	***RNA conc. (ng/μL)***	***RIN***	***Total reads***	***Avg. read length***	***Avg. quality****	***Total reads***	***Aligned (%)***	***Avg. length***	***Avg. quality****
ScAAK7	Static		1.2	9.1	25994148	42.55	33.60	25851954	95.38	42.45	33.83
ScAAK8	SMG	RNeasy	1.2	9.1	22585197	42.54	33.65	22464022	95.80	42.44	33.87
ScAAK9	Static	Minikits	2.2	8.6	23676028	42.54	33.65	23550183	96.06	42.44	33.87
ScAAK10	SMG		2.1	8.7	20942143	42.54	33.52	20829886	95.89	42.43	33.74
ScACS1.1	Static		44	10	21673085	42.50	34.08	21649968	96.20	42.40	34.27
ScACS1.2	SMG		83	9.3	26393415	42.52	34.08	26363008	95.26	42.41	34.32
ScACS2.1	Static		93	9.6	24756374	42.50	34.03	24728910	96.41	42.39	34.23
ScACS2.2	SMG		68	9.5	24302152	42.49	34.06	24276178	96.47	42.38	34.27
ScACS3.1	Static	PuroSPIN	61	10	20187929	42.48	33.94	20166326	96.42	42.36	34.13
ScACS3.2	SMG	Total DNA	33	9.3	24542608	42.50	34.12	24520924	96.89	42.40	34.25
ScACS4.1	Static	Purification	108	10	24586213	42.50	34.10	24563673	96.93	42.39	34.24
ScACS4.2	SMG	KIT	156	10	23942119	42.50	34.06	23920514	96.99	42.39	34.21
ScACS5.1	Static		110	9.8	24244159	42.50	34.10	24222229	96.93	42.39	34.24
ScACS5.2	SMG		181	9.9	25369559	42.50	34.06	25347026	96.84	42.39	34.22
ScACS6.1	Static		126	9.7	23496618	42.50	34.12	23473652	96.64	42.40	34.26
ScACS6.2	SMG		175	10	23589464	42.50	34.06	23567332	96.80	42.39	34.21

To account for the effect of the donor variability observed in the previous analyses, a stratification strategy was introduced to separate donors into sub-groups based on the OA-inducing propensity of SMG. Female donors were stratified into high respondents with a higher fold change of *COL10A1* (female donor # 2: 6.84-fold and female donor # 4: 6.78-fold) and low respondents with a lower fold change of *COL10A1* (female donor # 1: 1.56-fold and female donor # 3: 2.17-fold). Male donors all had similar expression fold change of *COL10A1* and remained in one group. The stratification strategy was verified by the Venn diagram showing the overlap of DEGs between the SMG and static in each subgroup and the PCA plot (Figure 4.3b). All DEGs that appeared in the Venn diagram are listed in Supplement Tables 4.1–4.7. The majority of DEGs were unique to each identified group and the samples were well separated by treatment type on the first two principal component (PC) for both female high and female low respondent groups. Further, Table 4.4 shows a panel of selected OA-related genes that are only significantly modulated in SMG compared to static control for the Female High Respondents cohort. These genes were not significant in the Female Low Respondents or the Male cohorts.

Table 4.4 Select panel of OA-related genes from RNA sequencing.

Gene	**Fold Change for SMG vs Static**		
	Female High Respondent	**Female Low Respondent**	**Male**
BMP8A	8.51 **	-1.23 ns	-1.59 ns
CD36	11.8 *	1.93 ns	1.10 ns
COL10A1	6.81 ***	1.57 ns	1.17 ns
COL9A3	5.21 *	2.77 ns	-2.32 ns
FGF1	3.11 *	-2.99 ns	-5.48 ns
IBSP	46.1 *	1.19 ns	1.21 ns
IHH	4.38 *	-1.61 ns	-1.99 ns
MMP10	43.8 **	-3.42 ns	-5.29 ns
PHOSPHO1	2.42 *	1.34 ns	-1.45 ns
S100A1	3.42 *	2.01 ns	-2.34 ns
SPP1	46.8***	10.9 ns	4.2 ns

*p < 0.05; **p < 0.01; ***p < 0.001; ns = not significant

4.2.11 Code availability

The bioinformatics software used for this study is Partek® Flow® software (Version 10.0.21.0302, Copyright © 2021, Partek Inc., St. Louis, MO, USA) and the link of online REVIGO tool used is: http://revigo.irb.hr/.

4.3 Results

4.3.1 Transcriptome analysis

The transcriptome of a total of eight donors was analyzed by RNA sequencing. The entire dataset contained expression profiles of engineered meniscus tissues exposed to both static and SMG (16 in total). After a series of pre-processing steps as described in the methods, a total of 13199 genes were identified to be present in all sequenced tissues and therefore were used for downstream analysis.

4.3.2 Donor stratification

To account for the effect of the donor variability observed in the previous analyses, we introduced a stratification strategy to separate donors into sub-groups based on the osteoarthritis-inducing propensity of SMG. Although no single marker was sufficient to reflect the induction of osteoarthritic-like transcriptome profile, the expression of *COL10A1* has been shown to be indicative of osteoarthritic-like chondrocytes hypertrophic differentiation. Therefore, sequenced donors were stratified by normalization of (i.e., SMG to static) *COL10A1* expression level (Figure 4.3a). In this way, female donor 2 and female donor 6 with 6.84-fold and 6.78-fold *COL10A1* up-regulation were categorized into the high respondent group. Female donor 1 (1.56-fold change) and 3 (2.17-fold change) were categorized into the low respondent group. SMG regulated the expression of *COL10A1* for all male donors to a similar extent, with the fold change of 1.62-fold, 0.74-fold, 0.84-fold, and 1.75-fold for donors 1, 2, 3, and 5, respectively. All male donors were categorized into one group.

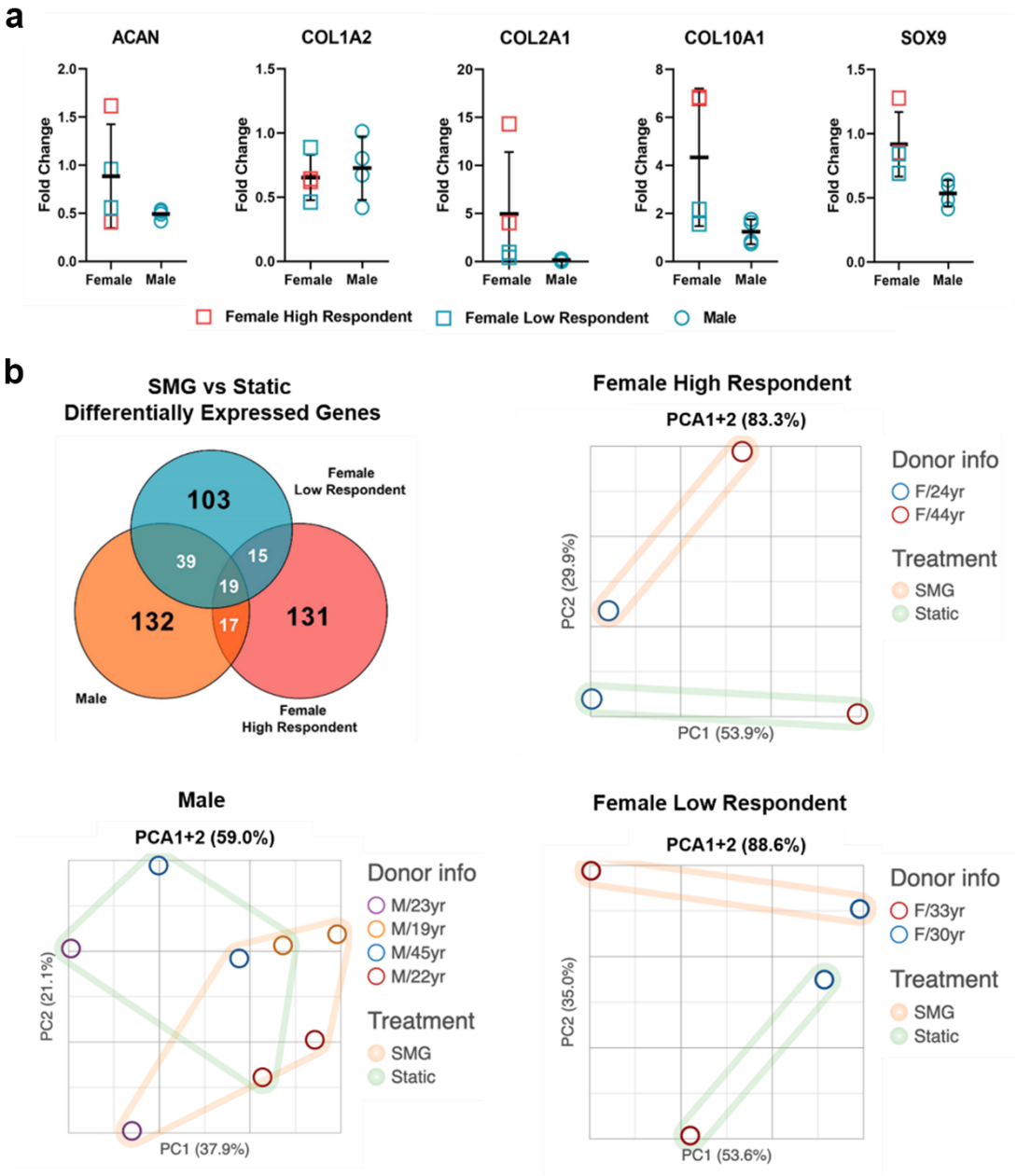

Figure 4.3 Donor stratification and distinct effect of SMG on sub-groups.

a. Gene expression by RNA sequencing. b. Distinct effect of SMG on each sub-group. DEGs of each group were overlaid and principal component analysis (PCA) was conducted for individual sub-groups.

4.3.3 Distinct effect of SMG on stratified donor groups

After stratifying the donors with the above-mentioned strategy, we overlaid the DEGs of each sub-group to compare the effect of SMG on the transcriptional profiles and to explore the direct relationship between the three donor groups (Figure 4.3b). The results showed that most genes differentially regulated by SMG were unique to each group with only 19 genes commonly shared by three groups, indicating the distinct effect of SMG on biological sex groups. Principal component analysis (PCA) on the transcription profiles exhibited the trend to separate donors by treatment for both female sub-groups, and the first two principles combined accounted for over 80% of the variance (Figure 4.3b). However, for the male group, the donors were not separated by treatment and only 59% of the variance was explained by the first two principal components (Figure 4.3b). The clustering pattern of PCA validated the distinct effect of SMG on different biological sex groups.

4.3.4 The effect of SMG on female high respondent

To further explore the specific effects of SMG on each female sub-group, we separated DEGs by the direction of modulation (up or down-regulation) and used the gene correlation network (GCN) approach to identify the co-expressed gene modules. Furthermore, the enriched gene ontology (GO) terms associated with each gene module were determined. The top significant enrichment terms for the female high respondent group are shown in Figure 4.4 and the genes of selected ECM or osteoarthritic relative GO terms are listed in Table 4.5 and Table 4.6.

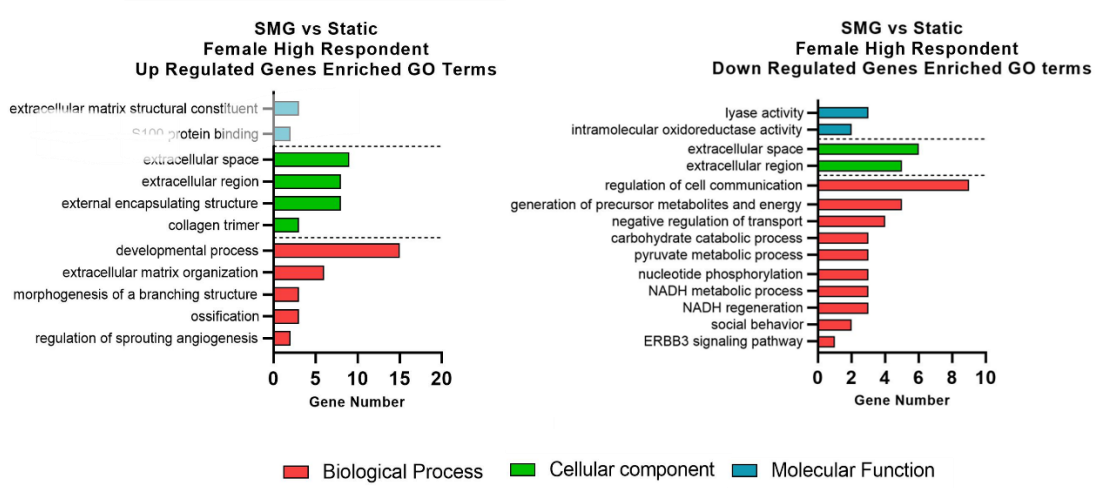

Figure 4.4 Transcriptome response of female high respondent to SMG.

Non-redundant, enriched Gene Ontology (GO) terms were selected by p-value. Top GO terms enriched by upregulated and downregulated genes were plotted by the number of genes in the GO terms.

Table 4.5 Selected upregulated genes enriched Gene Ontology (GO) terms of female high respondent to SMG.

GO Terms	*P-Value*	*Gene Symbol*	*Description*	*Fold Change (SMG vs Static)*
Extracellular matrix organization	4.49E-6	*IBSP*	Integrin Binding Sialoprotein	46.07
		MMP10	Matrix Metallopeptidase 10	43.75
		COL2A1	Collagen Type II Alpha 1 Chain	9.44
		COL10A1	Collagen Type X Alpha 1 Chain	6.81
		COL9A3	Collagen Type IX Alpha 3 Chain	5.21
		IHH	Indian Hedgehog Signaling Molecule	4.38
Extracellular region	1.73E-4	*IBSP*	Integrin Binding Sialoprotein	46.07
		MMP10	Matrix Metallopeptidase 10	43.75
		COL2A1	Collagen Type II Alpha 1 Chain	9.44
		SUSD4	Sushi Domain Containing 4	8.98
		COL10A1	Collagen Type X Alpha 1 Chain	6.81
		COL9A3	Collagen Type IX Alpha 3 Chain	5.21
		S100A1	S100 Calcium Binding Protein A1	3.43
		FGF1	Fibroblast Growth Factor 1	3.11
Collagen Trimmer	1.74E-4	*COL2A1*	Collagen Type II Alpha 1 Chain	9.44
		COL10A1	Collagen Type X Alpha 1 Chain	6.81
		COL9A3	Collagen Type IX Alpha 3 Chain	5.21
Regulation of sprouting angiogenesis	3.11E-4	*S100A1*	S100 Calcium Binding Protein A1	3.43
		FGF1	Fibroblast Growth Factor 1	3.11
Ossification	5.10E-4	*COL2A1*	Collagen Type II Alpha 1 Chain	9.44
		BMP8A	Bone Morphogenetic Protein 8a	8.51
		PHOSPHO1	Phosphoethanolamine/Phosphocholine Phosphatase 1	2.42

Table 4.6 Selected downregulated genes enriched Gene Ontology (GO) terms of female high respondent to SMG.

GO Terms	P-Value	Gene Symbol	Description	Fold Change (SMG vs Static)
Extracellular space	3.49E-3	*EPGN*	Epithelial Mitogen	-4.43
		MIF	Macrophage Migration Inhibitory	-2.49
		LOXL2	Lysyl Oxidase Like 2	-2.43
		CKB	Creatine Kinase B	-2.25
		PGK1	Phosphoglycerate Kinase 1	-2.21
		TPI1	Triosephosphate Isomerase 1	-2.14
Extracellular region	3.10E-2	*EPGN*	Epithelial Mitogen	-4.43
		RSPO2	R-Spondin 2	-3.16
		ALDOC	Aldolase, Fructose-Bisphosphate	-2.76
		MIF	Macrophage Migration Inhibitory	-2.49
		PRSS53	Serine Protease 53	-2.31

SMG was found to induce osteoarthritic-like transcriptome profiles in the female high respondents. Genes regulated by SMG exclusively enriched ECM-related cellular component GO terms, with genes up-regulated by SMG involved in essential osteoarthritic-related biological processes such as “ossification” and “regulation of sprouting angiogenesis" (Figure 4.4). Most of the enriched GO terms by up-regulated genes were related to chondrocyte-specific activities, whereas down-regulated genes were involved in more general cellular functions such as metabolic process and transportation (Figure 4.4).

The potential osteoarthritic inductive effect of SMG on the female high respondent was also confirmed by the alteration of individual gene expression. Except for *COL10A1*, which was used as donor stratification criteria, other osteoarthritis-related genes such as *IHH*, *MMP10*, *BMP8A*, and *PHOSPHO1* were upregulated by 4.38-fold, 43.75-fold, 8.51-fold, and 2.42-fold, respectively.

4.3.5 Comparison of the female high respondent, female low respondent, and male

The effect of SMG on other sub-groups was also analyzed by the above-mentioned method, the top enriched GO terms are plotted in Figure 4.5. Certain GO terms were shared by the female high respondent and low respondent, such as “NADH regeneration”, “oxidoreductase activity” and “developmental process”, but the chondrocytes specific activities were confined to the female high respondent sub-group.

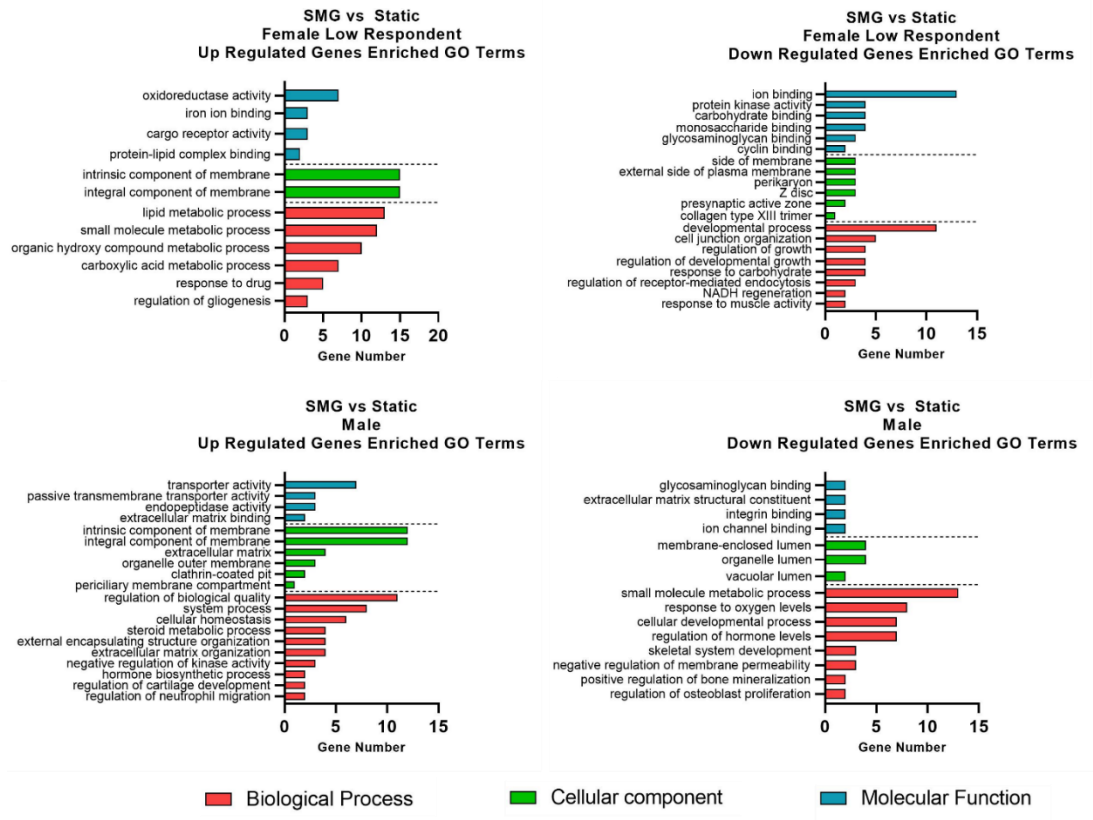

Figure 4.5 Transcriptome response of female low respondent and male to SMG.

Non-redundant, enriched Gene Ontology (GO) terms were selected by p-value. Top GO terms enriched by upregulated and downregulated genes were plotted by the number of genes in the GO terms.

It is noteworthy that the majority of cellular component GO terms enriched by SMG regulated genes were involved in membrane structure for female low respondents. For male donors, the DEGs enriched GO terms were mainly involved in general biological functions, with a few bone-related biological processes enriched by SMG downregulated genes, such as “regulation of osteoblast proliferation”, “skeletal system development” and “positive regulation of bone mineralization”. The two genes in the “positive regulation of bone mineralization” GO term, *CCN1* and *SLC8A1*, were down-regulated by 2.04-fold and 2.90-fold, respectively. Taken together, SMG had distinct effects between biological sex and within biological sex subgroups, with the female high

respondent subgroup having the highest propensity to express osteoarthritis-like transcriptome profile.

Given that the overlay of results in Figure 4.3 revealed the three distinct molecular signatures for the male, female high and low respondent subgroups, we performed an *in silico surfaceome* query (216), to uncover cell-surface protein-encoding genes. The query generated a total of 81 significantly modulated genes by SMG (Figure 4.6). Thirteen genes were shared by the three groups, and 33, 23 and 12 were respectively unique to the male, female high and low respondent subgroups (Figure 4.6). Of the 23 genes that are unique to the female high respondent subgroup, we identified *CD36* to be the highest modulated by ~12-fold (p-value =8.32x10^{-4}); Supplementary Table 4.3.

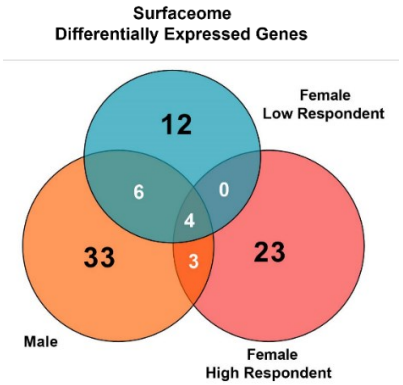

Figure 4.6 Surfaceome query of male and female subgroups.

Venn diagram displaying the number of *significantly* expressed surfaceome encoding genes between male, female high respondents, and female low respondents' subgroups.

4.3.6 Mechanical properties

For all three tested strain levels (10%, 20%, and 30%), the female high respondent had the least static baseline peak modulus. Three-week mechanical unloading by SMG increased the peak modulus for all three groups (males, female high respondent, and female low respondents), and the female high respondent had the least modulus (Figure 4.7a) among the groups. At 30% strain, the peak modulus of the female high respondent (61.7 kPa) was less than 50% of female low respondents (130.2 kPa) in the SMG group.

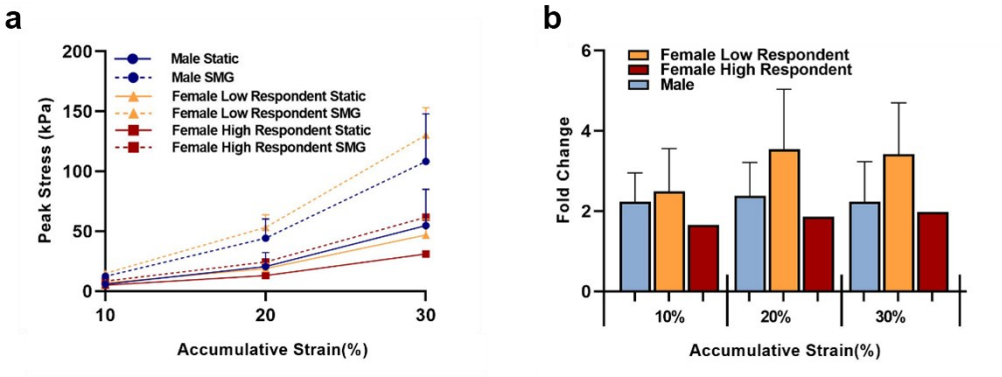

Figure 4.7 Mechanical property of engineered meniscus tissues.

a. Peak stress and b. fold change of peak moduli was calculated at 10%, 20% and 30% strain for all treatment groups. Values were normalized to the corresponding static control group. For all three groups (males, female low respondents, and female high respondent), peak modulus increased in the SMG group and the effect was least prominent in the female high respondent.

To compare the extent of the SMG effect, the fold change of peak modulus was calculated by normalizing the peak modulus in the SMG group to its corresponding static group (Figure 4.7b). At each strain level, the fold increase in peak modulus was highest in female low respondents, followed by males, and the female high respondent had the least fold increase. Although the result was not significant due to donor variability, the trend of tissue stiffening by SMG was observed and the effect was least prominent in female high respondents.

4.4 Discussion

In the present study, we investigated the effect of simulated microgravity (SMG) on tissue-engineered models of the human meniscus formed after chondrogenic culture of monolayer expanded meniscus fibrochondrocytes (MFC) in 3D porous bovine-derived type I collagen scaffolds. We first examined and established that the deposited matrix within the tissue-engineered models was consistent with the functional ECM components and characteristics of the native human meniscus (3, 26). Histological and immunofluorescence assessments for safranin O positive matrix, human types I and II collagen confirmed the deposition of these major biomechanically functional ECM

components of the meniscus within the tissue models. This finding albeit with some MFC donor variability was largely consistent with tissue-engineered constructs developed from human MFC (26, 56, 78, 155, 217, 218). Furthermore, our finding that SMG accentuated the intensities of Safranin O staining and type II collagen in the models is consistent with previous findings (219). But the finding of SMG enhancing safranin O intensity is inconsistent with the histological findings that after 30 days of spaceflight microgravity, a reduction in the level of toluidine blue or safranin O positive proteoglycan ECM in male mice's menisci occurred (111). The basis for these diametrically opposed findings between SMG and spaceflight microgravity's impact on meniscus may be associated with the enhanced mass transfer of nutrients, chondrogenic factors, gases, and low shear stress experienced during SMG culture in the RWV bioreactor (177, 220).

The finding that SMG increased the transcription and translation of type X collagen in meniscus models is consistent with previous reports on the impact of SMG during chondrogenic stimulation of adipose-derived mesenchymal stem cells (219, 221), but inconsistent with spaceflight microgravity induced downregulation of *COL10A1* expression in mice's articular cartilage (111). While mass transfer effects may contribute to the difference in outcomes between SMG and spaceflight microgravity effect on *COL10A1* expression, our main findings indicate that meniscus models from female MFC displayed a dichotomous response to SMG relative to models from male MFC. This finding demonstrated for the first time to the best of our knowledge that a subgroup of female donor MFC are highly susceptible to hypertrophic chondrogenesis while another female subgroup is less so and of a similar degree of hypertrophic chondrogenesis of MFC from male donors.

Given the significantly high chondrocyte differentiation index in the female high respondent subgroup, the lack of *COL10A1* expression in normal healthy articular chondrocytes but in osteoarthritic articular chondrocytes (149, 222-224), and more importantly the expression of *COL10A1* in osteoarthritic human meniscus (140, 154), we deemed the female high respondent subgroup as phenotypically osteoarthritic.

Further transcriptomic analysis via Gene Ontology confirmed significant upregulation of genes associated with osteoarthritis-related developmental processes such as ossification

and angiogenesis in the female high respondent subgroup (Figure 4.5 and Table 4.6), while the other female subgroup and male group displayed upregulated transcriptomes associated with lipid metabolism and general biological function, respectively (Figure 4.5). Additional bioinformatic analysis via surfaceome query (216) revealed *CD36* to be significantly characteristic of the MFC in the female high respondent subgroup. Interestingly, *CD36* has been implicated in the prevalence and progression of knee osteoarthritis in females (225, 226).

Early biomechanical changes of menisci have been reported to occur as early as 6 weeks in an anterior cruciate ligament transection (ACLT) posttraumatic knee osteoarthritis rabbit model (227). The report demonstrated a significant reduction in the mechanical properties of osteoarthritic menisci. Although, there was no statistical difference between the compressive properties of the male, female low- and high -respondents regardless of the tested mechanical strain in this study, it is interesting to note that the meniscus models of the female high respondent displayed the least mechanical measures. This finding further suggests that SMG may have induced osteoarthritis-like changes in the meniscus models in the female high respondents. But additional experiments with a larger donor cohort need to be done to substantiate the biomechanical findings herein.

Chondrocyte hypertrophy is associated with osteophyte formation in osteoarthritic cartilage (228). Premature hypertrophic chondrogenesis of bone marrow mesenchymal stem cells has been correlated with vascular invasion and *in vivo* calcification (229). Chondrocyte hypertrophy precedes vascularization and calcification of articular cartilage in the growth plate during developmental endochondral ossification (230). Chondrocyte hypertrophy markers including *COL10A1* and *MMP13* expression increased with severity of osteoarthritis, and type X collagen colocalized with calcium crystals in human menisci from osteoarthritic joints suggesting the role of MFC in the development of osteoarthritis (154). In view of these notable findings along with the highly significant hypertrophic characteristics of the female high respondent subgroup relative to the male group and female low respondent subgroup, it is reasonable to speculate that the meniscus models from the female high respondent subgroup will undergo vascular invasion and *in vivo*

calcification more readily. However, this expectation will have to be validated after *in vivo* implantation.

4.5 Conclusion

Taken together, our data demonstrate for the first time that mechanical unloading of engineered human meniscus models via SMG results in a sex-dependent dichotomous response of relevance to the development of osteoarthritis which may advance our understanding of the disproportionate incidence of knee osteoarthritis in females.

4.6 Acknowledgements

We thank Ms. Tara Stach and her team at the University of British Columbia Biomedical Research Centre for their RNA sequencing service.

4.7 Funding

ZM: NSERC (NSERC RGPIN-2018-06290 Adesida) DL: NSERC Undergraduate Student Research Awards RC: Alberta Innovates and WCHRI Summer Studentship MK: Alberta Cancer Foundation-Mickleborough Interfacial Biosciences Research Program (ACF-MIBRP 27128 Adesida) AMS: Canadian Institutes of Health Research (CIHR MOP 125921 Adesida) LW: University of Alberta Pilot Seed Grant Program (UOFAB PSGP); University of Alberta Women and Children's Health Research Institute Innovation Grant (UOFAB WCHRIIG 3126) DG: University of Alberta Pilot Seed Grant Program (UOFAB PSGP); University of Alberta Women and Children's Health Research Institute Innovation Grant (UOFAB WCHRIIG 3126) AA: Natural Sciences and Engineering Research Council (NSERC RGPIN-2018-06290 Adesida), NSERC RTI-2019-00310 Adesida; the Canadian Institutes of Health Research (CIHR MOP 125921 Adesida); the Canada Foundation for Innovation (CFI 33786); University Hospital of Alberta Foundation (UHF; RES0028185 Adesida); the Edmonton Orthopaedic Research Committee the Cliff Lede Family Charitable Foundation (RES00045921 Adesida); University of Alberta Pilot Seed Grant Program (UOFAB PSGP); University of Alberta Women and Children's Health Research Institute Innovation Grant (UOFAB WCHRIIG 3126); the Alberta Cancer Foundation-Mickleborough Interfacial Biosciences Research

Program (ACF-MIBRP 27128 Adesida). Research grant funding for the work was provided by Natural Sciences and Engineering Research Council (NSERC RGPIN- 2018-06290 Adesida), NSERC RTI-2019-00310 Adesida; the Canadian Institutes of Health Research (CIHR MOP 125921 Adesida); the Canada Foundation for Innovation (CFI 33786); University Hospital of Alberta Foundation (UHF; RES0028185 Adesida); the Edmonton Orthopaedic Research Committee; the Cliff Lede Family Charitable Foundation (RES00045921 Adesida); University of Alberta Pilot Seed Grant Program (UOFAB PSGP); University of Alberta Women and Children's Health Research Institute Innovation Grant (UOFAB WCHRIIG 3126); the Alberta Cancer Foundation-Mickleborough Interfacial Biosciences Research Program (ACF-MIBRP 27128 Adesida).

4.8 Competing interests

The authors declare no competing interests.

4.9 Supplementary materials

Supplementary table 4.1-4.7 are deposited and available at Figshare: https://doi.org/10.6084/m9.figshare.26366929.v1

Supplemental Figure 4.1 Correlation validation of RT-qPCR and RNA-Seq data. The value was reported as fold change (SMG to Static). Each data point corresponded to a single donor.

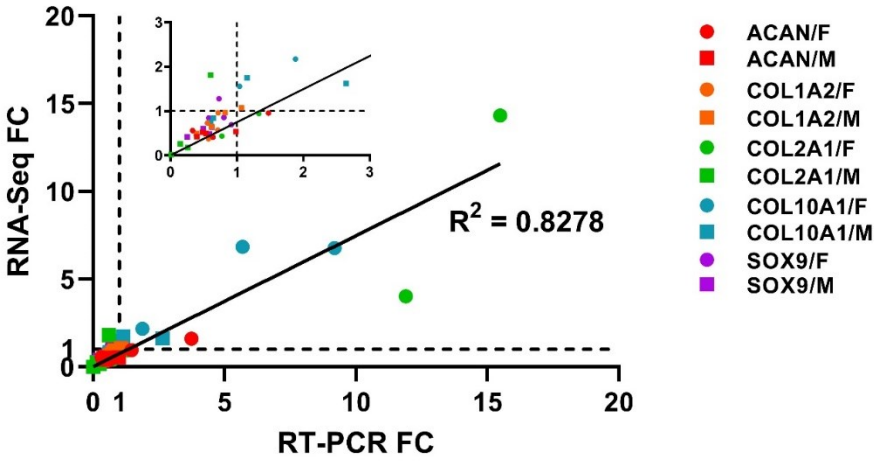

Chapter 5

Exploring Simulated Microgravity's Impact on Osteoarthritis Progression: CD36 and Sex-Specific Responses

Zhiyao Ma, Haiming Li, Daniel Graf, Maria Febbraio, Adetola Adesida

5.1 Introduction

Osteoarthritis (OA) is a prevalent and debilitating disease that predominantly affects load-bearing joints (231). Knee osteoarthritis (KOA) is characterized by the progressive degradation of nearly all structures within the knee joint, leading to pain, stiffness, and reduced joint mobility (141, 232, 233). The knee meniscus, a critical fibrocartilaginous structure, plays an essential role in joint stability, load distribution, and shock absorption (234). Meniscus degeneration is one of the earliest pathological changes observed in the onset of knee OA (5, 99), highlighting the importance of understanding the molecular mechanisms contributing to its deterioration.

Sex differences are well established as significant pathogenetic characteristics of KOA (103, 143, 145). Epidemiological studies reveal that females are more likely to develop OA and often suffer from more severe symptoms at an earlier age compared to males (235). While it is demonstrated that sex hormones regulate joint homeostasis in a sex-dependent manner (203, 236), hormonal differences alone cannot account for the disproportionate incidence of KOA in females (194). Other potential factors include variations in joint biomechanics, metabolic variables, and genetic factors (197, 200, 237-239).

CD36, a transmembrane glycoprotein, plays a key role in several physiological processes, including fatty acid metabolism, inflammation, and angiogenesis (240). Numerous studies have highlighted the importance of CD36 in tissue repair and degeneration, particularly in cardiovascular and metabolic diseases (241-244). Despite extensive

research in these areas, the role of CD36 in KOA, especially within the meniscus, remains largely unexplored. Some studies have suggested that CD36 may contribute to cartilage degradation and inflammation in OA (245-247). However, there is a significant gap in understanding how CD36 functions specifically in meniscal tissue and its interaction with sex in KOA. Given CD36's influence on angiogenesis, inflammation, and fatty acid metabolism—processes associated with tissue remodeling and OA development—investigating its role in these interconnected pathways could provide valuable insights into KOA pathogenesis.

The meniscus operates under constantly loaded biomechanical environments, making appropriate mechanical stress critical for maintaining a healthy phenotype. Conditions of reduced mechanical stress on Earth or microgravity induced by parabolic flight or spaceflight have been demonstrated to induce the onset of KOA phenotype and initiate tissue degeneration in both animal models (93, 111, 208, 248) and human subjects (88, 109, 175, 249). Simulated microgravity (SMG) provides a unique platform to study the mechanical unloading environment of microgravity on Earth, making it a relevant model system for investigating OA mechanisms. Previous studies on both short-term and long-term SMG have shown that SMG can initiate the development of OA phenotypes and promote tissue degeneration, with observed sex differences (92, 97, 110, 112, 250).

This study aims to enhance our understanding of the mechanisms behind sex differences in KOA and the effects of CD36, particularly its interaction with sex. We hypothesize that CD36 knockout will alleviate the adverse effects of simulated microgravity (SMG) on meniscus calcification and ECM degradation, with outcomes influenced by sex-specific differences.

To test this hypothesis, we employed both human and mouse meniscus models. First, we examined sex-dependent differences in meniscus tissue and gene expression using samples from late-stage male and female patients and analyzed CD36 expression at both gene and cell surface levels. Next, we utilized wild-type and CD36 knockout mice at various ages to investigate the role of CD36 in spontaneous meniscus calcification. Finally, we cultured menisci from CD36 wild-type and knockout mice, both male and female, under SMG conditions, assessing calcification levels, hypertrophic

differentiation, ECM degradation, and angiogenesis. These investigations aim to provide a comprehensive understanding of how CD36 and sex differences influence KOA pathogenesis using meniscus models.

5.2 Methods

5.2.1 Ethic statement

Human total knee arthroplasty (TKA) samples used in this study were collected from donors undergoing surgery with the approval of the University of Alberta Health Research Ethics Board (Study ID: Pro00018778). The animal research was conducted in accordance with the protocol approved by the University of Alberta Animal Care and Use Committee (Study ID: AUP00001363).

5.2.2 Primary meniscus fibrochondrocytes isolation

Human meniscus sample were collected from 7 female and 7 male donors. Non-identifiable donor information is detailed in Supplementary Table 5.1. Primary meniscus fibrochondrocytes were isolated from the inner region of the meniscus obtained from TKA samples. The inner region of the meniscus was excised from the whole meniscus tissue and cut into small pieces, approximately 1 mm^3 each. These meniscus fragments were then digested in a 50 mL Falcon tube containing 0.15% w/v collagenase type 2 solution (Worthington, LS004176) for 22 hours on a shaking bed at 250 rpm and 37°C. After digestion, primary meniscus fibrochondrocytes were filtered out and plated in cell culture flasks with DMEM complete medium (Dulbecco's Modified Eagle's Medium - High Glucose (D6429, Sigma-Aldrich), supplemented with 1% v/v Penicillin-Streptomycin-L-Glutamine (PSG) (10378, Gibco), 1% v/v 4-(2-hydroxyethyl)-1-piperazineethanesulfonic acid (HEPES) (H4034, Sigma-Aldrich), and 10% v/v inactivated Fetal Bovine Serum (FBS) (F1051, Sigma-Aldrich)) for 48 hours in an incubator (95% air, 5% CO_2, and 37°C) to recover. After 48 hours of recovery, adherent primary meniscus fibrochondrocytes were washed with Gibco Dulbecco's Phosphate Buffered Solution (DPBS) (14040133, ThermoFisher Scientific) and detached using Accutase solution (25-058-CI, CORNING) for flow cytometry analysis and RT-qPCR analysis.

5.2.3 Flow cytometry

A portion of the cells collected after 48 hours of recovery was used for flow cytometry analysis. These cells were washed twice with ice-cold FACS buffer (DPBS supplemented with 10% v/v FBS and 1% sodium azide (S2002, Sigma-Aldrich)) and 1×10^6 cells were transferred to each FACS tube (12 x 75 mm polystyrene round-bottom tubes, Becton Dickinson). For primary meniscus fibrochondrocytes from each donor, three groups were set up: cell-only control, isotype control, and CD36. For the cell-only control, 100 µL of FACS buffer were added. For the isotype control, cells were stained with FITC Mouse IgG2a, κ Isotype Control Antibody (100 uL, 1:100 dilution, 400210, Biolegend). For CD36, cells were stained with FITC anti-human CD36 Antibody (100 uL, 1:100 dilution, 336204, Biolegend). All groups were incubated for 30 minutes at 4°C. After incubation, all groups were washed once with ice-cold FACS buffer before measurement.

The labeled cells were analyzed on a BD FACS Canto II flow cytometer (Becton Dickinson) and data acquisition was performed with BD FACSDiva™ software (Becton Dickinson). FITC was excited using the blue laser at 488 nm and the emission was detected using a 525/50 filter. Data analysis was performed with FlowJo software (Version 10). Cells were gated using forward scatter vs. side scatter properties to exclude debris and aggregates. The percentage of positive labeled cells with each marker was calculated.

5.2.4 RT-qPCR

The rest of the cells collected after 48 hours of recovery were used for RT-qPCR. These cells were preserved in TRIzol (15596018, Life Technologies) and frozen at -80°C prior to RNA extraction. RNA was extracted using the PuroSPIN Total RNA Purification KIT (NK051-250, Luna Nanotech) according to the manufacturer's instructions. The extracted RNA was reverse transcribed into complementary DNA (cDNA) using Goscript Reverse Transcriptase (A5004, Promega). Quantification was performed by reverse transcription-quantitative polymerase chain reaction (RT-qPCR) using gene-specific primers (Supplementary Table 5.3) with Takyon No Rox SYBR MasterMix dTTP Blue detection.

Gene expression was normalized to the geometric mean of three housekeeping genes (*RPL13A*, *YWHAZ*, and *B2M*), and the data was presented using the $2^{-\Delta CT}$ method.

5.2.5 KOA meniscus histology and immunofluorescence

Before excising the inner region of the meniscus for cell isolation, an approximately 1 mm thick cross-section (perpendicular to the tibial plateau) of the whole meniscus was cut out for 5 female and 5 male donors and fixed in 10% (v/v) formalin (Anachemia). The fixed meniscus cross-section was washed with PBS, dehydrated, and embedded in paraffin wax. The embedded constructs were sectioned at 5 μm thickness for histological analysis and immunofluorescence. To visualize sulfated glycosaminoglycan (GAG) deposition, the sections were stained with 0.1% (w/v) Safranin-O (S2255-25G, Sigma) and 1% (w/v) Fast Green FCF (F7258-25G, Sigma). For immunofluorescence staining of type I collagen, antigen retrieval was performed by treating the sections with protease XXV (AP-9006-005, Thermo Scientific) and hyaluronidase (H6254, Sigma-Aldrich). Following antigen retrieval, the sections were blocked with 5% (w/v) BSA (A7906, Sigma-aldrich) , labeled with a rabbit anti-human collagen I antibody (1:200, CL7812AP, Cedarlane Laboratories Ltd), and incubated overnight at 4°C.The following day, the sections were washed and incubated for 30 minutes at room temperature with an Alexa Fluor® 594 conjugated goat anti-rabbit secondary antibody (A11012, Thermo Fisher). 4',6-diamidino-2-phenylindole (DAPI) was applied to visualize the nuclei. Immunofluorescence imaging was conducted using the Nikon Eclipse Ti-S microscope.

5.2.6 Animal

Littermate-derived established wild type (WT) and CD36 knockout (KO) mice (251), syngeneic to the C57Bl/6J strain, were bred as homozygotes under specific pathogen-free conditions with ad libitum access to normal chow and water. The housing room maintained a 12:12 light cycle, and all cage components, food, and bedding were sterilized. Sex and age-matched mice were used in this study.

5.2.7 4, 12, 24-week calcification

To investigate the effect of CD36 and sex on spontaneous calcification of the meniscus, four groups of mice were established: WT female, WT male, KO female, and KO male. At the ages of 4, 12, and 24 weeks, 5 mice from each group were euthanized by cervical dislocation and the knee joints were dissected and examined for calcification using micro-CT scanner (U-CT, MILabs). Most of the calcification was observed in the anterior horn region of the meniscus; therefore, only the anterior region was used to quantify the level of calcification. The acquired scans were reconstructed with MILabs Reconstruction software (version 11.01) at a resolution of 5 μm. The volume of calcification was quantified using 3D Slicer software (version 5.6.1). At each time point, twenty menisci were quantified for each of the four groups.

5.2.8 Meniscus isolation and hydrogel encapsulation

Mice from the aforementioned four groups were euthanized by cervical dislocation at the age of 4 weeks, and all four menisci were surgically dissected out. The isolated menisci were then encapsulated in a 1% (w/v) agarose hydrogel (A9539-50G, Sigma) to form cylindrical constructs with a diameter of 6 mm and a height of 3 mm.

5.2.9 Simulated microgravity culture

Hydrogel-encapsulated meniscus constructs were assigned to either static conditions as control (24-well culture plate) or simulated microgravity (SMG) conditions using a commercially available bioreactor (RCCS-4, Synthecon Inc). This setup created six groups: static control WT female, static control WT male, SMG WT female, SMG WT male, SMG KO female, and SMG KO male. The hydrogel-encapsulated meniscus constructs in both conditions were cultured in DMEM-High glucose medium supplemented with 20% FBS, 1% PSG, 1% insulin/transferrin/selenium (ITS+) Premix (Corning 354352), and 50 μg/mL ascorbic acid 2-phosphate. For the SMG condition, the rotating speed was set at 40 rpm. Constructs in all six groups were cultured for three weeks, with medium changes performed once a week. For each group, the menisci from minimal of 10 mice were cultured.

5.2.10 Calcification assessment

Calcification of the hydrogel-encapsulated meniscus for all six groups was assessed at four time points using a micro-CT scanner: baseline calcification immediately after hydrogel encapsulation before assignment to different mechanical stimulation groups, at the end of week 1 and week 2 during medium changes, and at the end of the three-week culture period. Most of the calcification was observed in the anterior horn region of the meniscus; therefore, only the anterior region was used to quantify the level of calcification and follow up histological and immunofluorescence analysis. Calcification data acquisition and quantification followed the same protocol mentioned previously.

5.2.11 Histology and immunofluorescence

At the end of three weeks of mechanical stimulation treatment, the meniscus samples underwent the same protocol for fixation, dehydration, embedding, sectioning, and GAG visualization as previously described. For the visualization of type I collagen (COL I), type II collagen (COL II), type X collagen (COL X), vascular endothelial growth factor (VEGF), and osteopontin (OPN), the 5 μm thick slices underwent the same antigen retrieval process mentioned above. Following antigen retrieval, a 0.2% (v/v) Triton X-100 (BP151-1, ThermoFisher) solution was applied at room temperature for 10 minutes to permeabilize the cell membrane, followed by 30 minutes of blocking with 5% (w/v) BSA. After blocking, the slides were individually stained with the optimal concentration of primary antibodies (as detailed in Supplementary Table 5.2) at 4°C overnight, and with the corresponding secondary antibodies (Supplementary Table 5.2) the following day. To quantitatively measure the expression of OPN at the anterior horn area of the meniscus, the total fluorescent signal intensity OPN was calculated using a self-developed Python script. The number of cells was counted by staining with DAPI and analyzing the images using a self-developed Python script. The quantification result for each marker was expressed as the average fluorescent signal intensity per cell (Intensity/Cell Number). For the quantification was conducted for the menisci of three mice per group.

5.2.12 Statistical analysis

All statistical analyses in this study were conducted using Prism GraphPad software (Version 10.1.2). For the RT-qPCR results of human TKA meniscus samples, outliers were first identified using the ROUT method (Q = 1%) and removed if present. The cleaned data were then tested for normal. If the normality test was passed, the statistical significance between the two groups was assessed using an unpaired parametric t-test with Welch's correction. If the normality test was not passed, the significance between the two groups was tested using the unpaired nonparametric Kolmogorov-Smirnov test. For the calcification date at 4, 12, and 24 week, the outlier and normality of sample distribution were first tested using the same method, all data passed normality test. The interaction of sex and CD36 at each point were assessed by two-way ANOVA. For each time point, the significance of result between WT and KO within each sex group were tested by unpaired parametric t-test with Welch's correction. For the calcification data under static and SMG culture, the outlier and normality of sample distribution were first tested using the same method. If the normality test was passed, the statistical significance between the two groups at the same time point was assessed using an unpaired parametric t-test with Welch's correction. If the normality test was not passed, the significance between the two groups at the same time point was tested using the unpaired nonparametric Kolmogorov-Smirnov test. (* $p<0.05$, ** $p<0.01$, *** $p< 0.001$, **** $p<0.0001$)

5.3 Results

5.3.1 GAG and type I collagen content in male vs female TKA meniscus

To compare the sex-dependent differences in late-stage OA meniscus, we examined the tissue-level content of two cartilaginous ECM components: GAG and type I collagen. Among the five female donors, nearly no GAG content was visible, with only donors 3 and 7 showing faint Safranin O staining in the outer meniscus region (Figure 5.1a). In contrast, three out of five male donors exhibited intense Safranin O staining in regions of the meniscus cross-section. Specifically, donors 3 and 4 had staining in the outer region

of the meniscus, while donor 5 showed a larger area of coverage, including both the outer region and part of the inner region (Figure 5.1a).

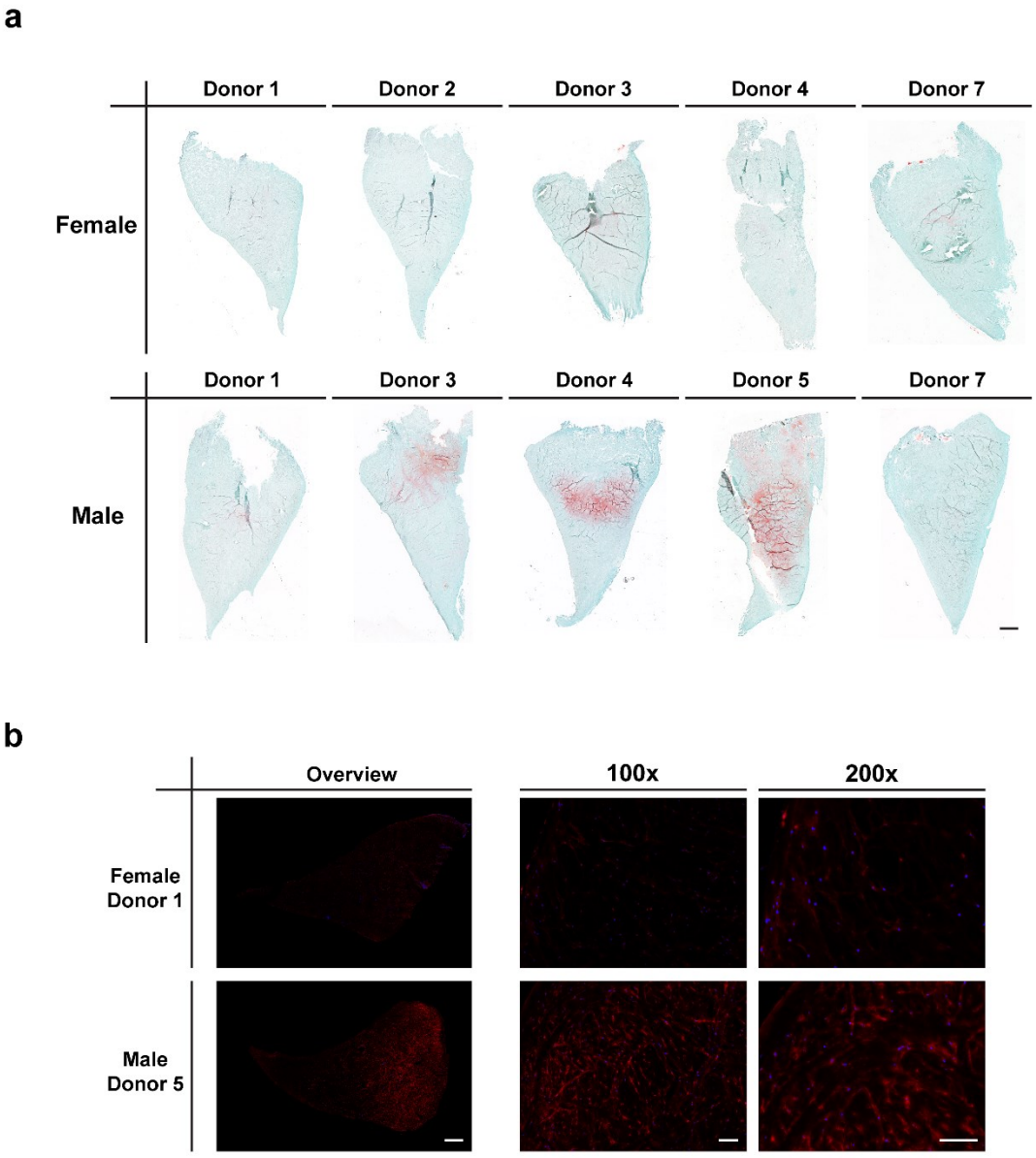

Figure 5.1 GAG and Type I Collagen Content in Male and Female TKA Meniscus.

a. Safranin O staining of cross-sections of TKA meniscus from five female and five male donors. Scale bar: 1 mm. b. Immunofluorescent staining of type I collagen in cross-sections of TKA meniscus from five female and five male donors. Scale bar: Overview 1 mm; 100x and 200x: 100 µm.

For type I collagen, two age-matched donors were selected: one female (donor 1, age 69) and one male (donor 5, age 69). Immunofluorescent staining revealed that in both male and female donors, type I collagen staining was most intense in the outer region of the meniscus and decreased towards the inner region. However, the male donor exhibited significantly more intense overall staining. Closer observation showed that type I collagen primarily existed in the pericellular matrix for both male and female donors, with a few buddle-shaped extensions into the extracellular space observed only in the male donor (Figure 5.1b).

5.3.2 Sex-dependent differences in OA-Related gene expression and CD36 in TKA meniscus

Following the analysis of GAG and type I collagen content, we investigated the gene expression levels of chondrogenic and OA-related markers in female and male donors. For the chondrogenic markers (*ACAN, COL1A2, COL2A1,* and *SOX9*), male donors showed higher average expression levels than female donors; however, the differences were not significant due to large donor variability. Specifically, for the GAG and type I collagen-encoding genes *ACAN* and *COL1A2*, male donors exhibited 1.82-fold and 1.33-fold higher expression levels, respectively, corresponding to the tissue-level content (Figure 5.2b).

We also examined OA-related markers. Female donors had significantly higher average expression of the hypertrophic differentiation marker *COL10A1* (12.82-fold) compared to male donors. The expression levels of matrix remodeling enzymes (*MMP3*, *MMP13*, and *ADAMTS5*) were comparable between sexes. The angiogenesis marker *VEGFA* showed a 1.7-fold higher average expression in males, though this difference was not significant. For bone formation markers *SPP1* and *BMP2*, females showed higher average expression levels, with *BMP2* being significantly 3.15-fold higher. The Indian hedgehog pathway marker (*IHH*) was also significantly higher in females, with an average fold change of 11.18. Expression levels of transcription factors *JUN* and *RUNX2* were slightly higher in female and male donors, respectively, but these differences were not significant (Figure 5.2c). For mechanotransduction markers, *TPRV4* expression was similar in both sexes;

however, females had a 1.59-fold higher average expression of *PIEZO1*, with marginal significance (p = 0.0828) (Figure 5.2d).

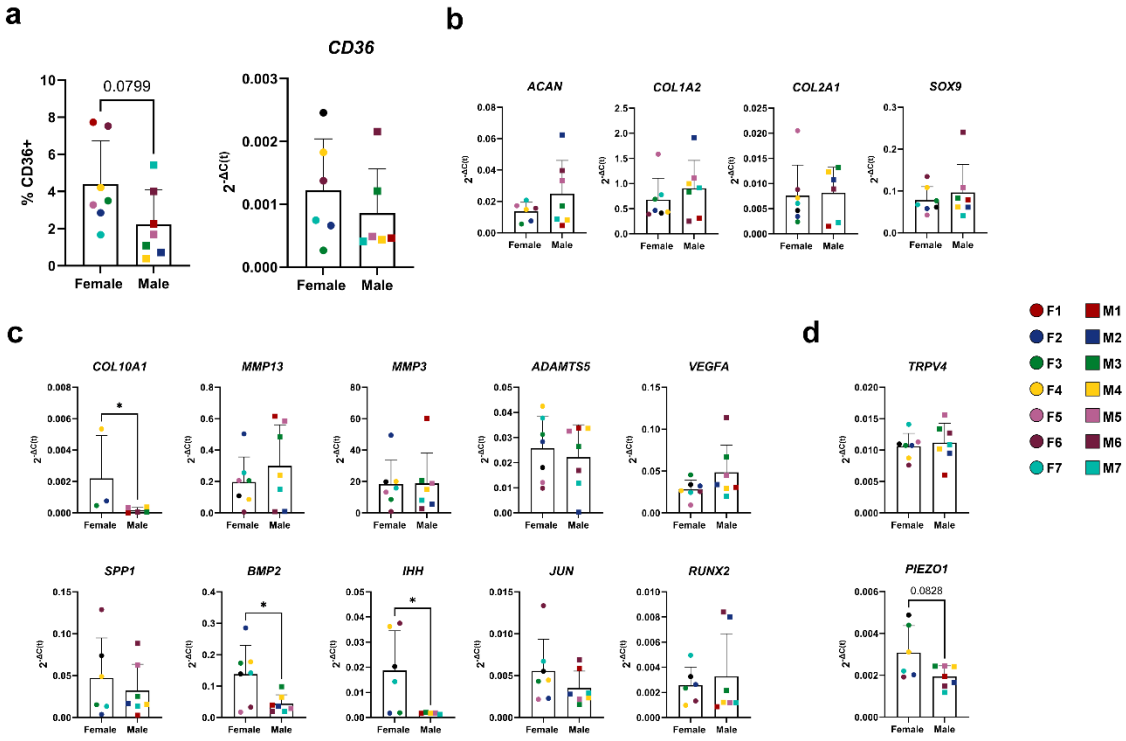

Figure 5.2 Gene and CD36 Expression in Male and Female TKA Meniscus.

a. Population of isolated fibrochondrocytes positive for CD36 on the cell surface examined by flow cytometry, and *CD36* expression by RT-qPCR. b. Expression of selected chondrogenic markers (*ACAN*, *COL1A2*, *COL2A1*, and *SOX9*) by RT-qPCR. c. Expression of selected OA-related genes (*COL10A1*, *MMP13*, *MMP3*, *ADAMTS5*, *VEGFA, SPP1, BMP2, IHH, JUN,* and *RUNX2*) by RT-qPCR. d. Expression of mechanotransduction markers (*TRPV4* and *PIEZO1*) by RT-qPCR.

Regarding *CD36* expression, females had an average 1.42-fold higher expression than males, but this was not significant due to large donor variability. Flow cytometry analysis showed that only a small population of cells from the inner meniscus expressed CD36 on the cell surface, with females having about a two-fold higher average population (4.39%) than males (2.23%), showing marginal significance (p = 0.0799) (Figure 5.2a).

5.3.3 CD36 knockout reduces spontaneous meniscus calcification in female mice at 12 weeks

We next studied the effect of CD36 and sex on spontaneous meniscus calcification and the development of KOA in a mouse model. Wild-type (WT) and CD36 knockout (KO) mice were examined at 4, 12, and 24 weeks. The meniscus was segmented in the reconstructed knee joint (Figure 5.3a), and the calcification volume at the anterior horn was quantified. At 4 weeks, there were no significant differences in calcification volume between WT and KO mice, nor between male and female mice. By 12 weeks, the calcification volume in WT mice had increased approximately twofold compared to 4 weeks. CD36 knockout significantly reduced calcification volume in female mice by about 15%, while male KO mice showed an increase of about 8%. Two-way ANOVA indicated a significant interaction between CD36 knockout and sex at this time point ($p < 0.0001$). By 24 weeks, the calcification volume in WT mice remained similar to the 12-week level, and CD36 knockout did not significantly alter calcification volume in either female or male mice (Figure 5.3b).

5.3.4 SMG accelerates calcification; CD36 knockout reduces progression in female mice

To further investigate the role of CD36 and sex in OA development, we combined the CD36 knockout mouse model with simulated microgravity (SMG) by culturing hydrogel-encapsulated meniscus constructs in a rotating wall vessel SMG bioreactor. Menisci were dissected at the 4-week time point, where no differences in calcification were observed (Figure 5.3c). Calcification volume was assessed at baseline (day 0) and weekly over three weeks (days 7, 14, and 21) using micro-CT (Figure 5.3d). The increase in calcification volume was normalized to the baseline measurement. To first validate the OA-inducing effect of SMG culture, we compared calcification volumes within wild-type mice between SMG and static control groups for both males and females (Figure 5.3e). In female mice, SMG culture significantly increased calcification volume by about 25% as early as day 7, an effect that persisted throughout the three-week culture period. In contrast, male mice showed less than a 10% increase in calcification volume on average under SMG, which was not significant.

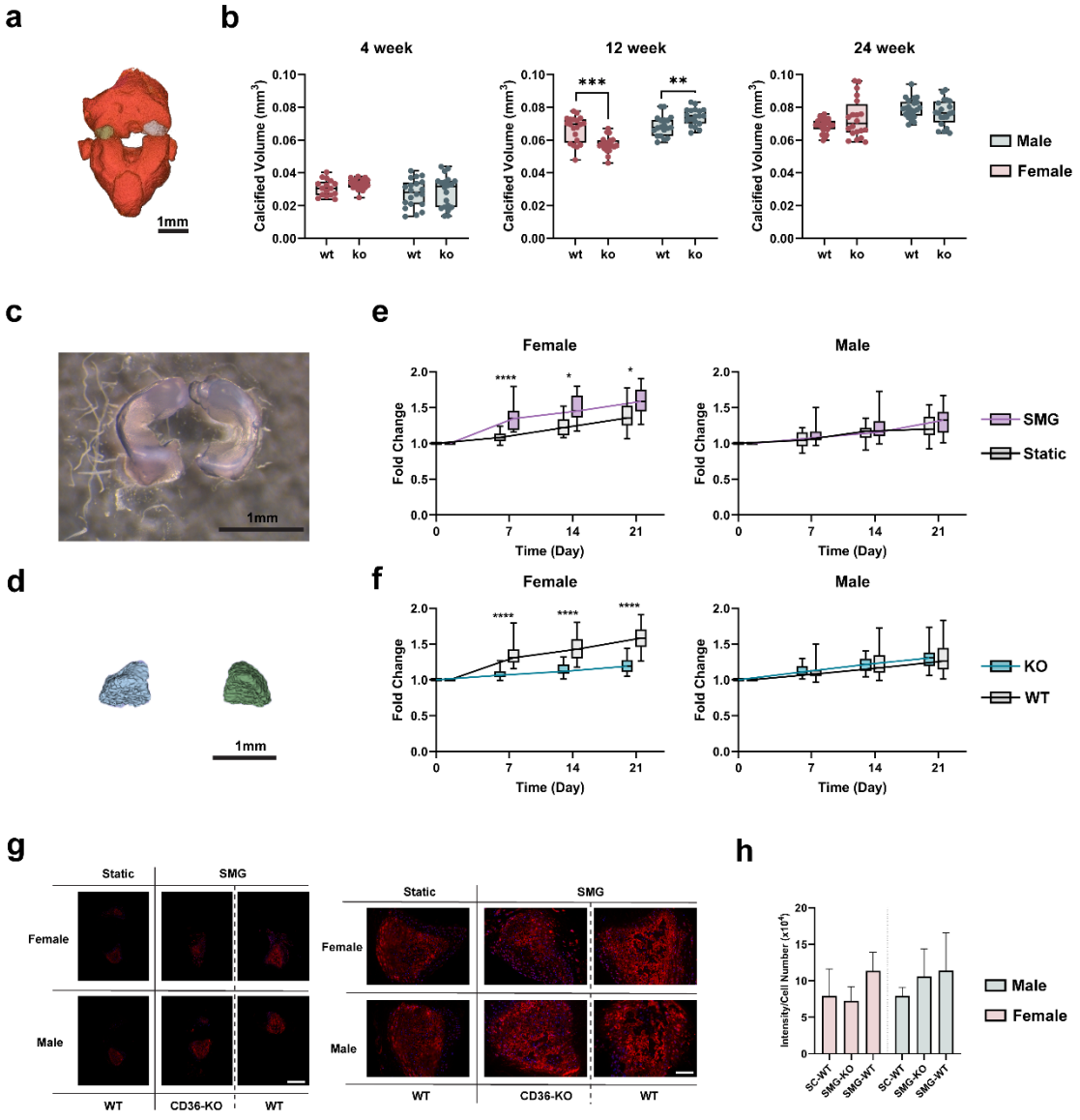

Figure 5.3 Sex-dependent Effect of SMG and CD36 on the Calcification of Mice Meniscus and the Expression of OPN.

a. Reconstructed mouse knee joint from micro-CT scan with calcified regions of the anterior horn of medial and lateral meniscus segmented out (light and dark gray). Scale bar: 1 mm. b. Volume of spontaneous meniscus calcification at the ages of 4, 12, and 24 weeks in WT and KO mice for both females and males. C. Surgically dissected meniscus at 4 weeks old before hydrogel encapsulation. Scale bar: 1 mm. d. Reconstructed calcified region of mouse meniscus from micro-CT scan. Scale bar: 1 mm. e. Temporal profile of relative volume of calcification at baseline (day 0) and days 7, 14, and 21 after

static and SMG culture of hydrogel-encapsulated WT meniscus for both males and females. Fold change is defined as the relative volume of calcification at each time point normalized to the volume of calcification at baseline. f. Temporal profile of relative volume of calcification at baseline (day 0) and days 7, 14, and 21 after SMG culture of hydrogel-encapsulated WT and KO meniscus for both males and females. Fold change is defined as the relative volume of calcification at each time point normalized to the volume of calcification at baseline. g. Immunofluorescence staining of osteopontin (OPN) in the cross-section of mouse meniscus. Scale bar: left panel 500 μm, right panel 100 μm. h. Quantification of OPN immunofluorescent staining based on three mice per group.

We then investigated the effect of CD36 knockout and compared the calcification volumes between sexes within the SMG culture condition (Figure 5.3f). In females, CD36 knockout significantly reduced calcification volume, with this reduction observable from day 7 and persisting throughout the three-week culture period. By day 21, the knockout reduced calcification volume by about 30%. However, in males, calcification volumes were comparable between knockout and wild-type groups throughout the entire culture period, indicating no significant effect of CD36 knockout in male mice.

5.3.5 CD36 knockout reduces OPN expression in female mice

The potential mechanism of CD36 and sex effects on calcification levels was examined by immunofluorescent staining of osteopontin (OPN) (Figure 5.3g). OPN intensity was lowest in the static control group and highest in the SMG WT group. CD36 knockout reduced OPN levels in the SMG KO group to those similar to the static control in females, but not in males. In males, the SMG KO group had OPN levels comparable to the SMG WT group. This observation was supported by quantification, although the trend was not statistically significant due to large variability (Figure 5.3h). For females, higher magnification revealed uniform and mild OPN deposition in the inner meniscus of the static control group, with minimal deposition in the superficial region. In the SMG WT group, OPN deposition increased, covering almost the entire anterior horn of the meniscus, with cyst formation in the middle region where OPN was strongly deposited

around the contour. The SMG KO group showed an OPN deposition pattern closer to the static control (Figure 5.3g).

5.3.6 SMG induces OA-like phenotype in mice meniscus

Contrary to the overall expression of OPN, the content of cartilaginous ECM components GAG and type II collagen was highest in the static wild-type group and lowest in the SMG WT group (Figure 5.4a, 5.4b). In the static control group, the superficial region of the anterior horn displayed a hyaline-cartilage-like phenotype with dense and homogeneous deposition of GAG and type II collagen in the ECM space. Toward the inner region, the phenotype transitioned to a slightly hypertrophic phenotype with reduced GAG and type II collagen content, mainly concentrated in the pericellular region instead of being homogeneously distributed throughout the ECM space. In the SMG WT group, the thickness of the superficial region and the content of GAG and type II collagen were significantly reduced compared to the static control, while the inner calcified region showed a severe hypertrophic phenotype and cyst formation. The SMG KO group for both females and males showed partial restoration of type II collagen in the superficial region and an increase in thickness compared to the SMG WT group, though not to the levels observed in the static control.

The differences in hypertrophic differentiation were further validated by type X collagen immunofluorescent staining (Figure 5.4c). For both males and females, the overall content of type X collagen showed a similar trend to OPN, with the highest deposition in the SMG WT group and the lowest in the static control group. In the anterior horn of the static control group, there was mild deposition in the calcified inner region and almost no type X collagen in the superficial region. In the SMG WT group, there was a significant increase in type X collagen content in the pericellular space of the inner calcified region, as well as increased intracellular content in the superficial region, especially in females. CD36 knockout reduced the content of type X collagen in females, particularly in the superficial region.

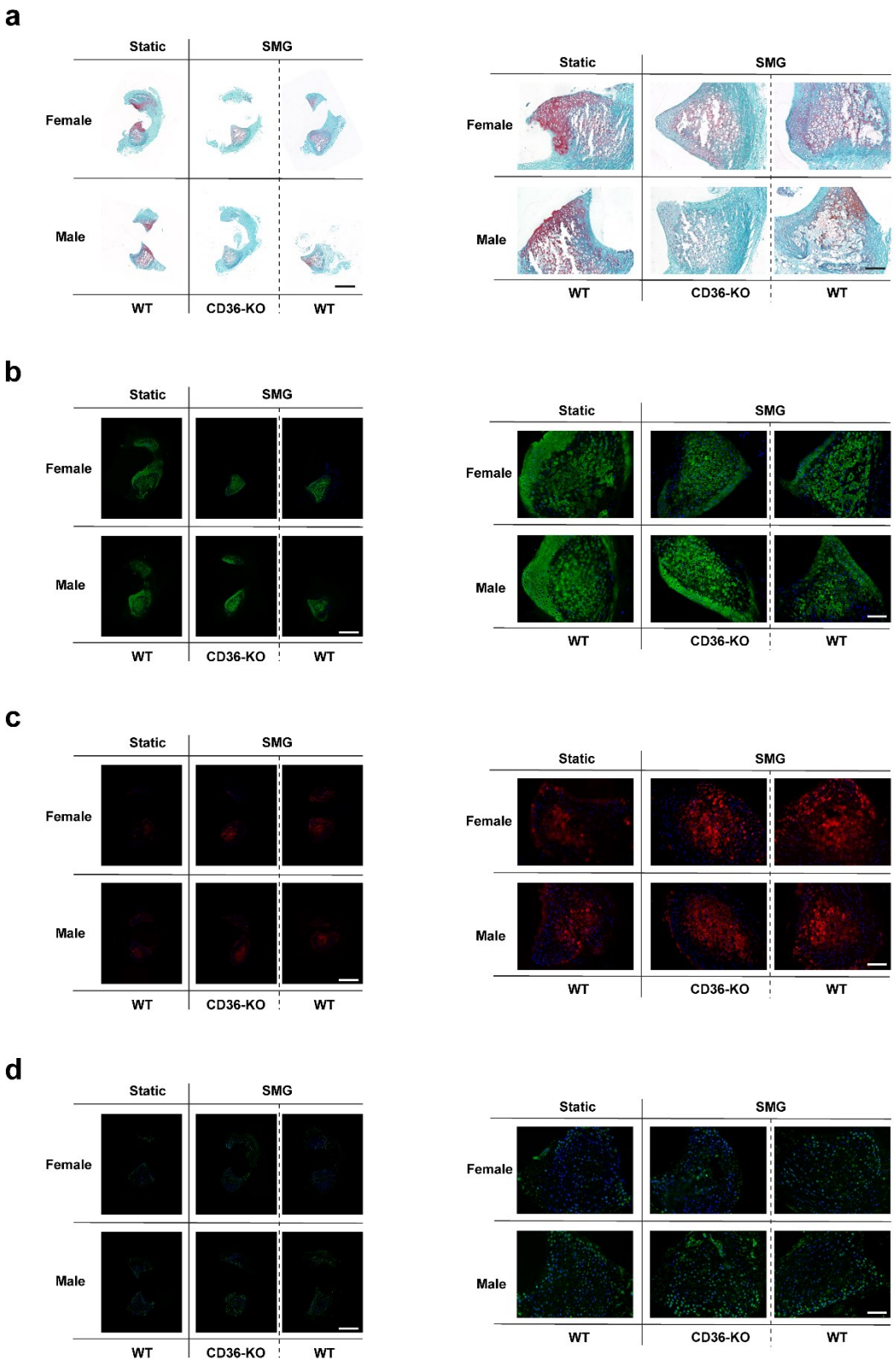
a
Static
SMG
Female
Male
WT
CD36-KO
WT
b
c
d

Figure 5.4 Histological and Immunofluorescent Analysis of Mouse Meniscus.

a. Safranin O staining of mouse meniscus cross-section. Scale bar: left panels 500 μm, right panels 100 μm. b. Immunofluorescent staining of type II collagen in mouse meniscus cross-section. Scale bar: left panels 500 μm, right panels 100 μm. c. Immunofluorescent staining of type X collagen in mouse meniscus cross-section. Scale bar: left panels 500 μm, right panels 100 μm. d. Immunofluorescent staining of VEGF in mouse meniscus cross-section. Scale bar: left panels 500 μm, right panels 100 μm.

5.3.7 SMG and CD36 effects on VEGF expression

Since CD36 influences angiogenesis, analyzing VEGF may reveal how CD36 knockout affects the processes of ECM degradation, hypertrophic differentiation, and calcification in the meniscus under SMG conditions. In both sex groups, VEGF content was relatively consistent across the three experimental conditions, with the superficial region showing slightly more intense staining than the inner calcified region. Knocking out CD36 did not significantly affect VEGF expression (Figure 5.4d).

5.4 Discussion

The observed sex differences in KOA are well documented, with females more likely to develop KOA and experience severe symptoms earlier than males (98, 103, 143, 145). However, the underlying molecular mechanisms remain unclear. This study aimed to elucidate these mechanisms by focusing on the meniscus, a crucial structure for joint stability and load distribution (11), which undergoes early degenerative changes that can initiate KOA (5, 100, 252, 253). By examining the specific marker CD36, known for its roles in fatty acid metabolism, inflammation, and angiogenesis (240), this study utilized both human and mouse meniscus models to investigate the molecular pathways contributing to sex differences in KOA.

Given the crucial role of the meniscus in the onset of KOA, several studies have investigated human meniscus degradation, primarily focusing on trauma-related evaluations and imaging-based technologies (28, 254-257). However, there is limited knowledge about the pathological changes in the meniscus at the histopathological level, particularly regarding sex differences. For example, studies have assessed the histological

and molecular features of meniscus degeneration using TKA meniscus samples and have focused on the changes associated with aging (258). Despite these efforts, there remains a gap in understanding the sex-specific pathological changes in the meniscus in the context of KOA.

In this study, we conducted a histological and molecular evaluation of meniscus samples from TKA patients with a specific focus on sex differences. Safranin O staining revealed that male donors generally had higher GAG content compared to females, with GAG primarily distributed in the outer vascular zone. This finding aligns with previous studies on meniscus degeneration with aging, which reported increased Safranin O staining intensity in aged, degenerated menisci as an adaptation attempt (258). However, in OA meniscus, there was extensive variability in Safranin O staining patterns, and no clear conclusions regarding sex differences were reported.

The lack of Safranin O staining in female donors may indicate a failure of adaptation in the meniscus tissue. Meniscus development follows a sequence where collagen fibers form early, and GAG deposition occurs later, increasing with age due to mechanical load-bearing activities (4, 259). The sensitivity of ECM GAG composition to mechanical conditions suggests that KOA-induced changes in knee joint mechanical environment could alter meniscus ECM composition. The severe matrix disruption in the menisci from TKA female donors likely impairs their ability to retain hydrophilic GAG, which is essential for maintaining meniscus elasticity. Similarly, type I collagen content was found to accumulate mostly in the outer avascular region of the meniscus for both age-matched female and male donors, decreasing towards the inner avascular region. This is in agreement with previous findings (260), with females showing a significantly reduced content of type I collagen.

The observed tissue-level differences were also reflected at the gene expression level. On average, meniscus samples from male TKA patients showed higher expression of type I collagen (*COL1A2*) and aggrecan (*ACAN*) compared to females. In contrast, female donors exhibited significantly higher average expression levels of the hypertrophic differentiation marker type X collagen (*COL10A1*), a well-established marker for OA development associated with matrix catabolism (147, 261). Similarly, bone

morphogenetic protein-2 (*BMP2*) also showed significantly higher expression in females. BMPs are secreted signaling molecules that belong to the transforming growth factor-beta (TGF-β) superfamily and play crucial roles in bone and cartilage formation (262). While some studies indicate that BMP2 can induce chondrogenesis and act as a reparative response to mechanical injury of cartilage (263-265), increased *BMP2* expression could also be an indicator of OA progression. It is suggested that BMP2 could elevate the degradation of aggrecan in knee articular cartilage through a process mediated by MMPs and ADAMTS (266). In our study using the meniscus model, only *ADAMTS5* showed higher expression levels in females, but the difference was not significant.

Transient receptor potential cation channel subfamily V member 4 (*TRPV4*) and *Piezo1* are key Ca^{2+} permeable ion channels in chondrocytes that mediate cellular responses to mechanical stimulation (267). The activation of these channels depends on the type and amplitude of mechanical stimuli. *TRPV4* responds to moderate physiological mechanical loading, enhancing anabolic responses (268, 269), whereas *Piezo1* is activated by injurious forces, often resulting in cartilage degradation and inflammation (167, 270). In this study, the expression of *TRPV4* showed no significant difference between female and male donors, while females exhibited a marginally higher expression of *Piezo1* compared to males. With the onset and progression of KOA, the structural and mechanical environment alters, shifting loading patterns and potentially causing excessive loading (271). Our data on the sex differences in *Piezo1* expression support these findings, suggesting that mechanotransduction pathways mediated by *Piezo1* could be a contributing factor to the observed sex differences in KOA.

Our study explored the role of CD36 in knee osteoarthritis (KOA) using meniscus models, focusing on its involvement in KOA mechanisms and sex-specific differences. CD36, known for its multifunctional roles in fatty acid metabolism, inflammation, and angiogenesis (240), has been extensively studied in cardiovascular and metabolic diseases (241, 243, 272). However, its role in KOA, particularly in relation to sex differences, remains poorly understood. Our findings revealed nearly twice the number of CD36-expressing cells on the surface in females compared to males in the inner meniscus of TKA samples, a marginally significant difference despite the overall low positive

population. This cell surface expression correlated with higher average CD36 gene expression in females, though not significantly. Previous study on CD36 expression in human OA articular cartilage showed that CD36-expressing chondrocytes were mostly distributed in a zone-dependent manner, and the number of CD36-stained cells significantly increased with KOA severity (245). In our study, cells from the inner meniscus region were pooled for analysis. Future studies should examine the histological distribution of CD36 in the meniscus and its correlation with KOA severity for more comprehensive comparison between sex groups.

Other than its correlation with KOA severity, CD36 expression has been found to be concentrated at cartilage injury sites and colocalized with developing chondrocyte hypertrophy and aggrecan cleavage in articular cartilage (273). Our findings validated this observation at the gene expression level and GAG deposition. Correlated with higher *CD36* expression, females showed significantly higher expression of the hypertrophic marker *COL10A1,* and reduced Safranin O staining compared to males.

CD36 has also been demonstrated to colocalize with caveolin-1 in specialized membrane structures called caveolae (274). Caveolae are mechanosensitive plasma membrane invaginations, present in many types of cells, including fibrochondrocytes isolated from the inner region of the meniscus, with high caveolin-1 expression (41). Both mechanotransduction channels *TRPV4* (275) and *Piezo1* (276) have been indicated to interact with caveolae. The observed higher expression of *CD36* and *Piezo1* in females could be mediated through the effects of caveolae.

Despite the development of various model systems to study KOA (169), animal models remain crucial in OA research due to their ability to mimic human disease pathophysiology and facilitate the study of complex interactions within the knee joint (277, 278). The C57BL/6J inbred strain of mice is extensively utilized for studying developmental biology and the pathogenesis of OA (279-282). These mice are also known to develop spontaneous OA with aging (281, 283, 284). While there have been studies examining the histopathological changes in the meniscus of C57BL/6J mice (285-287), data on the degree of calcification at an early age and comparisons between sex groups are lacking. Although meniscal ossification is a natural process in mouse and

rarely observed in human KOA, studying it in mouse models can provide crucial insights into the factors and molecular pathways that may trigger ossification during human disease progression, particularly in late-stage osteoarthritis. Moreover, mouse models allow us to observe the relationship between meniscal ossification and other KOA-related phenotypic changes. Ossification in mouse could serve as a measurable parameter to track disease progression, which may correlate with changes in tissue remodeling in human KOA. Our findings show that meniscus calcification in C57BL/6J mice can be detected as early as 4 weeks, with a significant increase in calcification volume by 12 weeks. No sex-dependent differences were observed in the WT group. Notably, CD36 knockout reduced calcification in females at three months, but this effect did not persist to six months, likely due to high variability among donors. This suggests that CD36 may influence calcification in a specific subset of females, emphasizing the need to consider the correlation with factors.

Although animal models are effective at mimicking the complex mechanical and physiological environments of OA, the outcomes of experimental studies can be significantly influenced by the genetic background of the animals and the experimental protocols used. For instance, one study compared six mouse models of OA using the C57BL/6J strain and found that CD36 upregulation is a hallmark of all four mechanical models of KOA (247). Microgravity environments, induced by space flight (111, 208), parabolic flight (93, 114), and simulated on Earth using various reactors (110, 250, 288), have proven effective as OA models by altering the mechanical environment. In this study, menisci were dissected from 4-week-old mice, encapsulated in agarose hydrogel to reduce shear stress typically observed with rotating wall bioreactors (289) and for easier handling, and cultured under simulated microgravity as an OA-inducing platform. The SMG culture significantly increased calcification in female WT mice compared to static controls, with a less pronounced effect on male meniscus calcification. Menisci under SMG conditions also exhibited other histopathological signs of OA development, including degeneration of the superficial hyaline cartilage region, hypertrophic differentiation, and cyst-like formation in the inner avascular zone (287).

Knocking out CD36 under SMG conditions significantly reduced meniscus calcification in female mice from day 7, with this effect persisting throughout the three-week culture period. Additionally, the rate of calcification growth was slower in the KO group compared to WT. To understand the tissue-level mechanisms behind CD36's protective effect on female meniscus calcification in an OA-inducing mechanical environment, we examined the expression levels of osteopontin (OPN). OPN is a highly phosphorylated glycoprotein present in almost every tissue (290), acting as a signaling protein and important substrate in matrix mineralization (291). In cartilage, OPN, encoded by *SPP1*, is secreted by chondrocytes and is mainly distributed in the pericellular space, signaling through integrins on the cell surface (292). Although OPN is present in both normal and pathological knee joints (293-296), its expression increases in OA articular cartilage, showing territorial deposition and colocalizing with hypertrophic chondrocytes (297). It also promotes pathological mineralization in OA cartilage (298). The overall intensity of immunofluorescent staining for OPN correlated with the trend of calcification volume, with the strongest expression observed in the SMG WT group for both males and females. This staining covered the entire anterior horn and was primarily distributed in the pericellular space and around cysts, colocalizing with type X collagen. The observed increase in hypertrophic differentiation and calcification are consistent with previous studies using the ACL injury model (75). In females, CD36 KO reduced OPN expression to levels similar to the static control group. These findings suggest that CD36 alleviates meniscus calcification by mediating OPN expression or its signaling pathway.

In addition to cellular hypertrophic differentiation, another well-recognized pathological process in KOA is angiogenesis, defined as the abnormal growth of blood vessels from pre-existing vasculature. Angiogenesis is abnormally increased in the synovium, osteophytes, and menisci of KOA joints (299). correlating with disease severity and pain sensation (300). In microvascular endothelial cells, CD36 functions as a negative regulator of angiogenesis through its interaction with thrombospondin-1 (TSP-1) (240). In cartilage, TSP-1 expression is confirmed, with severe osteoarthritic cartilage showing a significant reduction in TSP-1 synthesizing chondrocytes and matrix deposition, while its receptor, CD36, is upregulated (245). However, the specific effects of CD36 in cartilage remain unclear. To investigate this, we examined the expression of vascular

endothelial growth factor (VEGF), a proangiogenic factor. Our findings showed no significant differences in VEGF expression across sex and experimental groups, suggesting that KOA-related angiogenesis may not be directly influenced by CD36 under the conditions tested, or three weeks of SMG culture is insufficient to observe these changes.

5.5 Limitation and future study

Despite the significant findings of this study, several limitations should be acknowledged. Firstly, while we employed both human and mouse meniscus models to investigate the role of CD36 in KOA, our analyses were primarily qualitative, relying heavily on histological and immunofluorescent staining. Future studies should incorporate more quantitative methods. Advanced proteomic analyses of the meniscus and culture medium, which are preserved, can provide valuable insights into the proteins and growth factors secreted under different conditions, further elucidating the molecular mechanisms.

Additionally, while we focused on the expression of CD36 and its correlation with key markers like osteopontin (OPN) and vascular endothelial growth factor (VEGF), it is crucial to explore CD36's role in fatty acid metabolism, inflammation, and angiogenesis more deeply. This could be achieved by examining pathways related to these processes, such as RNA sequencing (RNA-seq) data, to provide a comprehensive overview of gene expression profiles and pathways involved. This approach could help elucidate the molecular mechanisms underlying the sex-specific effects of CD36 in KOA.

Moreover, the current study utilized simulated microgravity (SMG) as an OA-inducing platform. Future research should explore other mechanical models and longer culture periods to capture the progression of KOA more accurately. Investigating the temporal and spatial distribution of CD36 and its associated pathways in different meniscal regions and under varying mechanical conditions will be essential to understanding its comprehensive role in KOA pathogenesis.

5.6 Conclusion

This study provides significant insights into the role of CD36 in knee osteoarthritis (KOA) pathogenesis, particularly focusing on sex-specific differences using both human and mouse meniscus models. Our findings indicate that CD36 modulates meniscus calcification and hypertrophic differentiation in a sex-specific manner under KOA-inducing conditions. CD36 knockout significantly reduced meniscus calcification and osteopontin (OPN) expression in female mice, suggesting a potential protective effect. These findings underscore the importance of considering sex differences in KOA research and suggest that CD36 may be a potential therapeutic target. Future research should focus on further elucidating the molecular pathways involving CD36, including its roles in fatty acid metabolism, inflammation, and angiogenesis, to develop targeted treatments for KOA.

5.7 Supplementary materials

Supplementary Table 5.1 Non-identifiable Donor Information

Donor	Sex	Age	Donor	Sex	Age
1	Female	69	1	Male	66
2	Female	56	2	Male	72
3	Female	81	3	Male	63
4	Female	73	4	Male	75
5	Female	69	5	Male	69
6	Female	85	6	Male	67
7	Female	62	7	Male	57

Supplementary Table 5.2 Detailed information on primary and secondary antibody used for mice meniscus immunofluorescent staining in this study.

Primary Antibodies						
Marker	**Host**	**Clonality**	**Isotype**	**Dilution**	**Company**	**Product Code**
COL II	Mouse	Monoclonal	IgG	1:200	DSHB	II-II6B3
COL X	Rabbit	Polyclonal	IgG	1:200	Invitrogen	PA5-97603
VEGF	Mouse	Monoclonal	IgG	1:100	Novus Biologicals	NB100-664
OPN	Rabbit	Polyclonal	IgG	1:400	Abcam	ab181440
Secondary Antibodies						
Fluorochrome	**Host**	**Clonality**	**Target**	**Dilution**	**Company**	**Product Code**
Alexa Fluor Plus 488	Goat	Polyclonal	Mouse	1:200	Thermo Fisher	PIA32723
Alexa Fluor 594	Goat	Polyclonal	Rabbit	1:200	Thermo Fisher	A11012

Supplementary Table 5.3 Detailed primer sequence information of genes analyzed by RT-qPCR

Gene		Primer Sequences	Accession number
RPL13A	Forward	CCTGGAGGAGAAGAGGAAAGAGA	NM_012423.4
	Reverse	TTGAGGACCTCTGTGTATTTGTCAA	
B2M	Forward	TGCTGTCTCCATGTTTGATGTATCT	NM_004048.2
	Reverse	TCTCTGCTCCCCACCTCTAAGT	
YWHAZ	Forward	TCTGTCTTGTCACCAACCATTCTT	NM_003406
	Reverse	TCATGCGGCCTTTTTCCA	
ACAN	Forward	AGGGCGAGTGGAATGATGTT	NM_001135.3
	Reverse	GGTGGCTGTGCCCTTTTTAC	
COL1A2	Forward	GCTACCCAACTTGCCTTCATG	NM_000089.3
	Reverse	GCAGTGGTAGGTGATGTTCTGAGA	
COL2A1	Forward	CTGCAAAATAAAATCTCGGTGTTCT	NM_033150
	Reverse	GGGCATTTGACTCACACCAGT	
COL10A1	Forward	GAAGTTATAATTTACACTGAGGGTTTCAAA	NM_000493.3
	Reverse	GAGGCACAGCTTAAAAGTTTTAAACA	
SOX9	Forward	CTTTGGTTTGTGTTCGTGTTTTG	NM_000346.3
	Reverse	AGAGAAAGAAAAAGGGAAAGGTAAGTTT	
MMP3	Forward	AGGCATCCACACCCTAGGTTT	NM_002422
	Reverse	ATCAGAAATGGCTGCATCGAT	
MMP13	Forward	CATCCAAAAACGCCAGACAA	NM_002427.4
	Reverse	CGGAGACTGGTAATGGCATCA	
RUNX2	Forward	GGAGTGGACGAGGCAAGAGTTT	NM_001024630.4
	Reverse	AGCTTCTGTCTGTGCCTTCTGG	
BMP2	Forward	ACGAGGTCCTGAGCGAGTTC	NM_001200.3
	Reverse	GAAGCTCTGCTGAGGTGATAA	
SPP1	Forward	TGAGCATTCCGATGTGATTGA	NM_001040058.
	Reverse	TGTGGAATTCACGGCTGACTT	
ADAMTS5	Forward	TGTAGCCTGCATTCCACAACA	NM_007038.5
	Reverse	CCCAAACGGCTCAGTTCAA	
VEGFA	Forward	GCACGGTCCCTCTTGGAA	NM_001025366.2
	Reverse	CGGTGATTTAGCAGCAAGAAAA	
JUN	Forward	CGGAGAGGAAGCGCATGA	NM_002228.4
	Reverse	TTCCTTTTTCGGCACTTGGA	
IHH	Forward	CCTTGTCAGCCGTGAGGCCG	NM 002181.4
	Reverse	GCTGCCGGCTCCGTGTGATT	
CD36	Forward	TTCCTGCAGCCCAATGGT	NM_001001548.3
	Reverse	GTCAGCCTCTGTTCCAACTGATAG	
TRPV4	Forward	GGCTGCTCCCATTCTTGCT	NM_021625.5
	Reverse	GATGGCTCTCGAAACTCCTCAT	
PIEZO1	Forward	CGCACGCACCGAAATTCT	NM_001330751.2
	Reverse	ACGGCTGTAGGGCGATCTT	

Chapter 6

Discussion and future directions

6.1 Discussion

The overarching theme of this thesis centers on using SMG as an innovative platform to induce OA-like phenotypes in meniscus models, with a focused exploration of sex-dependent differences in disease progression. The findings compellingly demonstrate SMG's efficacy in replicating KOA-related changes in the meniscus models, validated through a comprehensive approach involving both human and mouse models. The effectiveness of SMG in inducing OA-like phenotypes was confirmed through detailed analyses at both the transcriptome and tissue levels, including the upregulation of key KOA markers and notable changes in ECM degradation, calcification, and mechanical properties. These results underscore SMG's potential as a powerful tool for studying KOA. The consistency of these changes across human and mouse menisci further reinforces the platform's relevance and utility as a disease model.

A significant contribution of this thesis is the identification of sex-dependent differences in KOA progression, particularly the roles of key markers such as JUN and CD36. The research reveals a higher expression of *CD36* in females, highlighting its protective effect against calcification under SMG conditions. These findings suggest that CD36 is a critical mediator of the observed sex-specific differences in KOA, emphasizing the importance of considering sex as a vital factor in KOA research and in the development of targeted therapeutic strategies. Moreover, the thesis successfully integrates findings across different experimental models, varying durations of exposure, and multiple levels of analysis. This integrative approach not only provides a comprehensive understanding of how SMG induces OA-like changes but also strengthens the validity of the conclusions drawn. By adopting a multi-faceted methodology, this research establishes a robust framework for future studies aimed at unraveling the complexities of KOA pathogenesis, offering new insights into the disease's underlying mechanisms and potential avenues for intervention.

This thesis is structured through a series of interconnected studies that build on one another to deepen the understanding of KOA pathogenesis. Chapter 2 explores the short-term responses of primary meniscus fibrochondrocytes to SMG, revealing significant enrichment of genes and pathways related to inflammation and immune response in early KOA onset. This study suggests that short-term SMG can induce molecular events mimicking early KOA, with sex dimorphism in cellular proliferation and *JUN* expression potentially influencing early disease progression. Chapter 3 extends these findings by examining long-term effects on engineered meniscus models, demonstrating that SMG induces an OA-like profile while cyclic hydrostatic pressure (CHP) promotes chondrogenesis. Sex-dependent differences were evident in the magnitude and direction of gene expression changes, tissue constructs contraction, and the correlation of contractile genes with other factors. Chapter 4 builds on the SMG study from Chapter 3, focusing on the transcriptome profile and identifying CD36 as a marker for higher osteoarthritis development propensity in females. Chapter 5 further investigates the role of CD36 in sex differences related to KOA using human knee arthroplasty meniscus samples and a CD36 knockout mouse model, finding that CD36 modulates meniscus calcification and hypertrophic differentiation in a sex-specific manner, with knockout reducing calcification and osteopontin (OPN) expression in female mice.

Contextualizing these findings within broader literature, this thesis aligns with previous research establishing that microgravity environments can induce significant musculoskeletal degeneration similar to KOA (301-303). This thesis demonstrates that SMG effectively induces OA-like phenotypes in meniscus models, including the upregulation of key KOA markers and alterations in molecular pathways associated with inflammation, ECM degradation, and calcification. This further validates microgravity as a model for KOA and highlights its utility in exploring early molecular events in the disease.

Building on these aligned findings, this thesis introduces several critical insights that advance the field in meaningful ways. First, this thesis stands out by utilizing human tissue to model OA-like phenotypes under SMG conditions, a significant departure from the predominant focus on animal models in spaceflight research. While animal studies

have provided valuable insights into musculoskeletal degeneration in microgravity, the use of human meniscus tissue in this study directly addresses the translational gap and enhances the relevance of the findings to human health. This approach not only increases the applicability of the results to clinical settings but also provides a more accurate reflection of human physiological responses to microgravity.

Second, the focus on the meniscus, rather than the more commonly studied articular cartilage, represents a novel and significant shift in research perspective. The meniscus is a highly mechanosensitive tissue, known to exhibit OA-like pathology often before changes are observed in the articular cartilage. This study highlights the importance of the meniscus as an early indicator of KOA development, particularly under altered mechanical conditions such as SMG. By shifting the focus to the meniscus, this research uncovers early molecular and structural changes that may precede the degeneration of articular cartilage, offering a more comprehensive understanding of the disease's progression.

Moreover, this thesis examines the effects of SMG across various durations, from short-term to long-term exposure, within the same human meniscus model. This temporal profiling provides a detailed understanding of how OA-like changes evolve over time under SMG, revealing the progression of molecular and tissue-level alterations. Such a temporal analysis is crucial for identifying the stages at which interventions may be most effective, thereby contributing valuable information for the development of time-sensitive therapeutic strategies.

The focus on sex differences further distinguishes this work from the existing literature. While the impact of microgravity on musculoskeletal health has been studied extensively, the role of sex in mediating these effects has often been overlooked. This thesis demonstrates that sex-specific responses are not only significant but may also dictate the progression and severity of KOA under SMG conditions. The identification of CD36 as a key molecule that accounts for these sex differences offers a new avenue for research and potential therapeutic targets. The observed higher expression of *CD36* in females, and its protective role against calcification under SMG, underscores the necessity of considering sex as a critical variable in KOA research and treatment.

Despite the significant insights provided by this research, several limitations should be acknowledged. First, while the use of SMG to model OA-like phenotypes in meniscus models offers a novel approach, it is important to recognize the limitations associated with the bioreactors used to simulate microgravity. These bioreactors, while effective in creating a low-shear, microgravity-like environment, may not perfectly replicate the nuanced mechanical unloading that occurs in actual microgravity. Factors such as potential variations in fluid dynamics, the uniformity of microgravity simulation, and the constraints on the size and shape of the samples used can influence the outcomes.

Second, although this thesis successfully incorporates both human and mouse models to explore KOA progression under SMG, the extrapolation of these findings to broader human populations should be done with caution. The study's sample size for human tissue, while informative, would benefit from being larger to ensure the robustness and generalizability of the findings.

Another limitation lies in the duration of SMG exposure used in the experiments. While the study examined both short-term and long-term effects, the specific durations chosen may not fully encompass the range of exposure times relevant to spaceflight or the chronic nature of KOA development. The absence of even longer duration studies may limit the understanding of the full temporal progression of OA-like changes under SMG conditions.

Moreover, the study's focus on the meniscus, while providing novel insights into an often-overlooked tissue in KOA research, inherently limits the scope of the findings. KOA is a multifactorial disease affecting the entire joint, including articular cartilage, subchondral bone, synovium, and surrounding tissues. While the meniscus is a critical component, the interactions between these various joint tissues under SMG conditions were not explored in this thesis. Future studies should aim to integrate the meniscus findings with investigations into other joint components to develop a more comprehensive understanding of KOA pathogenesis under altered mechanical environments.

Lastly, while this research highlights the importance of sex differences in KOA progression, the underlying mechanisms driving these differences remain incompletely

understood. The identification of CD36 as a key mediator is a significant step forward, but the broader network of molecular interactions and pathways that contribute to sex-specific responses to SMG is still not fully elucidated. Further research is needed to dissect these pathways and to explore potential therapeutic interventions that could mitigate the observed sex differences in KOA progression.

In summary, this thesis demonstrates the effectiveness of SMG as a platform to model OA-like phenotypes in meniscus models, with a particular focus on sex-dependent differences. The research highlights the role of CD36 in mediating these differences, underscoring the importance of considering sex in KOA research and therapy development. Despite limitations, the findings provide valuable insights into KOA pathogenesis and establish a strong foundation for future studies aimed at unraveling the complexities of KOA and its treatment.

6.2 Future directions

The findings of this thesis open several avenues for further research to enhance our understanding of sex-dependent KOA pathology and improve therapeutic strategies. By building on the insights gained from this study, future research can address remaining questions and explore new areas to advance the field. Key areas for future work include:

Understand the mechanotransduction mechanisms in the meniscus during KOA: Further exploration is needed to deepen our understanding of the mechanotransduction pathways in meniscus cells specifically under osteoarthritic conditions. Investigating how various mechanical stimuli influence cellular behaviors and extracellular matrix production in the context of KOA will provide insights into the fundamental processes driving KOA pathology.

Longitudinal studies with extended duration of SMG and more detailed transcriptome profiles: Conducting longitudinal studies with extended durations of SMG exposure will help to assess the chronic effects on meniscus pathology and KOA progression. These studies should focus on obtaining more detailed transcriptome profiles over time to capture the temporal dynamics of gene expression changes associated with prolonged mechanical unloading.

Application of more advanced bioinformatics techniques at various levels: Incorporating advanced bioinformatics techniques such as signal cell RNA sequencing, spatial transcriptomics, and proteomics will provide a comprehensive understanding of the molecular mechanisms involved in KOA. These techniques will help to identify complex molecular interactions and pathways that are critical for the pathological changes in KOA progression.

Functional validation of identified markers: Functional validation of identified markers, such as JUN and CD36, is crucial. This involves performing functional analyses such as protein interaction studies and pharmacological inhibitions to confirm their roles in sex-specific responses to KOA induced by mechanical unloading and their potential as therapeutic targets for mitigating KOA progression.

Include larger number of donors and more diverse backgrounds: Expanding the donor pool to include a larger and more diverse population will help to validate findings across different genetic backgrounds and demographics. This diversity is essential for developing therapeutic strategies that are effective across a broad range of patients.

Validate results in real microgravity: Validating the results obtained from simulated microgravity studies in real microgravity conditions, such as those experienced during space missions, will strengthen the findings. This validation will ensure that the observed molecular and cellular responses are not artifacts of the simulation but are truly indicative of how meniscus cells respond to mechanical unloading in KOA. Additionally, understanding these responses in real microgravity has important implications for space health, as it can provide insights into joint health and degeneration in astronauts.

By pursuing these research directions, the understanding of KOA pathology, sex-dependent differences, and its management can be significantly advanced, potentially leading to improved outcomes for patients suffering from this debilitating condition. Additionally, insights gained from this thesis can have important implications for space health, aiding in the development of strategies to mitigate joint degeneration and maintain musculoskeletal health during long-term space missions.

References

1. Bartels DW, Kyle Martin R, Levy BA. 14 - Meniscus Biomechanics. In: LaPrade RF, Chahla J, editors. Evidence-Based Management of Complex Knee Injuries. Philadelphia: Elsevier; 2022. p. 176-84.
2. Fox AJ, Bedi A, Rodeo SA. The basic science of human knee menisci: structure, composition, and function. Sports Health. 2012;4(4):340-51.
3. Makris EA, Hadidi P, Athanasiou KA. The knee meniscus: structure-function, pathophysiology, current repair techniques, and prospects for regeneration. Biomaterials. 2011;32(30):7411-31.
4. Clark CR, Ogden JA. Development of the menisci of the human knee joint. Morphological changes and their potential role in childhood meniscal injury. J Bone Joint Surg Am. 1983;65(4):538-47.
5. Seitz AM, Osthaus F, Schwer J, Warnecke D, Faschingbauer M, Sgroi M, et al. Osteoarthritis-Related Degeneration Alters the Biomechanical Properties of Human Menisci Before the Articular Cartilage. Front Bioeng Biotechnol. 2021;9:659989.
6. Canada BaJ. Osteoarthritis 2014 [Available from: http://boneandjointcanada.com/osteoarthritis/.
7. Breedveld FC. Osteoarthritis--the impact of a serious disease. Rheumatology (Oxford). 2004;43 Suppl 1:i4-8.
8. Roman MD, Russu O, Mohor C, Necula R, Boicean A, Todor A, et al. Outcomes in revision total knee arthroplasty (Review). Exp Ther Med. 2022;23(1):29.
9. Secretariat MA. Total knee replacement: an evidence based analysis. 2005.
10. Kohn D, Moreno B. Meniscus insertion anatomy as a basis for meniscus replacement: a morphological cadaveric study. Arthroscopy. 1995;11(1):96-103.
11. Walker PS, Erkman MJ. The role of the menisci in force transmission across the knee. Clin Orthop Relat Res. 1975(109):184-92.
12. Petersen W, Tillmann B. Collagenous fibril texture of the human knee joint menisci. Anat Embryol (Berl). 1998;197(4):317-24.

13. Abraham AC, Donahue TL. From meniscus to bone: a quantitative evaluation of structure and function of the human meniscal attachments. Acta Biomater. 2013;9(5):6322-9.
14. Sanchez-Adams J, Athanasiou KA. The Knee Meniscus: A Complex Tissue of Diverse Cells. Cellular and Molecular Bioengineering. 2009;2(3):332-40.
15. SP A. Gross and vascular anatomy of the meniscus and its role in meniscal healing, regeneration and remodeling. . Knee Meniscus: Basic and Clinical Foundations. 1992:1-14.
16. Petersen W, Tillmann B. Age-related blood and lymph supply of the knee menisci. A cadaver study. Acta Orthop Scand. 1995;66(4):308-12.
17. Arnoczky SP, Warren RF. Microvasculature of the human meniscus. Am J Sports Med. 1982;10(2):90-5.
18. Noyes FR, Chen RC, Barber-Westin SD, Potter HG. Greater than 10-year results of red-white longitudinal meniscal repairs in patients 20 years of age or younger. Am J Sports Med. 2011;39(5):1008-17.
19. Noyes FR, Barber-Westin SD. Arthroscopic repair of meniscal tears extending into the avascular zone in patients younger than twenty years of age. Am J Sports Med. 2002;30(4):589-600.
20. Barber-Westin SD, Noyes FR. Clinical healing rates of meniscus repairs of tears in the central-third (red-white) zone. Arthroscopy. 2014;30(1):134-46.
21. Herwig J, Egner E, Buddecke E. Chemical changes of human knee joint menisci in various stages of degeneration. Ann Rheum Dis. 1984;43(4):635-40.
22. Cheung HS. Distribution of type I, II, III and V in the pepsin solubilized collagens in bovine menisci. Connect Tissue Res. 1987;16(4):343-56.
23. Eyre DR, Wu JJ. Collagen of fibrocartilage: a distinctive molecular phenotype in bovine meniscus. FEBS Lett. 1983;158(2):265-70.
24. Eyre DR KT, Chun LE. Biochemistry of the meniscus: unique profile of collagen types and site dependent variations in composition. Orthop Trans. 1983;8:56.
25. Scott PG, Nakano T, Dodd CM. Isolation and characterization of small proteoglycans from different zones of the porcine knee meniscus. Biochim Biophys Acta. 1997;1336(2):254-62.

26. Nakata K, Shino K, Hamada M, Mae T, Miyama T, Shinjo H, et al. Human meniscus cell: characterization of the primary culture and use for tissue engineering. Clin Orthop Relat Res. 2001(391 Suppl):S208-18.
27. McDevitt CA, Webber RJ. The ultrastructure and biochemistry of meniscal cartilage. Clin Orthop Relat Res. 1990(252):8-18.
28. Ghadially FN, Lalonde JM, Wedge JH. Ultrastructure of normal and torn menisci of the human knee joint. J Anat. 1983;136(Pt 4):773-91.
29. Verdonk PC, Forsyth RG, Wang J, Almqvist KF, Verdonk R, Veys EM, et al. Characterisation of human knee meniscus cell phenotype. Osteoarthritis Cartilage. 2005;13(7):548-60.
30. Sun H, Wen X, Li H, Wu P, Gu M, Zhao X, et al. Single-cell RNA-seq analysis identifies meniscus progenitors and reveals the progression of meniscus degeneration. Ann Rheum Dis. 2020;79(3):408-17.
31. Sweigart MA, Athanasiou KA. Toward tissue engineering of the knee meniscus. Tissue Eng. 2001;7(2):111-29.
32. Sweigart MA, Zhu CF, Burt DM, DeHoll PD, Agrawal CM, Clanton TO, et al. Intraspecies and interspecies comparison of the compressive properties of the medial meniscus. Ann Biomed Eng. 2004;32(11):1569-79.
33. Fithian DC, Kelly MA, Mow VC. Material properties and structure-function relationships in the menisci. Clin Orthop Relat Res. 1990(252):19-31.
34. Eifler RL, Blough ER, Dehlin JM, Haut Donahue TL. Oscillatory fluid flow regulates glycosaminoglycan production via an intracellular calcium pathway in meniscal cells. J Orthop Res. 2006;24(3):375-84.
35. Guilak F, Hayes AJ, Melrose J. Perlecan in Pericellular Mechanosensory Cell-Matrix Communication, Extracellular Matrix Stabilisation and Mechanoregulation of Load-Bearing Connective Tissues. Int J Mol Sci. 2021;22(5).
36. Hellio Le Graverand MP, Ou Y, Schield-Yee T, Barclay L, Hart D, Natsume T, et al. The cells of the rabbit meniscus: their arrangement, interrelationship, morphological variations and cytoarchitecture. J Anat. 2001;198(Pt 5):525-35.

37. Wang C, Brisson BK, Terajima M, Li Q, Hoxha K, Han B, et al. Type III collagen is a key regulator of the collagen fibrillar structure and biomechanics of articular cartilage and meniscus. Matrix Biol. 2020;85-86:47-67.
38. Zhang Y, Wang F, Bao L, Li J, Shi Z, Wang J. Cyclic hydrostatic compress force regulates apoptosis of meniscus fibrochondrocytes via integrin alpha5beta1. Physiol Res. 2019;68(4):639-49.
39. Loeser RF. Integrins and chondrocyte-matrix interactions in articular cartilage. Matrix Biol. 2014;39:11-6.
40. Gao W, Hasan H, Anderson DE, Lee W. The Role of Mechanically-Activated Ion Channels Piezo1, Piezo2, and TRPV4 in Chondrocyte Mechanotransduction and Mechano-Therapeutics for Osteoarthritis. Front Cell Dev Biol. 2022;10:885224.
41. Vyhlidal MJ, Adesida AB. Mechanotransduction in meniscus fibrochondrocytes: What about caveolae? J Cell Physiol. 2022;237(2):1171-81.
42. Buwa N, Mazumdar D, Balasubramanian N. Caveolin1 Tyrosine-14 Phosphorylation: Role in Cellular Responsiveness to Mechanical Cues. J Membr Biol. 2020;253(6):509-34.
43. Echarri A, Del Pozo MA. Caveolae - mechanosensitive membrane invaginations linked to actin filaments. J Cell Sci. 2015;128(15):2747-58.
44. Kaji DA, Montero AM, Patel R, Huang AH. Transcriptional profiling of mESC-derived tendon and fibrocartilage cell fate switch. Nat Commun. 2021;12(1):4208.
45. Puetzer JL, Koo E, Bonassar LJ. Induction of fiber alignment and mechanical anisotropy in tissue engineered menisci with mechanical anchoring. J Biomech. 2015;48(8):1436-43.
46. Puetzer JL, Bonassar LJ. Physiologically Distributed Loading Patterns Drive the Formation of Zonally Organized Collagen Structures in Tissue-Engineered Meniscus. Tissue Eng Part A. 2016;22(13-14):907-16.
47. McCorry MC, Mansfield MM, Sha X, Coppola DJ, Lee JW, Bonassar LJ. A model system for developing a tissue engineered meniscal enthesis. Acta Biomater. 2017;56:110-7.

48. Kim J, Boys AJ, Estroff LA, Bonassar LJ. Combining TGF-beta1 and Mechanical Anchoring to Enhance Collagen Fiber Formation and Alignment in Tissue-Engineered Menisci. ACS Biomater Sci Eng. 2021;7(4):1608-20.
49. Han WM, Heo SJ, Driscoll TP, Boggs ME, Duncan RL, Mauck RL, et al. Impact of cellular microenvironment and mechanical perturbation on calcium signalling in meniscus fibrochondrocytes. Eur Cell Mater. 2014;27:321-31.
50. Meier EM, Wu B, Siddiqui A, Tepper DG, Longaker MT, Lam MT. Mechanical Stimulation Increases Knee Meniscus Gene RNA-level Expression in Adipose-derived Stromal Cells. Plast Reconstr Surg Glob Open. 2016;4(9):e864.
51. Liu C, Abedian R, Meister R, Haasper C, Hurschler C, Krettek C, et al. Influence of perfusion and compression on the proliferation and differentiation of bone mesenchymal stromal cells seeded on polyurethane scaffolds. Biomaterials. 2012;33(4):1052-64.
52. Petri M, Ufer K, Toma I, Becher C, Liodakis E, Brand S, et al. Effects of perfusion and cyclic compression on in vitro tissue engineered meniscus implants. Knee Surg Sports Traumatol Arthrosc. 2012;20(2):223-31.
53. Bahcecioglu G, Hasirci N, Bilgen B, Hasirci V. A 3D printed PCL/hydrogel construct with zone-specific biochemical composition mimicking that of the meniscus. Biofabrication. 2019;11(2):025002.
54. Szojka ARA, Li DX, Sopcak MEJ, Ma Z, Kunze M, Mulet-Sierra A, et al. Mechano-Hypoxia Conditioning of Engineered Human Meniscus. Front Bioeng Biotechnol. 2021;9:739438.
55. Szojka AR, Marqueti RC, Li DX, Molter CW, Liang Y, Kunze M, et al. Human engineered meniscus transcriptome after short-term combined hypoxia and dynamic compression. J Tissue Eng. 2021;12:2041731421990842.
56. Szojka ARA, Moore CN, Liang Y, Andrews SHJ, Kunze M, Mulet-Sierra A, et al. Engineered human meniscus' matrix-forming phenotype is unaffected by low strain dynamic compression under hypoxic conditions. PLoS One. 2021;16(3):e0248292.
57. Lueckgen J, Kraemer E, Reiner T, Richter W. Altered susceptibility to mechanical loading by hypertrophic degeneration of chondrocytes. Osteoarthritis and Cartilage. 2021;29.

58. Li Y, Zhou J, Yang X, Jiang Y, Gui J. Intermittent hydrostatic pressure maintains and enhances the chondrogenic differentiation of cartilage progenitor cells cultivated in alginate beads. Dev Growth Differ. 2016;58(2):180-93.
59. Mellor LF, Steward AJ, Nordberg RC, Taylor MA, Loboa EG. Comparison of Simulated Microgravity and Hydrostatic Pressure for Chondrogenesis of hASC. Aerosp Med Hum Perform. 2017;88(4):377-84.
60. Zellner J, Mueller M, Xin Y, Krutsch W, Brandl A, Kujat R, et al. Dynamic hydrostatic pressure enhances differentially the chondrogenesis of meniscal cells from the inner and outer zone. J Biomech. 2015;48(8):1479-84.
61. Ma Z, Li DX, Kunze M, Mulet-Sierra A, Westover L, Adesida AB. Engineered Human Meniscus in Modeling Sex Differences of Knee Osteoarthritis in Vitro. Front Bioeng Biotechnol. 2022;10:823679.
62. Puetzer JL, Ballyns JJ, Bonassar LJ. The effect of the duration of mechanical stimulation and post-stimulation culture on the structure and properties of dynamically compressed tissue-engineered menisci. Tissue Eng Part A. 2012;18(13-14):1365-75.
63. Zhang ZZ, Chen, Y. R., Wang, S. J., Zhao, F., Wang, X. G., Yang, F., Shi, J. J., Ge, Z. G., Ding, W. Y., Yang, Y. C., Zou, T. Q., Zhang, J. Y., Yu, J. K., & Jiang, D. . Orchestrated biomechanical, structural, and biochemical stimuli for engineering anisotropic meniscus. Science translational medicine. 2019;11:487.
64. Mayer-Wagner S, Hammerschmid F, Redeker JI, Schmitt B, Holzapfel BM, Jansson V, et al. Simulated microgravity affects chondrogenesis and hypertrophy of human mesenchymal stem cells. Int Orthop. 2014;38(12):2615-21.
65. Weiss WM, Mulet-Sierra A, Kunze M, Jomha NM, Adesida AB. Coculture of meniscus cells and mesenchymal stem cells in simulated microgravity. NPJ Microgravity. 2017;3:28.
66. Thomopoulos S, Fomovsky GM, Holmes JW. The development of structural and mechanical anisotropy in fibroblast populated collagen gels. J Biomech Eng. 2005;127(5):742-50.
67. Bowles RD, Williams RM, Zipfel WR, Bonassar LJ. Self-assembly of aligned tissue-engineered annulus fibrosus and intervertebral disc composite via collagen gel contraction. Tissue Eng Part A. 2010;16(4):1339-48.

68. Bell E, Ivarsson B, Merrill C. Production of a tissue-like structure by contraction of collagen lattices by human fibroblasts of different proliferative potential in vitro. Proc Natl Acad Sci U S A. 1979;76(3):1274-8.
69. Freutel M, Seitz AM, Galbusera F, Bornstedt A, Rasche V, Knothe Tate ML, et al. Medial meniscal displacement and strain in three dimensions under compressive loads: MR assessment. J Magn Reson Imaging. 2014;40(5):1181-8.
70. Peloquin JM, Santare MH, Elliott DM. Advances in Quantification of Meniscus Tensile Mechanics Including Nonlinearity, Yield, and Failure. J Biomech Eng. 2016;138(2):021002.
71. Zhao Z, Li Y, Wang M, Zhao S, Zhao Z, Fang J. Mechanotransduction pathways in the regulation of cartilage chondrocyte homoeostasis. J Cell Mol Med. 2020;24(10):5408-19.
72. Zelenski NA, Leddy HA, Sanchez-Adams J, Zhang J, Bonaldo P, Liedtke W, et al. Type VI Collagen Regulates Pericellular Matrix Properties, Chondrocyte Swelling, and Mechanotransduction in Mouse Articular Cartilage. Arthritis Rheumatol. 2015;67(5):1286-94.
73. Grad S, Eglin D, Alini M, Stoddart MJ. Physical stimulation of chondrogenic cells in vitro: a review. Clin Orthop Relat Res. 2011;469(10):2764-72.
74. O'Conor CJ, Case N, Guilak F. Mechanical regulation of chondrogenesis. Stem Cell Res Ther. 2013;4(4):61.
75. Du G, Zhan H, Ding D, Wang S, Wei X, Wei F, et al. Abnormal Mechanical Loading Induces Cartilage Degeneration by Accelerating Meniscus Hypertrophy and Mineralization After ACL Injuries In Vivo. Am J Sports Med. 2016;44(3):652-63.
76. Lund-Olesen K. Oxygen tension in synovial fluids. Arthritis Rheum. 1970;13(6):769-76.
77. Adesida AB, Grady LM, Khan WS, Hardingham TE. The matrix-forming phenotype of cultured human meniscus cells is enhanced after culture with fibroblast growth factor 2 and is further stimulated by hypoxia. Arthritis Res Ther. 2006;8(3):R61.
78. Szojka ARA, Lyons BD, Moore CN, Liang Y, Kunze M, Idrees E, et al. Hypoxia and TGF-beta3 Synergistically Mediate Inner Meniscus-Like Matrix Formation by Fibrochondrocytes. Tissue Eng Part A. 2019;25(5-6):446-56.

79. Tan GK, Dinnes DL, Myers PT, Cooper-White JJ. Effects of biomimetic surfaces and oxygen tension on redifferentiation of passaged human fibrochondrocytes in 2D and 3D cultures. Biomaterials. 2011;32(24):5600-14.
80. Huang T, Schor SL, Hinck AP. Biological activity differences between TGF-beta1 and TGF-beta3 correlate with differences in the rigidity and arrangement of their component monomers. Biochemistry. 2014;53(36):5737-49.
81. Bader DL, Salter DM, Chowdhury TT. Biomechanical influence of cartilage homeostasis in health and disease. Arthritis. 2011;2011:979032.
82. Miyanishi K, Trindade MC, Lindsey DP, Beaupre GS, Carter DR, Goodman SB, et al. Dose- and time-dependent effects of cyclic hydrostatic pressure on transforming growth factor-beta3-induced chondrogenesis by adult human mesenchymal stem cells in vitro. Tissue Eng. 2006;12(8):2253-62.
83. Miyanishi K, Trindade MC, Lindsey DP, Beaupre GS, Carter DR, Goodman SB, et al. Effects of hydrostatic pressure and transforming growth factor-beta 3 on adult human mesenchymal stem cell chondrogenesis in vitro. Tissue Eng. 2006;12(6):1419-28.
84. Wagner DR, Lindsey DP, Li KW, Tummala P, Chandran SE, Smith RL, et al. Hydrostatic pressure enhances chondrogenic differentiation of human bone marrow stromal cells in osteochondrogenic medium. Ann Biomed Eng. 2008;36(5):813-20.
85. Finger AR, Sargent CY, Dulaney KO, Bernacki SH, Loboa EG. Differential effects on messenger ribonucleic acid expression by bone marrow-derived human mesenchymal stem cells seeded in agarose constructs due to ramped and steady applications of cyclic hydrostatic pressure. Tissue Eng. 2007;13(6):1151-8.
86. Bahcecioglu G, Hasirci N, Bilgen B, Hasirci V. Hydrogels of agarose, and methacrylated gelatin and hyaluronic acid are more supportive for in vitro meniscus regeneration than three dimensional printed polycaprolactone scaffolds. Int J Biol Macromol. 2019;122:1152-62.
87. Daly AC, Critchley SE, Rencsok EM, Kelly DJ. A comparison of different bioinks for 3D bioprinting of fibrocartilage and hyaline cartilage. Biofabrication. 2016;8(4):045002.

88. Liphardt AM, Godonou ET, Dreiner M, Mundermann A, Tascilar K, Djalal N, et al. Immobilization by 21 days of bed rest results in type II collagen degradation in healthy individuals. Osteoarthritis Cartilage. 2024;32(2):177-86.
89. Day JR, Frank AT, O'Callaghan JP, DeHart BW. Effects of microgravity and bone morphogenetic protein II on GFAP in rat brain. J Appl Physiol (1985). 1998;85(2):716-22.
90. Cogoli A. Signal transduction in T lymphocytes in microgravity. Gravit Space Biol Bull. 1997;10(2):5-16.
91. Stamenkovic V, Keller G, Nesic D, Cogoli A, Grogan SP. Neocartilage formation in 1 g, simulated, and microgravity environments: implications for tissue engineering. Tissue Eng Part A. 2010;16(5):1729-36.
92. Jin L, Feng G, Reames DL, Shimer AL, Shen FH, Li X. The effects of simulated microgravity on intervertebral disc degeneration. Spine J. 2013;13(3):235-42.
93. Aleshcheva G, Wehland M, Sahana J, Bauer J, Corydon TJ, Hemmersbach R, et al. Moderate alterations of the cytoskeleton in human chondrocytes after short-term microgravity produced by parabolic flight maneuvers could be prevented by up-regulation of BMP-2 and SOX-9. FASEB J. 2015;29(6):2303-14.
94. Unsworth BR, Lelkes PI. Growing tissues in microgravity. Nat Med. 1998;4(8):901-7.
95. Herranz R, Anken R, Boonstra J, Braun M, Christianen PC, de Geest M, et al. Ground-based facilities for simulation of microgravity: organism-specific recommendations for their use, and recommended terminology. Astrobiology. 2013;13(1):1-17.
96. Wuest SL, Calio M, Wernas T, Tanner S, Giger-Lange C, Wyss F, et al. Influence of Mechanical Unloading on Articular Chondrocyte Dedifferentiation. Int J Mol Sci. 2018;19(5).
97. Wang Q, Zheng YP, Wang XY, Huang YP, Liu MQ, Wang SZ, et al. Ultrasound evaluation of site-specific effect of simulated microgravity on articular cartilage. Ultrasound Med Biol. 2010;36(7):1089-97.

98. Boyan BD, Tosi LL, Coutts RD, Enoka RM, Hart DA, Nicolella DP, et al. Addressing the gaps: sex differences in osteoarthritis of the knee. Biol Sex Differ. 2013;4(1):4.
99. Englund M, Guermazi A, Lohmander SL. The role of the meniscus in knee osteoarthritis: a cause or consequence? Radiol Clin North Am. 2009;47(4):703-12.
100. Ozeki N, Koga H, Sekiya I. Degenerative Meniscus in Knee Osteoarthritis: From Pathology to Treatment. Life (Basel). 2022;12(4).
101. Lange AK, Fiatarone Singh MA, Smith RM, Foroughi N, Baker MK, Shnier R, et al. Degenerative meniscus tears and mobility impairment in women with knee osteoarthritis. Osteoarthritis Cartilage. 2007;15(6):701-8.
102. Nicolella DP, O'Connor MI, Enoka RM, Boyan BD, Hart DA, Resnick E, et al. Mechanical contributors to sex differences in idiopathic knee osteoarthritis. Biol Sex Differ. 2012;3(1):28.
103. O'Connor MI. Sex differences in osteoarthritis of the hip and knee. J Am Acad Orthop Surg. 2007;15 Suppl 1:S22-5.
104. Kinney RC, Schwartz Z, Week K, Lotz MK, Boyan BD. Human articular chondrocytes exhibit sexual dimorphism in their responses to 17beta-estradiol. Osteoarthritis Cartilage. 2005;13(4):330-7.
105. Zaki S, Blaker CL, Little CB. OA foundations - experimental models of osteoarthritis. Osteoarthritis Cartilage. 2022;30(3):357-80.
106. Johnson CI, Argyle DJ, Clements DN. In vitro models for the study of osteoarthritis. Vet J. 2016;209:40-9.
107. Brandt KD, Dieppe P, Radin E. Etiopathogenesis of osteoarthritis. Med Clin North Am. 2009;93(1):1-24, xv.
108. Vanwanseele B, Lucchinetti E, Stussi E. The effects of immobilization on the characteristics of articular cartilage: current concepts and future directions. Osteoarthritis Cartilage. 2002;10(5):408-19.
109. Souza RB, Baum T, Wu S, Feeley BT, Kadel N, Li X, et al. Effects of unloading on knee articular cartilage T1rho and T2 magnetic resonance imaging relaxation times: a case series. J Orthop Sports Phys Ther. 2012;42(6):511-20.

110. Laws CJ, Berg-Johansen B, Hargens AR, Lotz JC. The effect of simulated microgravity on lumbar spine biomechanics: an in vitro study. Eur Spine J. 2016;25(9):2889-97.
111. Fitzgerald J, Endicott J, Hansen U, Janowitz C. Articular cartilage and sternal fibrocartilage respond differently to extended microgravity. NPJ Microgravity. 2019;5:3.
112. Ma Z, Li DX, Chee RKW, Kunze M, Mulet-Sierra A, Sommerfeldt M, et al. Mechanical Unloading of Engineered Human Meniscus Models Under Simulated Microgravity: A Transcriptomic Study. Sci Data. 2022;9(1):736.
113. Wehland M, Aleshcheva G, Schulz H, Saar K, Hubner N, Hemmersbach R, et al. Differential gene expression of human chondrocytes cultured under short-term altered gravity conditions during parabolic flight maneuvers. Cell Commun Signal. 2015;13:18.
114. Aissiou AK, Jha S, Dhunnoo K, Ma Z, Li DX, Ravin R, et al. Transcriptomic response of bioengineered human cartilage to parabolic flight microgravity is sex-dependent. NPJ Microgravity. 2023;9(1):5.
115. Adesida AB, Mulet-Sierra A, Laouar L, Jomha NM. Oxygen tension is a determinant of the matrix-forming phenotype of cultured human meniscal fibrochondrocytes. PLoS One. 2012;7(6):e39339.
116. Bornes TD, Jomha NM, Mulet-Sierra A, Adesida AB. Optimal Seeding Densities for In Vitro Chondrogenesis of Two- and Three-Dimensional-Isolated and -Expanded Bone Marrow-Derived Mesenchymal Stromal Stem Cells Within a Porous Collagen Scaffold. Tissue Eng Part C Methods. 2016;22(3):208-20.
117. Bradley PX, Thomas KN, Kratzer AL, Robinson AC, Wittstein JR, DeFrate LE, et al. The Interplay of Biomechanical and Biological Changes Following Meniscus Injury. Curr Rheumatol Rep. 2023;25(2):35-46.
118. Lieberthal J, Sambamurthy N, Scanzello CR. Inflammation in joint injury and post-traumatic osteoarthritis. Osteoarthritis Cartilage. 2015;23(11):1825-34.
119. Woodell-May JE, Sommerfeld SD. Role of Inflammation and the Immune System in the Progression of Osteoarthritis. J Orthop Res. 2020;38(2):253-7.
120. Sward P, Frobell R, Englund M, Roos H, Struglics A. Cartilage and bone markers and inflammatory cytokines are increased in synovial fluid in the acute phase of knee

injury (hemarthrosis)--a cross-sectional analysis. Osteoarthritis Cartilage. 2012;20(11):1302-8.
121. Clair AJ, Kingery MT, Anil U, Kenny L, Kirsch T, Strauss EJ. Alterations in Synovial Fluid Biomarker Levels in Knees With Meniscal Injury as Compared With Asymptomatic Contralateral Knees. Am J Sports Med. 2019;47(4):847-56.
122. Liu B, Goode AP, Carter TE, Utturkar GM, Huebner JL, Taylor DC, et al. Matrix metalloproteinase activity and prostaglandin E2 are elevated in the synovial fluid of meniscus tear patients. Connect Tissue Res. 2017;58(3-4):305-16.
123. Haslauer CM, Elsaid KA, Fleming BC, Proffen BL, Johnson VM, Murray MM. Loss of extracellular matrix from articular cartilage is mediated by the synovium and ligament after anterior cruciate ligament injury. Osteoarthritis Cartilage. 2013;21(12):1950-7.
124. Mills CD, Kincaid K, Alt JM, Heilman MJ, Hill AM. M-1/M-2 macrophages and the Th1/Th2 paradigm. J Immunol. 2000;164(12):6166-73.
125. Miotla Zarebska J, Chanalaris A, Driscoll C, Burleigh A, Miller RE, Malfait AM, et al. CCL2 and CCR2 regulate pain-related behaviour and early gene expression in post-traumatic murine osteoarthritis but contribute little to chondropathy. Osteoarthritis Cartilage. 2017;25(3):406-12.
126. Boehme KA, Rolauffs B. Onset and Progression of Human Osteoarthritis-Can Growth Factors, Inflammatory Cytokines, or Differential miRNA Expression Concomitantly Induce Proliferation, ECM Degradation, and Inflammation in Articular Cartilage? Int J Mol Sci. 2018;19(8).
127. Felka T, Rothdiener M, Bast S, Uynuk-Ool T, Zouhair S, Ochs BG, et al. Loss of spatial organization and destruction of the pericellular matrix in early osteoarthritis in vivo and in a novel in vitro methodology. Osteoarthritis Cartilage. 2016;24(7):1200-9.
128. Tallheden T, Bengtsson C, Brantsing C, Sjogren-Jansson E, Carlsson L, Peterson L, et al. Proliferation and differentiation potential of chondrocytes from osteoarthritic patients. Arthritis Res Ther. 2005;7(3):R560-8.
129. Diril MK, Ratnacaram CK, Padmakumar VC, Du T, Wasser M, Coppola V, et al. Cyclin-dependent kinase 1 (Cdk1) is essential for cell division and suppression of DNA

re-replication but not for liver regeneration. Proc Natl Acad Sci U S A. 2012;109(10):3826-31.
130. Saito M, Mulati M, Talib SZ, Kaldis P, Takeda S, Okawa A, et al. The Indispensable Role of Cyclin-Dependent Kinase 1 in Skeletal Development. Sci Rep. 2016;6:20622.
131. Huan X, Jinhe Y, Rongzong Z. Identification of Pivotal Genes and Pathways in Osteoarthritic Degenerative Meniscal Lesions via Bioinformatics Analysis of the GSE52042 Dataset. Med Sci Monit. 2019;25:8891-904.
132. Li C, Zheng Z. Identification of Novel Targets of Knee Osteoarthritis Shared by Cartilage and Synovial Tissue. Int J Mol Sci. 2020;21(17).
133. Melrose J, Roughley P, Knox S, Smith S, Lord M, Whitelock J. The structure, location, and function of perlecan, a prominent pericellular proteoglycan of fetal, postnatal, and mature hyaline cartilages. J Biol Chem. 2006;281(48):36905-14.
134. Bleuel J, Zaucke F, Bruggemann GP, Niehoff A. Effects of cyclic tensile strain on chondrocyte metabolism: a systematic review. PLoS One. 2015;10(3):e0119816.
135. Papachristou D, Pirttiniemi P, Kantomaa T, Agnantis N, Basdra EK. Fos- and Jun-related transcription factors are involved in the signal transduction pathway of mechanical loading in condylar chondrocytes. Eur J Orthod. 2006;28(1):20-6.
136. Sassi N, Laadhar L, Allouche M, Zandieh-Doulabi B, Hamdoun M, Klein-Nulend J, et al. Wnt signaling is involved in human articular chondrocyte de-differentiation in vitro. Biotech Histochem. 2014;89(1):29-40.
137. Wang Y, Fan X, Xing L, Tian F. Wnt signaling: a promising target for osteoarthritis therapy. Cell Commun Signal. 2019;17(1):97.
138. Luyten FP, Tylzanowski P, Lories RJ. Wnt signaling and osteoarthritis. Bone. 2009;44(4):522-7.
139. Lehtovirta S, Makitie RE, Casula V, Haapea M, Niinimaki J, Niinimaki T, et al. Defective WNT signaling may protect from articular cartilage deterioration - a quantitative MRI study on subjects with a heterozygous WNT1 mutation. Osteoarthritis Cartilage. 2019;27(11):1636-46.

140. Sun Y, Mauerhan DR, Honeycutt PR, Kneisl JS, Norton HJ, Zinchenko N, et al. Calcium deposition in osteoarthritic meniscus and meniscal cell culture. Arthritis Res Ther. 2010;12(2):R56.
141. Blackburn SG, Research & Rhodes, C. & Higginbottom, A. & Dziedzic, K.. . The OARSI standardised definition of osteoarthritis: A lay version. Osteoarthritis and Cartilage. 2016;24.
142. Murray CJ, Vos T, Lozano R, Naghavi M, Flaxman AD, Michaud C, et al. Disability-adjusted life years (DALYs) for 291 diseases and injuries in 21 regions, 1990-2010: a systematic analysis for the Global Burden of Disease Study 2010. Lancet. 2012;380(9859):2197-223.
143. Boyan BD, Tosi L, Coutts R, Enoka R, Hart DA, Nicolella DP, et al. Sex differences in osteoarthritis of the knee. J Am Acad Orthop Surg. 2012;20(10):668-9.
144. Pan Q, O'Connor MI, Coutts RD, Hyzy SL, Olivares-Navarrete R, Schwartz Z, et al. Characterization of osteoarthritic human knees indicates potential sex differences. Biol Sex Differ. 2016;7:27.
145. Badley EM, Kasman NM. The Impact of Arthritis on Canadian Women. BMC Womens Health. 2004;4 Suppl 1(Suppl 1):S18.
146. Dreier R. Hypertrophic differentiation of chondrocytes in osteoarthritis: the developmental aspect of degenerative joint disorders. Arthritis Res Ther. 2010;12(5):216.
147. Aigner T, Reichenberger E, Bertling W, Kirsch T, Stoss H, von der Mark K. Type X collagen expression in osteoarthritic and rheumatoid articular cartilage. Virchows Arch B Cell Pathol Incl Mol Pathol. 1993;63(4):205-11.
148. D'Angelo M, Yan Z, Nooreyazdan M, Pacifici M, Sarment DS, Billings PC, et al. MMP-13 is induced during chondrocyte hypertrophy. J Cell Biochem. 2000;77(4):678-93.
149. Leijten JC, Emons J, Sticht C, van Gool S, Decker E, Uitterlinden A, et al. Gremlin 1, frizzled-related protein, and Dkk-1 are key regulators of human articular cartilage homeostasis. Arthritis Rheum. 2012;64(10):3302-12.
150. Elder BD, Athanasiou KA. Hydrostatic pressure in articular cartilage tissue engineering: from chondrocytes to tissue regeneration. Tissue Eng Part B Rev. 2009;15(1):43-53.

151. Gunja NJ, Uthamanthil RK, Athanasiou KA. Effects of TGF-beta1 and hydrostatic pressure on meniscus cell-seeded scaffolds. Biomaterials. 2009;30(4):565-73.
152. Yu B, Yu D, Cao L, Zhao X, Long T, Liu G, et al. Simulated microgravity using a rotary cell culture system promotes chondrogenesis of human adipose-derived mesenchymal stem cells via the p38 MAPK pathway. Biochem Biophys Res Commun. 2011;414(2):412-8.
153. Mellor LF, Baker TL, Brown RJ, Catlin LW, Oxford JT. Optimal 3D culture of primary articular chondrocytes for use in the rotating wall vessel bioreactor. Aviat Space Environ Med. 2014;85(8):798-804.
154. Kiraly AJ, Roberts A, Cox M, Mauerhan D, Hanley E, Sun Y. Comparison of Meniscal Cell-Mediated and Chondrocyte-Mediated Calcification. The open orthopaedics journal. 2017;11:225-33.
155. Liang Y, Idrees E, Andrews SHJ, Labib K, Szojka A, Kunze M, et al. Plasticity of Human Meniscus Fibrochondrocytes: A Study on Effects of Mitotic Divisions and Oxygen Tension. Sci Rep. 2017;7(1):12148.
156. Anderson-Baron M, Liang Y, Kunze M, Mulet-Sierra A, Osswald M, Ansari K, et al. Suppression of Hypertrophy During in vitro Chondrogenesis of Cocultures of Human Mesenchymal Stem Cells and Nasal Chondrocytes Correlates With Lack of in vivo Calcification and Vascular Invasion. Front Bioeng Biotechnol. 2020;8:572356.
157. Hellemans J, Mortier G, De Paepe A, Speleman F, Vandesompele J. qBase relative quantification framework and software for management and automated analysis of real-time quantitative PCR data. Genome Biol. 2007;8(2):R19.
158. Schmittgen TD, Livak KJ. Analyzing real-time PCR data by the comparative C(T) method. Nat Protoc. 2008;3(6):1101-8.
159. Livak KJ, Schmittgen TD. Analysis of relative gene expression data using real-time quantitative PCR and the 2(-Delta Delta C(T)) Method. Methods. 2001;25(4):402-8.
160. Parreno J, Raju S, Wu PH, Kandel RA. MRTF-A signaling regulates the acquisition of the contractile phenotype in dedifferentiated chondrocytes. Matrix Biol. 2017;62:3-14.

161. Killion CH, Mitchell EH, Duke CG, Serra R. Mechanical loading regulates organization of the actin cytoskeleton and column formation in postnatal growth plate. Mol Biol Cell. 2017;28(14):1862-70.
162. Tang DD, Gerlach BD. The roles and regulation of the actin cytoskeleton, intermediate filaments and microtubules in smooth muscle cell migration. Respir Res. 2017;18(1):54.
163. Servin-Vences MR, Moroni M, Lewin GR, Poole K. Direct measurement of TRPV4 and PIEZO1 activity reveals multiple mechanotransduction pathways in chondrocytes. Elife. 2017;6.
164. Agarwal P, Lee HP, Smeriglio P, Grandi F, Goodman S, Chaudhuri O, et al. A dysfunctional TRPV4-GSK3beta pathway prevents osteoarthritic chondrocytes from sensing changes in extracellular matrix viscoelasticity. Nat Biomed Eng. 2021;5(12):1472-84.
165. McNulty AL, Guilak F. Mechanobiology of the meniscus. J Biomech. 2015;48(8):1469-78.
166. Hwang HS, Park IY, Hong JI, Kim JR, Kim HA. Comparison of joint degeneration and pain in male and female mice in DMM model of osteoarthritis. Osteoarthritis Cartilage. 2021;29(5):728-38.
167. Lee W, Nims RJ, Savadipour A, Zhang Q, Leddy HA, Liu F, et al. Inflammatory signaling sensitizes Piezo1 mechanotransduction in articular chondrocytes as a pathogenic feed-forward mechanism in osteoarthritis. Proc Natl Acad Sci U S A. 2021;118(13).
168. Benderdour M, Tardif G, Pelletier JP, Di Battista JA, Reboul P, Ranger P, et al. Interleukin 17 (IL-17) induces collagenase-3 production in human osteoarthritic chondrocytes via AP-1 dependent activation: differential activation of AP-1 members by IL-17 and IL-1beta. J Rheumatol. 2002;29(6):1262-72.
169. Cope PJ, Ourradi K, Li Y, Sharif M. Models of osteoarthritis: the good, the bad and the promising. Osteoarthritis Cartilage. 2019;27(2):230-9.
170. Youn I, Choi JB, Cao L, Setton LA, Guilak F. Zonal variations in the three-dimensional morphology of the chondron measured in situ using confocal microscopy. Osteoarthritis Cartilage. 2006;14(9):889-97.

171. Ohtsuki T, Shinaoka A, Kumagishi-Shinaoka K, Asano K, Hatipoglu OF, Inagaki J, et al. Mechanical strain attenuates cytokine-induced ADAMTS9 expression via transient receptor potential vanilloid type 1. Exp Cell Res. 2019;383(2):111556.
172. Antunes BP, Vainieri ML, Alini M, Monsonego-Ornan E, Grad S, Yayon A. Enhanced chondrogenic phenotype of primary bovine articular chondrocytes in Fibrin-Hyaluronan hydrogel by multi-axial mechanical loading and FGF18. Acta Biomater. 2020;105:170-9.
173. Huang Z, Zhou M, Wang Q, Zhu M, Chen S, Li H. Mechanical and hypoxia stress can cause chondrocytes apoptosis through over-activation of endoplasmic reticulum stress. Arch Oral Biol. 2017;84:125-32.
174. He Z, Leong DJ, Xu L, Hardin JA, Majeska RJ, Schaffler MB, et al. CITED2 mediates the cross-talk between mechanical loading and IL-4 to promote chondroprotection. Ann N Y Acad Sci. 2019;1442(1):128-37.
175. Fitzgerald J. Cartilage breakdown in microgravity-a problem for long-term spaceflight? NPJ Regen Med. 2017;2:10.
176. Wehland M, Steinwerth P, Aleshcheva G, Sahana J, Hemmersbach R, Lutzenberg R, et al. Tissue Engineering of Cartilage Using a Random Positioning Machine. Int J Mol Sci. 2020;21(24).
177. Freed LE, Vunjak-Novakovic G. Microgravity tissue engineering. In Vitro Cell Dev Biol Anim. 1997;33(5):381-5.
178. Gupta T, Haut Donahue TL. Role of cell location and morphology in the mechanical environment around meniscal cells. Acta Biomater. 2006;2(5):483-92.
179. Ferretti M, Srinivasan A, Deschner J, Gassner R, Baliko F, Piesco N, et al. Anti-inflammatory effects of continuous passive motion on meniscal fibrocartilage. J Orthop Res. 2005;23(5):1165-71.
180. Killian ML, Haut RC, Haut Donahue TL. Acute cell viability and nitric oxide release in lateral menisci following closed-joint knee injury in a lapine model of post-traumatic osteoarthritis. BMC Musculoskelet Disord. 2014;15:297.
181. Videman T, Eronen I, Friman C, Langenskiold A. Glycosaminoglycan metabolism of the medial meniscus, the medial collateral ligament and the hip joint

capsule in experimental osteoarthritis caused by immobilization of the rabbit knee. Acta Orthop Scand. 1979;50(4):465-70.
182. Klein L, Heiple KG, Torzilli PA, Goldberg VM, Burstein AH. Prevention of ligament and meniscus atrophy by active joint motion in a non-weight-bearing model. J Orthop Res. 1989;7(1):80-5.
183. Anderson DR, Gershuni DH, Nakhostine M, Danzig LA. The effects of non-weight-bearing and limited motion on the tensile properties of the meniscus. Arthroscopy. 1993;9(4):440-5.
184. Djurasovic M, Aldridge JW, Grumbles R, Rosenwasser MP, Howell D, Ratcliffe A. Knee joint immobilization decreases aggrecan gene expression in the meniscus. Am J Sports Med. 1998;26(3):460-6.
185. Mikic B, Johnson TL, Chhabra AB, Schalet BJ, Wong M, Hunziker EB. Differential effects of embryonic immobilization on the development of fibrocartilaginous skeletal elements. J Rehabil Res Dev. 2000;37(2):127-33.
186. Bray RC, Smith JA, Eng MK, Leonard CA, Sutherland CA, Salo PT. Vascular response of the meniscus to injury: effects of immobilization. J Orthop Res. 2001;19(3):384-90.
187. Aufderheide AC, Athanasiou KA. A direct compression stimulator for articular cartilage and meniscal explants. Ann Biomed Eng. 2006;34(9):1463-74.
188. McNulty AL, Moutos FT, Weinberg JB, Guilak F. Enhanced integrative repair of the porcine meniscus in vitro by inhibition of interleukin-1 or tumor necrosis factor alpha. Arthritis Rheum. 2007;56(9):3033-42.
189. McNulty AL, Guilak F. Integrative repair of the meniscus: lessons from in vitro studies. Biorheology. 2008;45(3-4):487-500.
190. McNulty AL, Estes BT, Wilusz RE, Weinberg JB, Guilak F. Dynamic loading enhances integrative meniscal repair in the presence of interleukin-1. Osteoarthritis Cartilage. 2010;18(6):830-8.
191. Riera KM, Rothfusz NE, Wilusz RE, Weinberg JB, Guilak F, McNulty AL. Interleukin-1, tumor necrosis factor-alpha, and transforming growth factor-beta 1 and integrative meniscal repair: influences on meniscal cell proliferation and migration. Arthritis Res Ther. 2011;13(6):R187.

192. Kiani C, Chen L, Wu YJ, Yee AJ, Yang BB. Structure and function of aggrecan. Cell Res. 2002;12(1):19-32.
193. Gao Y, Liu S, Huang J, Guo W, Chen J, Zhang L, et al. The ECM-cell interaction of cartilage extracellular matrix on chondrocytes. Biomed Res Int. 2014;2014:648459.
194. Ferre IM, Roof MA, Anoushiravani AA, Wasterlain AS, Lajam CM. Understanding the Observed Sex Discrepancy in the Prevalence of Osteoarthritis. JBJS Rev. 2019;7(9):e8.
195. Yang B, Yu JK, Zheng ZZ, Lu ZH, Zhang JY. Comparative study of sex differences in distal femur morphology in osteoarthritic knees in a Chinese population. PLoS One. 2014;9(2):e89394.
196. Wise BL, Liu F, Kritikos L, Lynch JA, Parimi N, Zhang Y, et al. The association of distal femur and proximal tibia shape with sex: The Osteoarthritis Initiative. Semin Arthritis Rheum. 2016;46(1):20-6.
197. Frysz M, Gregory J, Aspden RM, Paternoster L, Tobias JH. Sex differences in proximal femur shape: findings from a population-based study in adolescents. Sci Rep. 2020;10(1):4612.
198. Phinyomark A, Osis ST, Hettinga BA, Kobsar D, Ferber R. Gender differences in gait kinematics for patients with knee osteoarthritis. BMC Musculoskelet Disord. 2016;17:157.
199. Ro DH, Lee DY, Moon G, Lee S, Seo SG, Kim SH, et al. Sex differences in knee joint loading: Cross-sectional study in geriatric population. J Orthop Res. 2017;35(6):1283-9.
200. Allison K, Hall M, Wrigley TV, Pua YH, Metcalf B, Bennell KL. Sex-specific walking kinematics and kinetics in individuals with unilateral, symptomatic hip osteoarthritis: A cross sectional study. Gait Posture. 2018;65:234-9.
201. Brennan SL, Cicuttini FM, Shortreed S, Forbes A, Jones G, Stuckey SL, et al. Women lose patella cartilage at a faster rate than men: a 4.5-year cohort study of subjects with knee OA. Maturitas. 2010;67(3):270-4.
202. Wang XD, Kou XX, Meng Z, Bi RY, Liu Y, Zhang JN, et al. Estrogen aggravates iodoacetate-induced temporomandibular joint osteoarthritis. J Dent Res. 2013;92(10):918-24.

203. Antony B, Venn A, Cicuttini F, March L, Blizzard L, Dwyer T, et al. Association of Body Composition and Hormonal and Inflammatory Factors With Tibial Cartilage Volume and Sex Difference in Cartilage Volume in Young Adults. Arthritis Care Res (Hoboken). 2016;68(4):517-25.
204. Zazulak BT, Paterno M, Myer GD, Romani WA, Hewett TE. The effects of the menstrual cycle on anterior knee laxity: a systematic review. Sports Med. 2006;36(10):847-62.
205. Hooshmand S, Juma S, Khalil DA, Shamloufard P, Arjmandi BH. Women with osteoarthritis have elevated synovial fluid levels of insulin-like growth factor (IGF)-1 and IGF-binding protein-3. J Immunoassay Immunochem. 2015;36(3):284-94.
206. Kosek E, Finn A, Ultenius C, Hugo A, Svensson C, Ahmed AS. Differences in neuroimmune signalling between male and female patients suffering from knee osteoarthritis. J Neuroimmunol. 2018;321:49-60.
207. Centers for Disease C, Prevention. National and state medical expenditures and lost earnings attributable to arthritis and other rheumatic conditions--United States, 2003. MMWR Morb Mortal Wkly Rep. 2007;56(1):4-7.
208. Kwok AT, Mohamed NS, Plate JF, Yammani RR, Rosas S, Bateman TA, et al. Spaceflight and hind limb unloading induces an arthritic phenotype in knee articular cartilage and menisci of rodents. Sci Rep. 2021;11(1):10469.
209. Zhou Q, Wei B, Liu S, Mao F, Zhang X, Hu J, et al. Cartilage matrix changes in contralateral mobile knees in a rabbit model of osteoarthritis induced by immobilization. BMC Musculoskelet Disord. 2015;16:224.
210. Hinterwimmer S, Krammer M, Krotz M, Glaser C, Baumgart R, Reiser M, et al. Cartilage atrophy in the knees of patients after seven weeks of partial load bearing. Arthritis Rheum. 2004;50(8):2516-20.
211. Lu W, Wang L, Yao J, Wo C, Chen Y. C5a aggravates dysfunction of the articular cartilage and synovial fluid in rats with knee joint immobilization. Mol Med Rep. 2018;18(2):2110-6.
212. Mutsuzaki H, Nakajima H, Sakane M. Extension of knee immobilization delays recovery of histological damages in the anterior cruciate ligament insertion and articular cartilage in rabbits. J Phys Ther Sci. 2018;30(1):140-4.

213. Nagai M, Aoyama T, Ito A, Tajino J, Iijima H, Yamaguchi S, et al. Alteration of cartilage surface collagen fibers differs locally after immobilization of knee joints in rats. J Anat. 2015;226(5):447-57.
214. Sun Y, Mauerhan DR, Honeycutt PR, Kneisl JS, Norton JH, Hanley EN, Jr., et al. Analysis of meniscal degeneration and meniscal gene expression. BMC Musculoskelet Disord. 2010;11:19.
215. Mechanical Unloading of Engineered Human Meniscus Models Under Simulated Microgravity: A Transcriptomic Study. [Internet]. Figshare. 2022.
216. Bausch-Fluck D, Goldmann U, Muller S, van Oostrum M, Muller M, Schubert OT, et al. The in silico human surfaceome. Proc Natl Acad Sci U S A. 2018;115(46):E10988-E97.
217. Elkhenany HA, Szojka ARA, Mulet-Sierra A, Liang Y, Kunze M, Lan X, et al. Bone Marrow Mesenchymal Stem Cell-Derived Tissues are Mechanically Superior to Meniscus Cells. Tissue Eng Part A. 2021;27(13-14):914-28.
218. Baker BM, Nathan AS, Huffman GR, Mauck RL. Tissue engineering with meniscus cells derived from surgical debris. Osteoarthritis Cartilage. 2009;17(3):336-45.
219. Weiss WM, Mulet-Sierra A, Kunze M, Jomha NM, Adesida AB. Coculture of meniscus cells and mesenchymal stem cells in simulated microgravity. NPJ Microgravity. 2017;3(1):28.
220. Freed LE, Vunjak-Novakovic G. Cultivation of cell-polymer tissue constructs in simulated microgravity. Biotechnol Bioeng. 1995;46(4):306-13.
221. Yu B, Yu D, Cao L, Zhao X, Long T, Liu G, et al. Simulated microgravity using a rotary cell culture system promotes chondrogenesis of human adipose-derived mesenchymal stem cells via the p38 MAPK pathway. Biochemical and Biophysical Research Communications. 2011(0).
222. Martin I, Jakob M, Schafer D, Dick W, Spagnoli G, Heberer M. Quantitative analysis of gene expression in human articular cartilage from normal and osteoarthritic joints. Osteoarthritis Cartilage. 2001;9(2):112-8.
223. von der Mark K, Kirsch T, Nerlich A, Kuss A, Weseloh G, Gluckert K, et al. Type X collagen synthesis in human osteoarthritic cartilage. Indication of chondrocyte hypertrophy. Arthritis Rheum. 1992;35(7):806-11.

224. Leijten JC, Bos SD, Landman EB, Georgi N, Jahr H, Meulenbelt I, et al. GREM1, FRZB and DKK1 mRNA levels correlate with osteoarthritis and are regulated by osteoarthritis-associated factors. Arthritis Res Ther. 2013;15(5):R126.
225. Valdes AM, Hart DJ, Jones KA, Surdulescu G, Swarbrick P, Doyle DV, et al. Association study of candidate genes for the prevalence and progression of knee osteoarthritis. Arthritis Rheum. 2004;50(8):2497-507.
226. Bian Q, Wang YJ, Liu SF, Li YP. Osteoarthritis: genetic factors, animal models, mechanisms, and therapies. Front Biosci (Elite Ed). 2012;4:74-100.
227. Levillain A, Boulocher C, Kaderli S, Viguier E, Hannouche D, Hoc T, et al. Meniscal biomechanical alterations in an ACLT rabbit model of early osteoarthritis. Osteoarthritis Cartilage. 2015;23(7):1186-93.
228. Hoyland JA, Thomas JT, Donn R, Marriott A, Ayad S, Boot-Handford RP, et al. Distribution of type X collagen mRNA in normal and osteoarthritic human cartilage. Bone Miner. 1991;15(2):151-63.
229. Pelttari K, Winter A, Steck E, Goetzke K, Hennig T, Ochs BG, et al. Premature induction of hypertrophy during in vitro chondrogenesis of human mesenchymal stem cells correlates with calcification and vascular invasion after ectopic transplantation in SCID mice. Arthritis Rheum. 2006;54(10):3254-66.
230. van der Kraan PM, van den Berg WB. Chondrocyte hypertrophy and osteoarthritis: role in initiation and progression of cartilage degeneration? Osteoarthritis Cartilage. 2012;20(3):223-32.
231. Bortoluzzi A, Furini F, Scire CA. Osteoarthritis and its management - Epidemiology, nutritional aspects and environmental factors. Autoimmun Rev. 2018;17(11):1097-104.
232. Primorac D, Molnar V, Rod E, Jelec Z, Cukelj F, Matisic V, et al. Knee Osteoarthritis: A Review of Pathogenesis and State-Of-The-Art Non-Operative Therapeutic Considerations. Genes (Basel). 2020;11(8).
233. Clockaerts S, Bastiaansen-Jenniskens YM, Runhaar J, Van Osch GJ, Van Offel JF, Verhaar JA, et al. The infrapatellar fat pad should be considered as an active osteoarthritic joint tissue: a narrative review. Osteoarthritis Cartilage. 2010;18(7):876-82.

234. Ma Z, Vyhlidal MJ, Li DX, Adesida AB. Mechano-bioengineering of the knee meniscus. Am J Physiol Cell Physiol. 2022;323(6):C1652-C63.
235. Contartese D, Tschon M, De Mattei M, Fini M. Sex Specific Determinants in Osteoarthritis: A Systematic Review of Preclinical Studies. Int J Mol Sci. 2020;21(10).
236. Boyan BD, Hart DA, Enoka RM, Nicolella DP, Resnick E, Berkley KJ, et al. Hormonal modulation of connective tissue homeostasis and sex differences in risk for osteoarthritis of the knee. Biol Sex Differ. 2013;4(1):3.
237. Wang S, Wang H, Liu W, Wei B. Identification of Key Genes and Pathways Associated with Sex Differences in Osteoarthritis Based on Bioinformatics Analysis. Biomed Res Int. 2019;2019:3482751.
238. Kaprio J, Kujala UM, Peltonen L, Koskenvuo M. Genetic liability to osteoarthritis may be greater in women than men. BMJ. 1996;313(7051):232.
239. Black AL, Clark AL. Sexual dimorphism in knee osteoarthritis: Biomechanical variances and biological influences. J Orthop. 2022;32:104-8.
240. Febbraio M, Hajjar DP, Silverstein RL. CD36: a class B scavenger receptor involved in angiogenesis, atherosclerosis, inflammation, and lipid metabolism. Journal of Clinical Investigation. 2001;108(6):785-91.
241. Shu H, Peng Y, Hang W, Nie J, Zhou N, Wang DW. The role of CD36 in cardiovascular disease. Cardiovasc Res. 2022;118(1):115-29.
242. Chen Y, Zhang J, Cui W, Silverstein RL. CD36, a signaling receptor and fatty acid transporter that regulates immune cell metabolism and fate. J Exp Med. 2022;219(6).
243. Glatz JFC, Wang F, Nabben M, Luiken J. CD36 as a target for metabolic modulation therapy in cardiac disease. Expert Opin Ther Targets. 2021;25(5):393-400.
244. Umbarawan Y, Syamsunarno M, Koitabashi N, Obinata H, Yamaguchi A, Hanaoka H, et al. Myocardial fatty acid uptake through CD36 is indispensable for sufficient bioenergetic metabolism to prevent progression of pressure overload-induced heart failure. Sci Rep. 2018;8(1):12035.
245. Pfander D, Cramer T, Deuerling D, Weseloh G, Swoboda B. Expression of thrombospondin-1 and its receptor CD36 in human osteoarthritic cartilage. Ann Rheum Dis. 2000;59(6):448-54.

246. Sun J, Yan B, Yin W, Zhang X. Identification of genes associated with osteoarthritis by microarray analysis. Mol Med Rep. 2015;12(4):5211-6.
247. Maumus M, Noel D, Ea HK, Moulin D, Ruiz M, Hay E, et al. Identification of TGFbeta signatures in six murine models mimicking different osteoarthritis clinical phenotypes. Osteoarthritis Cartilage. 2020;28(10):1373-84.
248. Nomura M, Sakitani N, Iwasawa H, Kohara Y, Takano S, Wakimoto Y, et al. Thinning of articular cartilage after joint unloading or immobilization. An experimental investigation of the pathogenesis in mice. Osteoarthritis Cartilage. 2017;25(5):727-36.
249. Ganse B, Cucchiarini M, Madry H. Joint Cartilage in Long-Duration Spaceflight. Biomedicines. 2022;10(6).
250. Ma Z, Li DX, Lan X, Bubelenyi A, Vyhlidal M, Kunze M, et al. Short-term response of primary human meniscus cells to simulated microgravity. Cell Commun Signal. 2024;22(1):342.
251. Febbraio M, Abumrad NA, Hajjar DP, Sharma K, Cheng W, Pearce SF, et al. A null mutation in murine CD36 reveals an important role in fatty acid and lipoprotein metabolism. J Biol Chem. 1999;274(27):19055-62.
252. Driban JB, Davis JE, Lu B, Price LL, Ward RJ, MacKay JW, et al. Accelerated Knee Osteoarthritis Is Characterized by Destabilizing Meniscal Tears and Preradiographic Structural Disease Burden. Arthritis Rheumatol. 2019;71(7):1089-100.
253. Englund M. The role of the meniscus in osteoarthritis genesis. Med Clin North Am. 2009;93(1):37-43, x.
254. Englund M, Guermazi A, Roemer FW, Aliabadi P, Yang M, Lewis CE, et al. Meniscal tear in knees without surgery and the development of radiographic osteoarthritis among middle-aged and elderly persons: The Multicenter Osteoarthritis Study. Arthritis Rheum. 2009;60(3):831-9.
255. Mesiha M, Zurakowski D, Soriano J, Nielson JH, Zarins B, Murray MM. Pathologic characteristics of the torn human meniscus. Am J Sports Med. 2007;35(1):103-12.
256. Wesdorp MA, Eijgenraam SM, Meuffels DE, Bierma-Zeinstra SMA, Kleinrensink GJ, Bastiaansen-Jenniskens YM, et al. Traumatic Meniscal Tears Are Associated With Meniscal Degeneration. Am J Sports Med. 2020;48(10):2345-52.

257. Ahmad R. Intra-substance meniscal changes and their clinical significance: a meta-analysis. Sci Rep. 2021;11(1):3642.
258. Pauli C, Grogan SP, Patil S, Otsuki S, Hasegawa A, Koziol J, et al. Macroscopic and histopathologic analysis of human knee menisci in aging and osteoarthritis. Osteoarthritis Cartilage. 2011;19(9):1132-41.
259. McNicol D RP. Extraction and characterization of proteoglycan from human meniscus. Biochem J. 1980;185(3):705-13.
260. Sun Y, Mauerhan DR, Kneisl JS, James Norton H, Zinchenko N, Ingram J, et al. Histological examination of collagen and proteoglycan changes in osteoarthritic menisci. Open Rheumatol J. 2012;6:24-32.
261. Brew CJ, Clegg PD, Boot-Handford RP, Andrew JG, Hardingham T. Gene expression in human chondrocytes in late osteoarthritis is changed in both fibrillated and intact cartilage without evidence of generalised chondrocyte hypertrophy. Ann Rheum Dis. 2010;69(1):234-40.
262. Deng ZH, Li YS, Gao X, Lei GH, Huard J. Bone morphogenetic proteins for articular cartilage regeneration. Osteoarthritis Cartilage. 2018;26(9):1153-61.
263. Whitty C, Pernstich C, Marris C, McCaskie A, Jones M, Henson F. Sustained delivery of the bone morphogenetic proteins BMP-2 and BMP-7 for cartilage repair and regeneration in osteoarthritis. Osteoarthr Cartil Open. 2022;4(1):100240.
264. Gao X, Cheng H, Awada H, Tang Y, Amra S, Lu A, et al. A comparison of BMP2 delivery by coacervate and gene therapy for promoting human muscle-derived stem cell-mediated articular cartilage repair. Stem Cell Res Ther. 2019;10(1):346.
265. O'Brien MH, Dutra EH, Mehta S, Chen PJ, Yadav S. BMP2 Is Required for Postnatal Maintenance of Osteochondral Tissues of the Temporomandibular Joint. Cartilage. 2021;13(2_suppl):734S-43S.
266. Blaney Davidson EN, Vitters EL, van Lent PL, van de Loo FA, van den Berg WB, van der Kraan PM. Elevated extracellular matrix production and degradation upon bone morphogenetic protein-2 (BMP-2) stimulation point toward a role for BMP-2 in cartilage repair and remodeling. Arthritis Res Ther. 2007;9(5):R102.

267. Wang N, Lu Y, Rothrauff BB, Zheng A, Lamb A, Yan Y, et al. Mechanotransduction pathways in articular chondrocytes and the emerging role of estrogen receptor-alpha. Bone Res. 2023;11(1):13.
268. O'Conor CJ, Leddy HA, Benefield HC, Liedtke WB, Guilak F. TRPV4-mediated mechanotransduction regulates the metabolic response of chondrocytes to dynamic loading. Proc Natl Acad Sci U S A. 2014;111(4):1316-21.
269. Hattori K, Takahashi N, Terabe K, Ohashi Y, Kishimoto K, Yokota Y, et al. Activation of transient receptor potential vanilloid 4 protects articular cartilage against inflammatory responses via CaMKK/AMPK/NF-kappaB signaling pathway. Sci Rep. 2021;11(1):15508.
270. Brylka LJ, Alimy AR, Tschaffon-Muller MEA, Jiang S, Ballhause TM, Baranowsky A, et al. Piezo1 expression in chondrocytes controls endochondral ossification and osteoarthritis development. Bone Res. 2024;12(1):12.
271. Vincent KR, Conrad BP, Fregly BJ, Vincent HK. The pathophysiology of osteoarthritis: a mechanical perspective on the knee joint. PM R. 2012;4(5 Suppl):S3-9.
272. Febbraio M, Silverstein RL. CD36: implications in cardiovascular disease. Int J Biochem Cell Biol. 2007;39(11):2012-30.
273. Cecil DL, Appleton CT, Polewski MD, Mort JS, Schmidt AM, Bendele A, et al. The pattern recognition receptor CD36 is a chondrocyte hypertrophy marker associated with suppression of catabolic responses and promotion of repair responses to inflammatory stimuli. J Immunol. 2009;182(8):5024-31.
274. Lisanti MP SP, Vidugiriene J, Tang Z, Hermanowski-Vosatka A, Tu YH, Cook RF, Sargiacomo M. . Characterization of caveolin-rich membrane domains isolated from an endothelial-rich source: implications for human disease. J Cell Biol. 1994;126(1):111-26.
275. Shihata WA, Michell DL, Andrews KL, Chin-Dusting JP. Caveolae: A Role in Endothelial Inflammation and Mechanotransduction? Front Physiol. 2016;7:628.
276. Diem K, Fauler M, Fois G, Hellmann A, Winokurow N, Schumacher S, et al. Mechanical stretch activates piezo1 in caveolae of alveolar type I cells to trigger ATP release and paracrine stimulation of surfactant secretion from alveolar type II cells. FASEB J. 2020;34(9):12785-804.

277. Kuyinu EL, Narayanan G, Nair LS, Laurencin CT. Animal models of osteoarthritis: classification, update, and measurement of outcomes. J Orthop Surg Res. 2016;11:19.
278. Longo UG, Papalia R, De Salvatore S, Picozzi R, Sarubbi A, Denaro V. Induced Models of Osteoarthritis in Animal Models: A Systematic Review. Biology (Basel). 2023;12(2).
279. Kerr GJ, McCann MR, Branch JK, Ratneswaran A, Pest MA, Holdsworth DW, et al. C57BL/6 mice are resistant to joint degeneration induced by whole-body vibration. Osteoarthritis Cartilage. 2017;25(3):421-5.
280. Huang H, Skelly JD, Ayers DC, Song J. Age-dependent Changes in the Articular Cartilage and Subchondral Bone of C57BL/6 Mice after Surgical Destabilization of Medial Meniscus. Sci Rep. 2017;7:42294.
281. van der Kraan PM, Stoop R, Meijers TH, Poole AR, van den Berg WB. Expression of type X collagen in young and old C57Bl/6 and Balb/c mice. Relation with articular cartilage degeneration. Osteoarthritis Cartilage. 2001;9(2):92-100.
282. Otsuki S, Taniguchi N, Grogan SP, D'Lima D, Kinoshita M, Lotz M. Expression of novel extracellular sulfatases Sulf-1 and Sulf-2 in normal and osteoarthritic articular cartilage. Arthritis Res Ther. 2008;10(3):R61.
283. Stoop R, van der Kraan PM, Buma P, Hollander AP, Billinghurst RC, Poole AR, et al. Type II collagen degradation in spontaneous osteoarthritis in C57Bl/6 and BALB/c mice. Arthritis Rheum. 1999;42(11):2381-9.
284. Akoum J, Tahiri K, Corvol MT, Borderie D, Etienne F, Rannou F, et al. Aging Cartilage in Wild-Type Mice: An Observational Study. Cartilage. 2021;13(2_suppl):1407S-11S.
285. Ramos-Mucci L, Javaheri B, van 't Hof R, Bou-Gharios G, Pitsillides AA, Comerford E, et al. Meniscal and ligament modifications in spontaneous and post-traumatic mouse models of osteoarthritis. Arthritis Res Ther. 2020;22(1):171.
286. Yoshioka NK, Young GM, Khajuria DK, Karuppagounder V, Pinamont WJ, Fanburg-Smith JC, et al. Structural changes in the collagen network of joint tissues in late stages of murine OA. Sci Rep. 2022;12(1):9159.

287. Kwok J, Onuma H, Olmer M, Lotz MK, Grogan SP, D'Lima DD. Histopathological analyses of murine menisci: implications for joint aging and osteoarthritis. Osteoarthritis Cartilage. 2016;24(4):709-18.
288. Nordberg RC, Mellor LF, Krause AR, Donahue HJ, Loboa EG. LRP receptors in chondrocytes are modulated by simulated microgravity and cyclic hydrostatic pressure. PLoS One. 2019;14(10):e0223245.
289. Phelan MA, Gianforcaro AL, Gerstenhaber JA, Lelkes PI. An Air Bubble-Isolating Rotating Wall Vessel Bioreactor for Improved Spheroid/Organoid Formation. Tissue Eng Part C Methods. 2019;25(8):479-88.
290. Denhardt DT, Noda M, O'Regan AW, Pavlin D, Berman JS. Osteopontin as a means to cope with environmental insults: regulation of inflammation, tissue remodeling, and cell survival. J Clin Invest. 2001;107(9):1055-61.
291. Giachelli CM, Speer MY, Li X, Rajachar RM, Yang H. Regulation of vascular calcification: roles of phosphate and osteopontin. Circ Res. 2005;96(7):717-22.
292. Parikh AB, Lee GM, Tchivilev IV, Graff RD. A neocartilage ideal for extracellular matrix macromolecule immunolocalization. Histochem Cell Biol. 2003;120(5):427-34.
293. Yamaga M, Tsuji K, Miyatake K, Yamada J, Abula K, Ju YJ, et al. Osteopontin level in synovial fluid is associated with the severity of joint pain and cartilage degradation after anterior cruciate ligament rupture. PLoS One. 2012;7(11):e49014.
294. Standal T, Borset M, Sundan A. Role of osteopontin in adhesion, migration, cell survival and bone remodeling. Exp Oncol. 2004;26(3):179-84.
295. Bai R-J, Li Y-S, Zhang F-J. Osteopontin, a bridge links osteoarthritis and osteoporosis. Frontiers in Endocrinology. 2022;13.
296. Xu M, Zhang L, Zhao L, Gao S, Han R, Su D, et al. Phosphorylation of osteopontin in osteoarthritis degenerative cartilage and its effect on matrix metalloprotease 13. Rheumatol Int. 2013;33(5):1313-9.
297. Pullig O, Weseloh G, Gauer S, Swoboda B. Osteopontin is expressed by adult human osteoarthritic chondrocytes: protein and mRNA analysis of normal and osteoarthritic cartilage. Matrix Biol. 2000;19(3):245-55.

298. Rosenthal AK, Gohr CM, Uzuki M, Masuda I. Osteopontin promotes pathologic mineralization in articular cartilage. Matrix Biol. 2007;26(2):96-105.
299. Mapp PI, Walsh DA. Mechanisms and targets of angiogenesis and nerve growth in osteoarthritis. Nat Rev Rheumatol. 2012;8(7):390-8.
300. Ashraf S, Wibberley H, Mapp PI, Hill R, Wilson D, Walsh DA. Increased vascular penetration and nerve growth in the meniscus: a potential source of pain in osteoarthritis. Ann Rheum Dis. 2011;70(3):523-9.
301. Liphardt AM, Fernandez-Gonzalo R, Albracht K, Rittweger J, Vico L. Musculoskeletal research in human space flight - unmet needs for the success of crewed deep space exploration. NPJ Microgravity. 2023;9(1):9.
302. Moosavi D, Wolovsky D, Depompeis A, Uher D, Lennington D, Bodden R, et al. The effects of spaceflight microgravity on the musculoskeletal system of humans and animals, with an emphasis on exercise as a countermeasure: a systematic scoping review. Physiol Res. 2021;70(2):119-51.
303. Juhl OJt, Buettmann EG, Friedman MA, DeNapoli RC, Hoppock GA, Donahue HJ. Update on the effects of microgravity on the musculoskeletal system. NPJ Microgravity. 2021;7(1):28.